Bollettino della Società Paleontologica Italiana, 62 (2), 2023, 143-217. Modena

Physical and biological events across the Frasnian-Famennian boundary (Late Devonian) in continuous oxic carbonate successions in the western Tethys (Carnic Alps of Italy and Austria)

Enzo Farabegoli, Maria Cristina Perri*, Claudia Spalletta, Michael M. Joachimski, Anita Andrew & Monica Pondrelli

E. Farabegoli, Dipartimento di Scienze Biologiche, Geologiche e Ambientali, Alma Mater Studiorum - Università di Bologna, Via Zamboni 67, I-40126 Bologna, Italy.
M.C. Perri, Dipartimento di Scienze Biologiche, Geologiche e Ambientali, Alma Mater Studiorum - Università di Bologna, Via Zamboni 67, I-40126 Bologna, Italy; mariacristina.perri@unibo.it *corresponding author
C. Spalletta, Dipartimento di Scienze Biologiche, Geologiche e Ambientali, Alma Mater Studiorum - Università di Bologna, Via Zamboni 67, I-40126 Bologna, Italy; claudia.spalletta@unibo.it
M. Joachimski, GeoZentrum Nordbayern, Friedrich-Alexander Universität Erlangen-Nürnberg, Schlossgarten 5, D-91054 Erlangen, Germany; michaeljoachimski@fau.de
A. Andrew, Suite 8, Level 2, 141 Peats Ferry Road, Hornsby NSW 2077, Australia; anita.andrew53@gmail.com
M. Pondrelli, International Research School of Planetary Sciences, Università d'Annunzio, Viale Pindaro 42, I-65127 Pescara, Italy; monica.pondrelli@unich.it

KEY WORDS - Depositional environments, conodonts, biostratigraphy, stable isotopes, Lower Kellwasser Event, Upper Kellwasser Event, extinction, post-event recovery.

ABSTRACT - Two Upper Devonian stratigraphic sections Pramosio A (PRA) and Freikofel T (FRKT) in the Carnic Alps of Italy and adjacent southern Austria representing continuous, entirely calcareous oxic sedimentation spanning the Frasnian-Famennian (Fr-Fm) boundary, were analysed for conodont biostratigraphy, facies and geochemistry. Lithologies are mainly packstone and wackestone interbedded with rudstones. Microbial matter is associated with packstones and wackestones in the latest Frasnian continuing through to the base of the Famennian. Intervals of black limestone and anoxic black shale with bituminous layers are absent from both sections. Microfacies analysis, focused mainly on the Fr-Fm boundary interval, discriminated nine facies in the PRA section and six in the FRKT section, all representing water depths of a few dozens of metres. The former is interpreted as having been deposited along the middle or upper part of a slightly inclined carbonate ramp (<2°), the latter along or at the base of a metastable carbonate ramp (<6°). Pramosio A section ranges from Frasnian Zone 12 to the Pseudopolygnathus granulosus *Zone, Freikofel T from Zone 13a to the* Palmatolepis termini *Zone.*

The conodont study focused on biodiversity variation during the late Frasnian biologic crisis and across the Fr-Fm transition up to the end of recovery in the Palmatolepis minuta minuta *Zone. Polygnathids dominate until the upper part of Zone 13b when palmatolepids become prevalent. In Zone 13c, their dominance continued into the lower Famennian. Increase of icriodids was paralleled by the onset of palmatolepid dominance. The end-Frasnian biological crisis impacted heavily on conodonts, extinguishing the ancyrodellids and wiping out all palmatolepids except for a single species,* Palmatolepis ultima*. The scenario cannot be attributed to anoxia because the seawaters were well oxygenated. The Lower and Upper Kellwasser extinction events (LKWE and UKWE), connected with the end-Frasnian biologic crisis were identifiable by conodonts even in the absence of sedimentary signatures of anoxic facies. The Lower Kellwasser Event is associated with a decreasing-temperature trend. Two phases of the Upper Kellwasser Event have been discriminated. Both are connected with decreasing temperature based on conodont apatite $\delta^{18}O$. Enhanced burial of organic matter is indicated by increase in $\delta^{13}C$ measured on whole-rock carbonate in the Pramosio A section from the uppermost Zone 13b to the base of the Famennian. This positive shift in $\delta^{13}C_{carb}$ pre-dates the shift in $\delta^{18}O$. Conodont abundances are higher in Pramosio A than in Freikofel T. Exceptional abundances occur in Zone 13b in PRA section, peaking in pelagic environments with palmatolepid conodonts concurrent with increase of other pelagic biota, especially ammonoids and radiolarians. This is consistent with transgressive phases. Low abundances often coincide with rudstone levels equating with low-stand phases. Those in the early Famennian are inferred to reflect events during the worldwide biological crisis. Three transgressive-regressive cycles have been identified during Zone 13b in the Carnic Alps; the regressive trend of the last cycle persisted throughout Zone 13c when the basin reached low-stand conditions followed by a transgressive phase immediately above the Fr-Fm boundary. The transgressive-regressive cycles were of high frequency and possibly of fourth order because the time interval between the lower and upper Kellwasser positive $\delta^{13}C$ excursions, equivalent to the interval uppermost Zone 12 to uppermost Zone 13c, has been estimated at about 600 kyr.*

INTRODUCTION

In aggregate, the biological events across the Frasnian-Famennian (Fr-Fm) boundary constitute one of the most significant extinction intervals to have affected the evolution of life on Earth. Explanations proffered fall into two major groups: 1) long-term (LT) or short-term (ST) including cyclical variations in terrestrial climate and world-wide relative changes in sea level (RCSL) driven by multiple factors in the Earth-Sun system. These factors include LT global tectonics, LT to ST global or regional volcanic activity, and high-frequency orbitally-driven ST glacio-eustatic cycles (Walliser, 1984, 1996; Johnson et al., 1985; Sandberg et al., 1988; Becker et al., 1989; Goodfellow et al., 1989; Hallam & Wignall, 1997; Over et al., 1997; House et al., 2000; Girard & Lecuyer, 2002; House, 2002; Chen & Tucker, 2003; Bond et al., 2004; Hallam, 2004; McGhee, 2005; Racki, 2005; Courtillot & Olson, 2007; Bond & Wignall, 2008, 2014; Racki, 2020; Zhang et al., 2021; Zhao et al., 2022); 2) instantaneous or near-instantaneous extraterrestrial catastrophic events, especially impacts of bolides including comets

ISSN 0375-7633 doi:10.4435/BSPI.2023.06

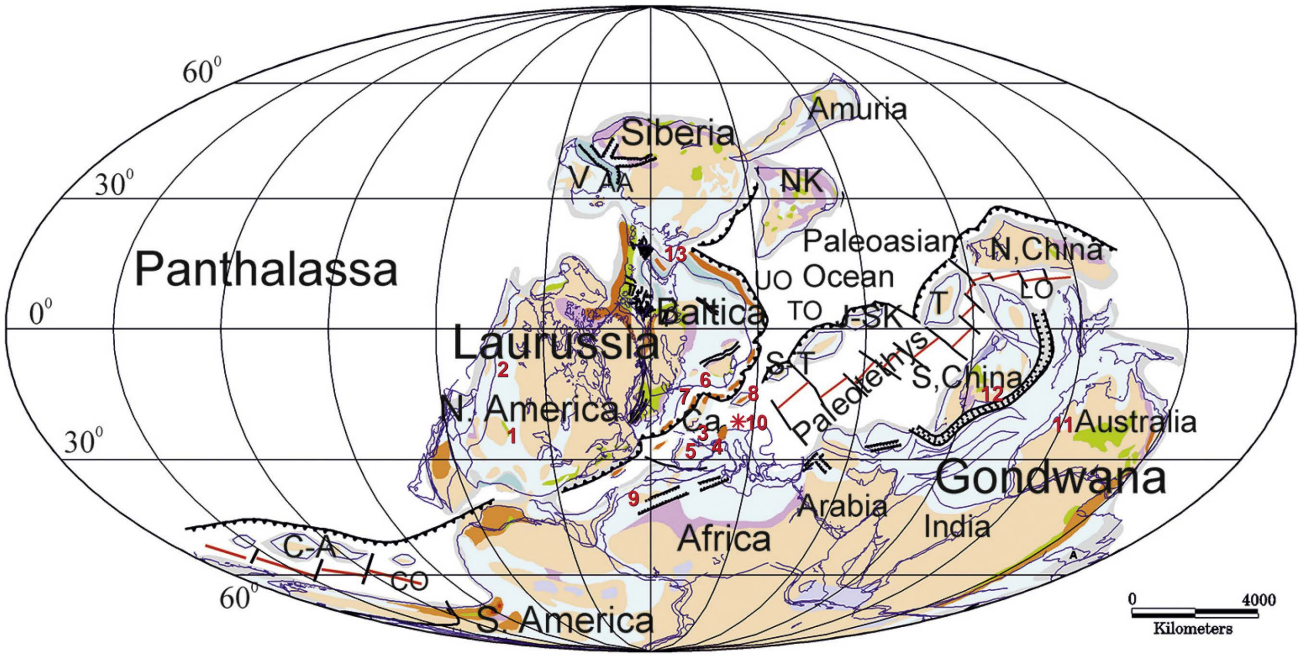

Fig. 1 - Late Devonian stratigraphic sections on the palaeogeographic-palaeotectonic map of Golonka (2020, modified). Legend: 1: Iowa basin (USA); 2: Manitoba (Canada); 3: Montagne Noire (France); 4: Sardinia (Italy); 5: Cantabrian Mountains (Spain); 6: Kowala (Poland); 7: Rheinisches Schiefergebirge (Germany); 8: Czech Republic; 9: Anti-Atlas (Morocco); 10: Carnic Alps; 11: Canning Basin (Australia); 12: Southern China; 13: Altair-Salair Region (Siberia).

(Claeys et al., 1996; Sandberg et al., 2002; Ellwood et al., 2003; Glikson et al., 2005; Racki, 2012). Evaluation of these hypotheses requires close analysis of numerous continuous depositional successions representing regional and even global phenomena, making use of sampling techniques guaranteeing maximum detail for the briefest events. To avoid increasing confusion, it is best to focus on successions lacking (or appearing to lack) unconformities, disconformities and hiatuses, as well as ones with condensed sedimentary packages, and/or sequences deposited in strongly stressed environments such as dysoxic-anoxic settings.

Because many of the well known and studied successions at the Fr-Fm boundary are affected by one or more limiting conditions, the debate on causes of extinction(s) may be strongly skewed one way or another. Two marine, anoxic-dysoxic, condensed, conspicuously black carbonate levels (Lower and Upper Kellwasserkalk, LKW and UKW) deposited immediately prior to the Fr-Fm boundary have famed case histories. Both have been discriminated in the GSSP section in the Upper Coumiac Quarry-base of Bed 32a the UKW, in the Montagne Noire of southern France (Klapper et al., 1994), as well as in sections in Germany (Buggisch et al., 1978; Schindler, 1990, 1993; Kaufmann et al., 2004; Gereke, 2007; Gereke & Schindler, 2012), Belgium (Sandberg et al., 1992; Mottequin & Poty, 2015), Poland (Racki, 1993; Joachimski et al., 2001; Olempska, 2002), Morocco (Belka & Wendt, 1992), parts of North America (Bratton et al., 1999; Over, 2002; Over & Schindler, 2003; Bond & Wignall, 2005), China (Carmichael et al., 2014; Huang & Gong, 2016; Song et al., 2017; Huang et al., 2018a, b) and Vietnam (Königshof et al., 2017). According to recent geochronologic studies, the KW-type beds have been deposited in only a few hundred thousand years (DeVleeschouwer et al., 2017; Becker et al., 2020). Many workers therefore opine that KW-type beds should be considered as: 1) isochronous horizons; 2) anoxic events produced by global transgressions; and 3) specifically in the case of the UKW that anoxia was primarily responsible for the Fr-Fm boundary extinction event (Upper Kellwasser Event), profoundly impacting on benthic and nektic faunas and floras (Copper, 1998, 2002).

Devonian geochronologic data are affected by significant degrees of uncertainty (see Becker et al., 2020). Despite acceptance of the Frasnian-Famennian GSSP in the Upper Coumiac Quarry, worldwide alignments of biologic and climatic events about that horizon continue to be disputed. The transgressive to high-stand nature for the KW horizons, postulated on basic rules of sequence stratigraphy, cannot be firmly established or disproved. This is not inconsequential, because it is consistent with the reinforcement of a world-wide transgressive marine anoxic event reflecting the dark levels and the UKW Event. The same reasons presently limit our ability to align the worldwide variations in the stable isotopes of oxygen and carbon, measured using conodont apatite and on whole carbonate rock. Pronounced variations in sea-water temperatures (5-7°C; Joachimski & Buggisch, 2002) around the Fr-Fm boundary, identified by measurements of stable oxygen isotopes in conodont apatite, require highest quality calibrations.

Keeping the above-mentioned in mind, we devoted our multiproxy research (based on conodont data for global correlations) on two oxic carbonate successions in the Carnic Alps. Continuous carbonate successions have been

described in other areas: Western Australia (Joachimski et al., 2002), Thailand (Savage et al., 2006) and China (Chang et al., 2019; Zhao et al., 2022). The Carnic Alps successions were deposited in shallow- to intermediate-depth pelagic marine environments (shelf sensu lato). These environments produced a readily discriminable and continuous record of facies tied to short-term as well as long-term patterns of climatic and sea-level changes. By doing so, it was possible to take account of a broad spectrum of sedimentologic (physical and isotopic) constraints to minimise conceivable misinterpretations.

GEOLOGICAL SETTING

During the Late Devonian, the Carnic microplate was located in the marine realm connecting the Rheic Ocean on the west to the Palaeotethys on the east at a latitude of ca 30° S, about the same latitude as the Canning Basin of Western Australia (Fig. 1). As with the Montagne Noire and Morocco farther west, it formed part of the North Gondwana margin, the first at about the same latitude, the second more to the south. The South and North China plates were located northeast of Gondwana. Portions of North America, Belgium, Germany, the Czech Republic and Poland were connected with the southern margin of Euroamerica. Relative to microplates located in the sea between Euroamerica and Gondwana, the Carnic microplate seems to have been more distal relative to land than other microplates (Vai, 1991; Schönlaub, 1992; Scotese, 1997, 2001; Schönlaub & Histon, 2000; Joachimski et al., 2004, 2009; von Raumer & Stampfli, 2008; Franke et al., 2017; Golonka, 2020; Ferretti et al., 2022).

The Devonian sequence of the Carnic Basin, spanning the Italian-Austrian border in the Carnic Alps, the easternmost part of the Southern Alps (N Italy-S Austria; Fig. 2) displays several major thrusts as well as minor high-angle indubitably Alpine faults. There is no agreement among authors regarding the scale of shortenings, suggested by some to be kilometric, by others to be hundreds of kilometres, and whether the main tectonic activity was Variscan or Alpine. The Carnic Alps consists mainly of a well preserved non- to low-metamorphic Palaeozoic sequence of ?upper Cambrian-Lower Ordovician to mid-Permian age (Selli, 1963; Vai, 1976; Spalletta et al., 1982; Schönlaub, 1985; Venturini, 1990, 1991; Venturini & Spalletta, 1998; Corradini & Suttner [eds], 2015; Pondrelli et al., 2020; Corradini & Pondrelli, 2021; Ferretti et al., 2023) subdivided into pre-Variscan and post-Variscan sequences. The former spans the ?upper Cambrian-Lower Ordovician to the Early Pennsylvanian, the latter the Pennsylvanian to the mid-Permian; the discrete sequences came into being with onset of the Variscan Orogeny. The Devonian is represented mainly by basin to reef calcareous facies. Deposition of shallow-water limestones commenced in the Pridoli with maximum development of reef facies during the Middle Devonian, extending into the Frasnian. The main Pragian to Frasnian reef plus back-reef and lagoonal complexes reached a maximum thickness of 1000 m at Mt Coglians.

The Givetian to Frasnian reef (Kellergrat Fm.) is ca 180 m thick (Kreutzer, 1990, 1992; Kido et al., 2015) at the Kellergrat section. Other calcareous lithosomes, often consisting mainly of amphiporoid facies, interpreted as patch reef and lagoonal environments a few hundred meters thick, crop out at Ombladet, Mooskofel, Polinik, Zermula (Ferrari & Vai, 1966; Corradini et al., 2019, 2020), and in the Cavallo di Pontebba Mountain (Fig. 3) (Corradini & Suttner [eds], 2015). The differing thicknesses and facies distribution of the Upper Devonian

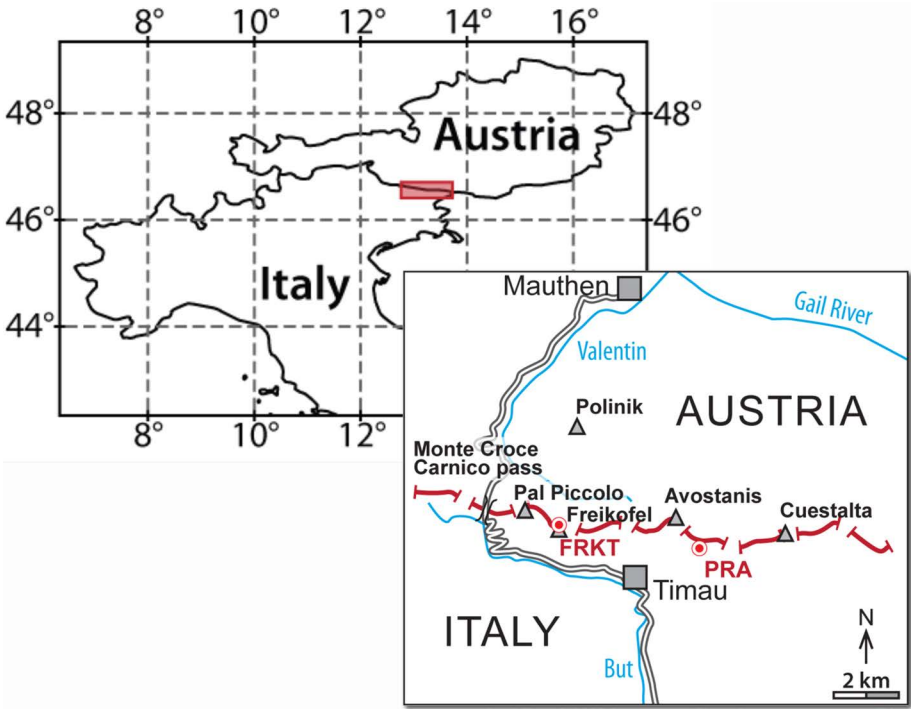

Fig. 2 - Location of the Carnic Alps (top left) and of the examined sections (bottom right).

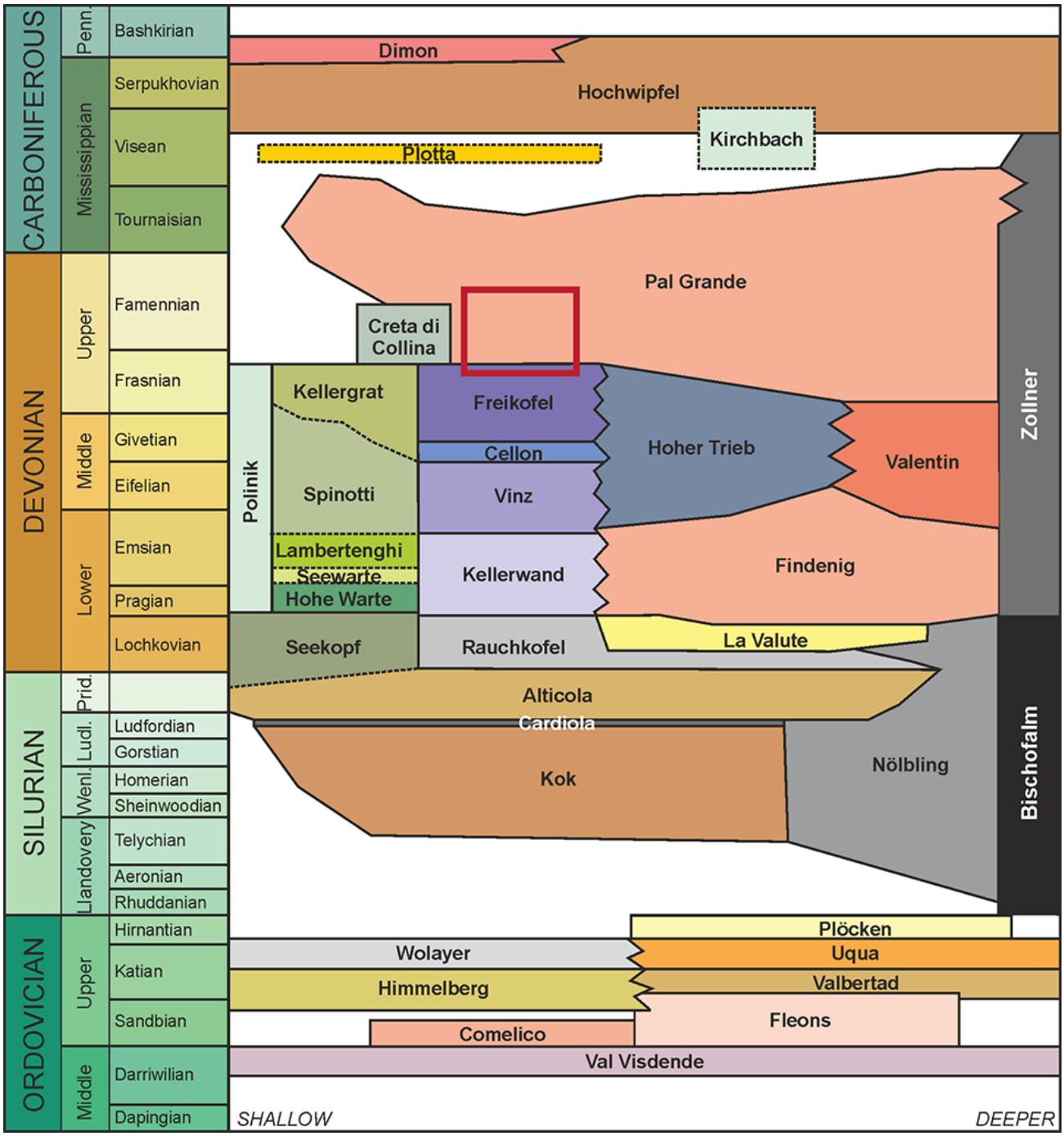

Fig. 3 - General lithostratigraphic scheme of a portion of the Devonian and Carboniferous pre-Variscan sequence (after Corradini et al., 2015, modified). The red box includes the Freikofel and Pal Grande formations outcropping along the Pramosio A and Freikofel T sections.

limestones were controlled by extensional tectonics (Spalletta et al., 1983; Spalletta & Venturini, 1995; Schönlaub, 1998). According to Vai (1976) and Schönlaub (1985, 1998), starting in the Frasnian and continuing in the Famennian, the previous limestone facies were replaced by a rather monotonous fine-grained limestone rich in pelagic fossils such as goniatites and clymenids, accumulated in a subsiding basin. This upper Frasnian-Famennian unit was recently formalized as the Pal Grande Formation (Spalletta et al., 2015b) (Fig. 3). Limestone facies deposited during at least the first part of the Famennian are less monotonous than reported in the literature. Near Mt Coglians, local brachiopod coquinites interbedded with breccias accumulated into the Famennian (Creta di Collina Fm.; Ferrari & Vai, 1973; Spalletta et al., 2015a). In terms of conodont biostratigraphy this formation equates with the interval Frasnian Zone 12 to the *Palmatolepis marginifera utahensis* Zone (Spalletta et al., 2015a). The brachiopod coquinites have been interpreted as representing "lime mud sedimentation in an open shallow pelagic sea" (Ferrari & Vai, 1973, p. 179). According to Spalletta et al. (2015a), the Creta di Collina Fm. was deposited in a relatively shallow environment of outer ramp and basin, periodically supplied by gravity-driven re-sedimented

material. Contemporaneously, the area between Mt Coglians and Mt Freikofel and the Pramosio area in the east was characterized by accumulation of interlayered breccias, and grainstones to packstone-wackestones of the Freikofel Fm. (Pas et al., 2014; Pondrelli et al., 2015b).

LITHOSTRATIGRAPHY

There are salient lithologic differences between the two sections in the field. In the Pramosio A section (PRA), beds and bed-sets often appear intensely weathered (Fig. 4). In the Freikofel T section (FRKT), the surfaces of bed-sets are mostly better defined (Fig. 5). The rock colour of the PRA section is almost exclusively grey with slight variation from light grey to dark grey, and with only two very thin (1-2 mm) pink brown layers (samples PRA6BA-PRA6BC). Colours in the FRKT section are grey, beige, brown, reddish and brick-red, the last two dominating in the middle and upper part. Because of weathering and thick surface coating produced by lichens, sedimentary structures are not readily discernible in either section.

Formal definition of 36 formations with strict application of the rules of the International Commission of Stratigraphy by a team of Italian and Austrian workers has been achieved (Corradini & Suttner [eds], 2015). In both studied sections, two of these formations have been identified: the Freikofel Fm. (below) and the Pal Grande Fm. (above) (Fig. 3). The former consists predominantly of rudstone-floatstone with subordinate packstone-grainstone and pelagic mudstone-wackestone (Pondrelli et al., 2015b). The overlying Pal Grande Fm. consists mainly of grey to reddish nodular beds of mudstone and wackestone with, in places, the presence in its basal part of calcarenites and breccias (Spalletta et al., 2015b). The boundary between the two formations is diachronous (Spalletta et al., 2015b). The top of the Freikofel Fm. in the Freikofel T section is within the Frasnian conodont Zone 13b, whereas in the Pramosio A section it is within Zone 13a. In the PRA section, rudstone facies occur up to the Famennian conodont *Palmatolepis glabra prima* Zone, in the FRKT section occur up to the *Palmatolepis termini* Zone. Microbialitic facies have been discriminated in both formations (Fig. 6).

Pramosio A section

This section (PRA), located less than 1 km north of the Casera Pramosio hut, at coordinates 46°35'37.9062" N, 13°1'42.3624" E, is about 85 m thick (Figs 2, 4). Its lower part was preliminary described by Perri & Spalletta (1998). The continuous carbonate succession spans the late Frasnian and most of the Famennian. A clear unconformity divides the Pal Grande Fm. from siltstones of the lower Carboniferous Hochwipfel Fm. Lithology, texture, fossil content, facies and chemostratigraphy of carbon and oxygen isotopes of the lowermost 16.4 meters (PRA-02-PRA15) of the closely sampled succession are represented in Fig. 6. The entire section was sampled for conodonts, $\delta^{18}O$ of conodont apatite (54 samples) and for microfacies analysis (86 thin sections ranging in size from 3×4 cm to 6×11 cm, the most frequent being 4×6 cm). The interval PRA4-PRA11 was sampled for carbon isotope analysis of whole-rock carbonates. The stratigraphic interval between samples PRA5 and PRA6B, ca 80 cm, was sampled in a continuous way using an electric cutting machine. The spatial distribution of the polished slabs from which thin sections were produced from a continuous vertical succession is illustrated in Fig. 4c. The vertical distance between the samples in the interval PRA6B-PRA8D spanning the Frasnian-Famennian boundary did not exceed 10 cm. Spacing between samples in the PRA8D-PRA14 interval increases gradually, reaching up to 50 cm. The distance between samples PRA14 and PRA15 is 150 cm; the sample distance up-section from PRA15 was increased to 3-5 meters. Due to weathering and the activity of lichens, meaningful macroscopic description of lithologies and textures proved to be very difficult, particularly for the finer grained limestones including microbialites.

Freikofel T section

The Freikofel T section (FRKT), located across the Italy-Austria border at an altitude of 1750 m and coordinates 46°36'05.3" N, 12°58'36.6" E (base of the section), 46°36'07.4" N, 12°58'36.2" E (top), is about 25 m thick (Figs 2, 5). The entire section was sampled for conodonts, $\delta^{18}O$ of conodont apatite (21 samples), and microfacies analysis (63 thin sections ranging in size from 3×4 cm to 6×11 cm with the most frequent size 4×6 cm). The interval between samples FRKT1 and FRKT72 is ca 12 m; it was sampled rather densely (Fig. 6). The interval FRKT21A-FRKT25 across the Frasnian-Famennian boundary was bed-by-bed sampled for thin sections; these, laid side by side, provide an almost continuous thin-section record through that critical interval. Bed-set surfaces are well stacked; the macroscopic description of lithology and texture is more reliable than in the Pramosio A section. The stratigraphic succession at Mt Freikofel has been analysed also by Pas et al. (2014).

FACIES AND FACIES-ASSOCIATIONS IN THE PRAMOSIO A AND FREIKOFEL T SECTIONS

The facies and facies associations we discriminated in the successions are here named facies A to facies I in the Pramosio A section and facies J to facies O in the Freikofel T section. In both sections, the facies changes (from bottom, up-section) are clearly responses to local highly dynamic depositional environments. Only facies B and H discriminated in the Pramosio A section are very similar to each other and, arguably, could be combined. In order to better appreciate similarities and differences between coeval depositional environments, we describe the facies, following where possible the vertical succession of conodont biostratigraphic units (see Chapter Conodont biostratigraphy).

Facies of the Frasnian Zone 12

This biozone has been identified only in the Pramosio A section where it is represented by facies A.

Facies A (PRA-02 and PRA1) consists of medium- to fine-grained fossiliferous packstones with planar, parallel laminae, alternating with rudstones in decimetric beds and bed-sets in grainstone matrix. Common components are shallow-water and lagoon-derived biogens, mixed with pelagic components such as radiolarians becoming more

Fig. 4 - Pramosio A section. a) The continuous carbonate succession belonging to the Freikofel and Pal Grande formations spans the upper Frasnian and most of the Famennian (Frasnian Zone 12 to the *Pseudopolygnathus granulosus* Zone, see Tab. 1). b) PRA4-PRA15. Location of the Frasnian-Famennian (Fr-Fm) boundary at the base of level PRA7A. c) PRA5B-PRA6D. Uppermost Frasnian. Field picture with superimposed composite photograph of continuous polished slabs of rocks collected using a flexible rock saw. PRA5A-PRA6B1: Frasnian Zone 13b; PRA6C-PRA6E: Frasnian Zone 13c. Bed PRA6A includes sample PRA6AA; bed PRA6B is subdivided in PRA6BA, PRA6BB, PRA6BC; bed PRA6B1 is subdivided in PRA6B1A and PRA6B1B (see Tabs 1, S5). PRA5B-PRA6B1 encompasses facies E consisting of dark grey rudstones alternating with grey, dark grey and light grey wackestones, packstones and grainstones. Two discontinuous, mm-sized, dark (orange where weathered) wavy layers border level PRA6B1. d) PRA6B-PRA8C. Top of Frasnian-base of Famennian. PRA6C-PRA6E: Frasnian Zone 13c (see explanation of Fig. 4c); PRA7A-PRA7B; *Pa. subperlobata* Zone; interval referred to facies G, consisting of microbialitic grey limestones, and lowermost part of facies H. PRA8A-PRA8B: *Pa. triangularis* Zone; PRA8C: *Pa. delicatula platys* Zone; interval always in facies H, consisting of microbialitic grey limestones.

Fig. 5 - Freikofel T section. a) Mt Freikofel; the red line indicates the location of the Freikofel T section. The continuous carbonate succession referred to the Freikofel and Pal Grande formations spans the upper Frasnian and the lower Famennian (Frasnian Zone 13a to the *Palmatolepis termini* Zone, see Tab. 2). b) Rudstone with grainstone matrix passing gradually upward to a decimetric reddish to ochre-coloured wavy bedded grainstone belonging to facies J, from the lower part of the section (Zone 13a). c) Location of the Frasnian-Famennian boundary at the base of level FRKT21F. Enzo Farabegoli digging for collecting samples provides the scale. d) FRKT53-FRKT63. *Palmatolepis minuta minuta* Zone. Beds referred to facies O constituted mainly by very fine to fine grey packstone and red-brick-coloured microbialitic limestone. FRKT59 is indicated by the red spot and detailed in the inset in thin section as a grainstone-wackestone interval. e) Uppermost part of the FRKT section constituted by grey rudstone with grainstone matrix. FRKT132 (red spot) is a grey wackestone bed, the last sampled for conodonts (*Palmatolepis termini* Zone).

frequent at the top (Figs 6, 7a-b). Bioturbation is pervasive. This facies association is similar to one described by Spalletta et al. (1980) from the Pramosio 327 section.

The conodont content decreases up-section from about 350 P_1 elements to less than 50 per kg. *Icriodus*, indicative of shallow water, increases significantly from 1% in microbialitic bed-sets capping rudstones to ca 40%. Data of level PRA1 are possibly indicative of the Lower Kellwasser Event. The $\delta^{18}O$ of conodont apatite displays a trend from 18.2 to 18.8 ‰ (Fig. 6).

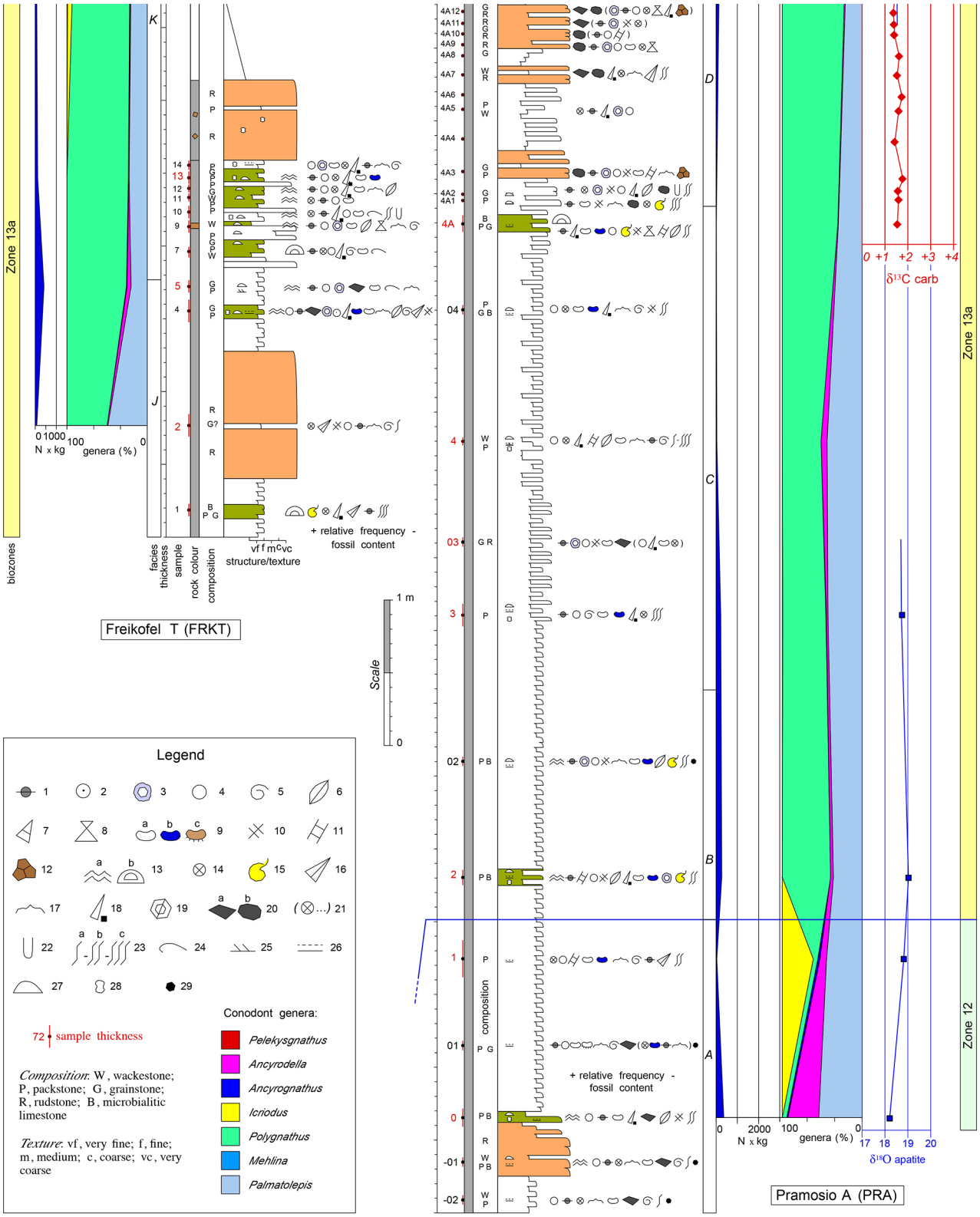

Fig. 6 - Stratigraphic columns (by Enzo Farabegoli) of Pramosio A section (PRA-02-PRA15) and Freikofel T section (FRKT1-FRKT72). Rudstone beds are coloured in orange and intervals of microbialitic limestone in green. Numbers of conodont samples are in red. Legend: 1: pellets; 2: oolite or ooid; 3: coated grain; 4: calcisphere; 5: foraminifer; 6: brachiopod; 7: gastropod; 8: bivalve; 9: ostracod as thin shell (a), closed valves (b) and ornamented valves (c); 10: crinoid ossicle; 11: calcareous algae; 12: coral; 13: microbialite as thin planar to undulate layers (a) or domal structure (b); 14: radiolarian; 15: ammonoid; 16: dacryoconarid; 17: trilobite; 18: spicule; 19: armoured ball; 20: intraclast as angular clast (a) or subrounded clast (b); 21: clast/bioclast component of breccia; 22: burrow; 23; bioturbation as scarce (a), medium (b) or frequent (c); 24: thin-shelled bivalve; 25: crossed lamination/stratification; 26: plane-parallel lamination/stratification; 27: diagenetic cavity with planar base; 28: domal cavity (microbialite?); 29: pyrite framboid.

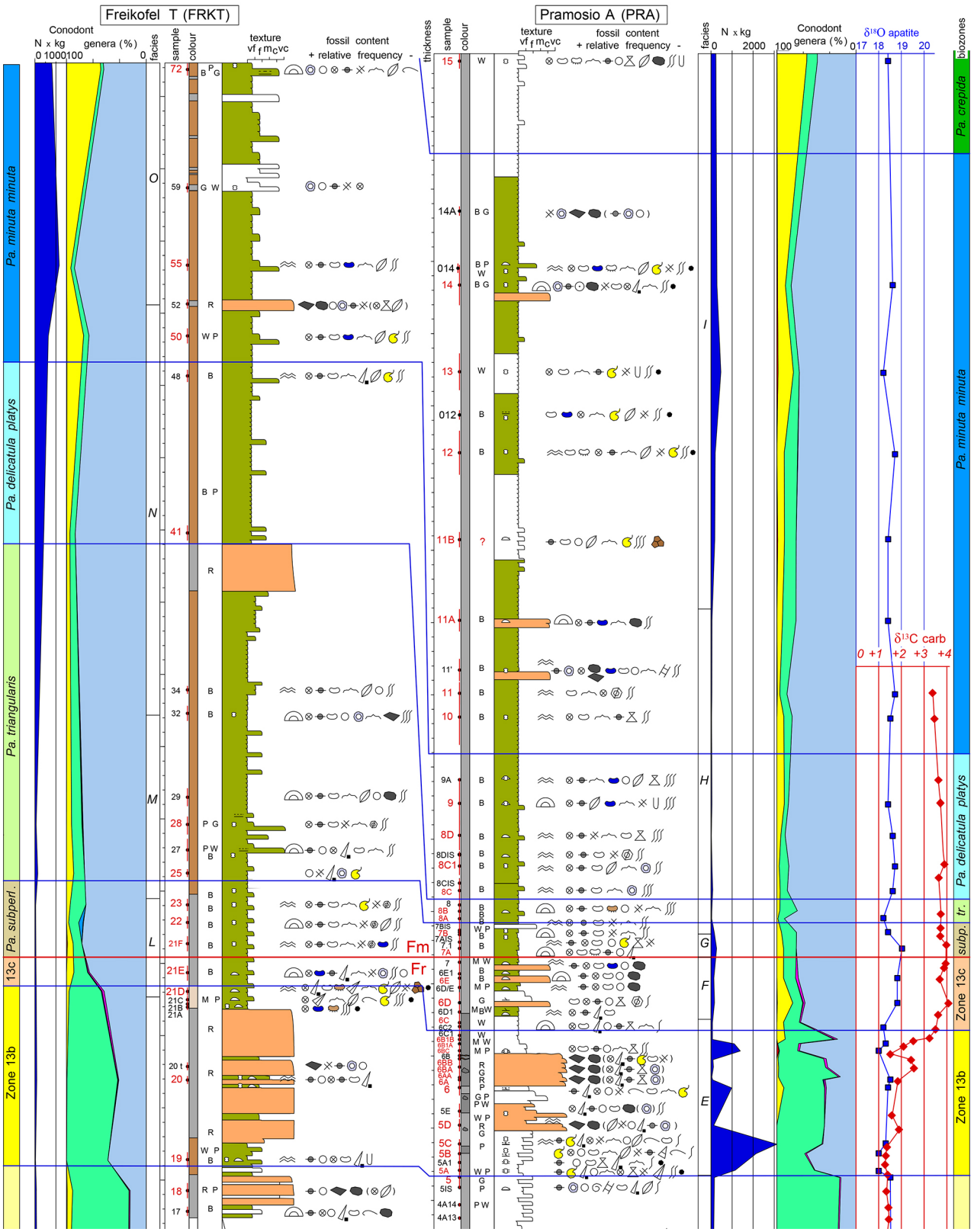

Fig. 6 - Continuation.

Facies of the Frasnian Zone 13a

Facies B, C and D were discriminated in the Pramosio A section; facies J and K p.p. in the Freikofel T section.

Facies B (sample PRA2-PRA02) consists of parallel, plane-bedded, fine-grained packstones containing shallow marine particles including abundant coated grains as well as pelagic components, especially ammonoids. Bioturbation is very frequent. These beds alternate with very thin microbialitic limestones, parallel plane-bedded to slightly wavy-bedded (Figs 6, 7c). This facies, at the

very base of Zone 13a, is interpreted as slightly post-dating the Lower Kellwasser Event.

Facies C (samples PRA3-PRA4A) consists of extensively bioturbated wackestones, packstones and grainstones. Shallow-water components (calcispheres, algae, foraminifers, brachiopods and bivalves) are frequently mixed with pelagic fossils (radiolarians and ammonoids) (Figs 6, 7d-f). The uppermost bed-set (sample PRA4A) is a microbialitic limestone containing pelagic fossils (radiolarians and ammonoids). We tentatively align this bed with the lowest sample of the Freikofel T section (FRKT1 referred to facies J).

Facies D (samples PRA4A1-PRA5) consists of grey wackestones, packstones and grainstones alternating with rudstones (Figs 6, 7i-j, l). The packstones and wackestones consist of abundant shallow marine to lagoon-derived components (coated grains, pellets, algae, corals and crinoids), but in some bed-sets pelagic components (radiolarians and ammonoids) are more frequent (e.g., PRA4A1, PRA4A2 and PRA4A5; Fig. 7i). Two rudstone bed-sets, a few decimetres thick, contain lithoclasts (corals, crinoids, coated grains, algae) eroded from a very shallow marine foreshore and from a more pelagic bedrock (radiolarians). All wackestone-packstone facies show centimetric-scale linear cavities typical of stromatactis. This facies in the Pramosio A section is coeval with facies J and with the lower part of facies K in the Freikofel T section.

Facies J (samples FRKT1-FRKT5) consists of thin- to medium-bedded (5-10 cm) packstones and grainstones which, in detail, are bed-sets of very thin cross-bedded layers 1-3 cm thick. Radiolarians and ammonoids are frequent; shallow marine components are rare; bioturbation is scarce. A thick rudstone-grainstone bed-set (ca 1 m) characterizes the middle part of this facies. The grey colour prevails, but the rudstone with grainstone matrix passes gradually upward to a decimetric reddish to ochre coloured wavy bedded grainstone (Figs 6, 7g-h). In our opinion this rudstone bed-set cannot be correlated with rudstones of facies D in the Pramosio A section.

Facies K p.p. (samples FRKT7-FRKT18) consists of microbialitic limestone bed-sets 3-6 cm thick alternating with 5 to 30 cm thick packstone- grainstone- and rudstone-bed-sets (Figs 6, 7m-n). The pelagic components in the microbialities decrease upwards concurrent with increasing shallow water components. The rudstone clasts are both angular and sub-rounded. Bioturbation is scarce, though sub-vertical burrows occur locally. The prevailing colour of the rudstones is grey, whereas the predominant colour of the microbialites is brown to pink. Stromatactis-type elongate and globular cavities are frequent in the mudstones, microbialites and packstones.

Conodont abundance is variable in both sections reaching a maximum of 425 P_1 elements/kg (sample FRKT5) across the boundary between facies J and K of the Freikofel T section. *Polygnathus* is the dominant genus in both sections. A peak of *Icriodus* is present in facies K (FRKT18) at the top of the biozone.

The $\delta^{18}O$ of conodont apatite increases in facies B (PRA2, 19‰) and decreases significantly in facies C (PRA4, 18.1‰). The $\delta^{13}C$ measured on total rock has two moderate positive peaks (from 1.5 to 1.9‰) corresponding approximately to two rudstone bed-sets (Fig. 6).

Facies of the Frasnian Zone 13b

The interval consists of facies E p.p. in the Pramosio A section, and of the upper part of facies K and the very base of facies L in the Freikofel T section.

Facies E p.p. (samples PRA5A-PRA6C2) consists entirely of grey and dark grey rudstones in two major decimetric bed-sets alternating with grey, dark grey and light grey wackestones, packstones and grainstones containing very frequent ammonoids and radiolarians mixed with less shallow-water particles (Figs 6, 7o-p). Bioturbation ranges from scarce to frequent. The rudstone in the uppermost part of the succession is overlain by two discontinuous, mm-sized, dark (orange where weathered) wavy layers separated by 3 cm of grey limestone (sample PRA6BC, upper part of PRA6B, see Fig. 4c).

The upper part of facies K (samples FRKT19-FRKT21C) consists of rudstones alternating with subordinate centimetric-decimetric microbialitic bed-sets rich in shallow-water fossils (Figs 6, 7q). The colour of the rock ranges from grey (rudstone, locally with reddish angular clasts) to reddish and beige. Bioturbation is scarce, locally with sub-vertical burrows.

The very base of facies L (sample FRKT21D) is represented by beige microbialites rich in pelagic fossils including ammonoids. The sedimentation rate of this biostratigraphic interval in the Freikofel T section is about twice that in the Pramosio A section; the difference being connected with abundance of rudstone in the first section.

The conodont abundance shows three peaks in the Pramosio A section, corresponding with wackestone-

Fig. 7 - Microfacies of Frasnian beds from the Pramosio A and Freikofel T sections grouped according to conodont biozones. a) Facies A, PRA0, bioturbated fine- to medium-grained packstone; Frasnian Zone 12. b) Facies A, PRA1, medium-grained to fine-grained packstone; Frasnian Zone 12. c) Facies B, PRA2, fine-grained packstone with ammonoids (left corner) and radiolarians; Zone 13a. d) Facies C, PRA3, bioturbated graded packstone with radiolarians (R), calcispheres (C), ostracods and brachiopod fragments; Zone 13a. e) Facies C, PRA4, packstone with stromatactis-type cavities; Zone 13a. f) Facies C, PRA4A, fine-grained packstone with microbialitic laminae rich in radiolarians, ostracods and brachiopods; Zone 13a. g) Facies J, FRKT1, bioturbated packestone; Zone 13a. h) Facies J, FRKT5, bioturbated, medium grained packstone containing coated grains (CG); Zone 13a. i) Facies D, PRA4A2, fine-grained wackstone to packstone with stromatactis-type cavity, rich in radiolarians; Zone 13a. j) Facies D, PRA4A7, rudstone constituted of angular and subrounded clasts containing pellets, coated grains and radiolarians; Zone 13a. k) Field picture of the interval about level PRA4; Zone 13a. l) Facies D, PRA4A12, rudstone consisting of subrounded clasts eroded from a shallow marine foreshore with crinoids (CR) and coated grains and from a more pelagic bedrock with radiolarians; Zone 13a. m) Facies K, FRKT7, fine- to medium grained packstone alternating with microbialitic thin layers; Zone 13a. n) Facies K: FRKT11, microbialitic limestone passing sharply upward to packstone-grainstone; Zone 13a. o) Facies E, PRA5B, ammonoid-bearing packstone with entomozoan ostracod (E) and radiolarians (R); Zone 13b. p) Facies E, PRA6, wackestone-packstone with frequent radiolarians, rare rounded clasts and geopetally filled bioclast; Zone 13b. q) Facies K, FRKT20, microbialitic limestone passing upward to wackestone-packstone; Zone 13c. r) Facies F, PRA6E, rudstone in which rounded, sub-rounded clasts seem to have been produced by disruption and transport of an early-lithified microbialite; Zone 13c. s) Facies L, FRKT21E, bioturbated microbialitic limestone with planar and undulating bedding, ostracods, trilobites (T), bivalves and frequent radiolarians (R); Zone 13c.

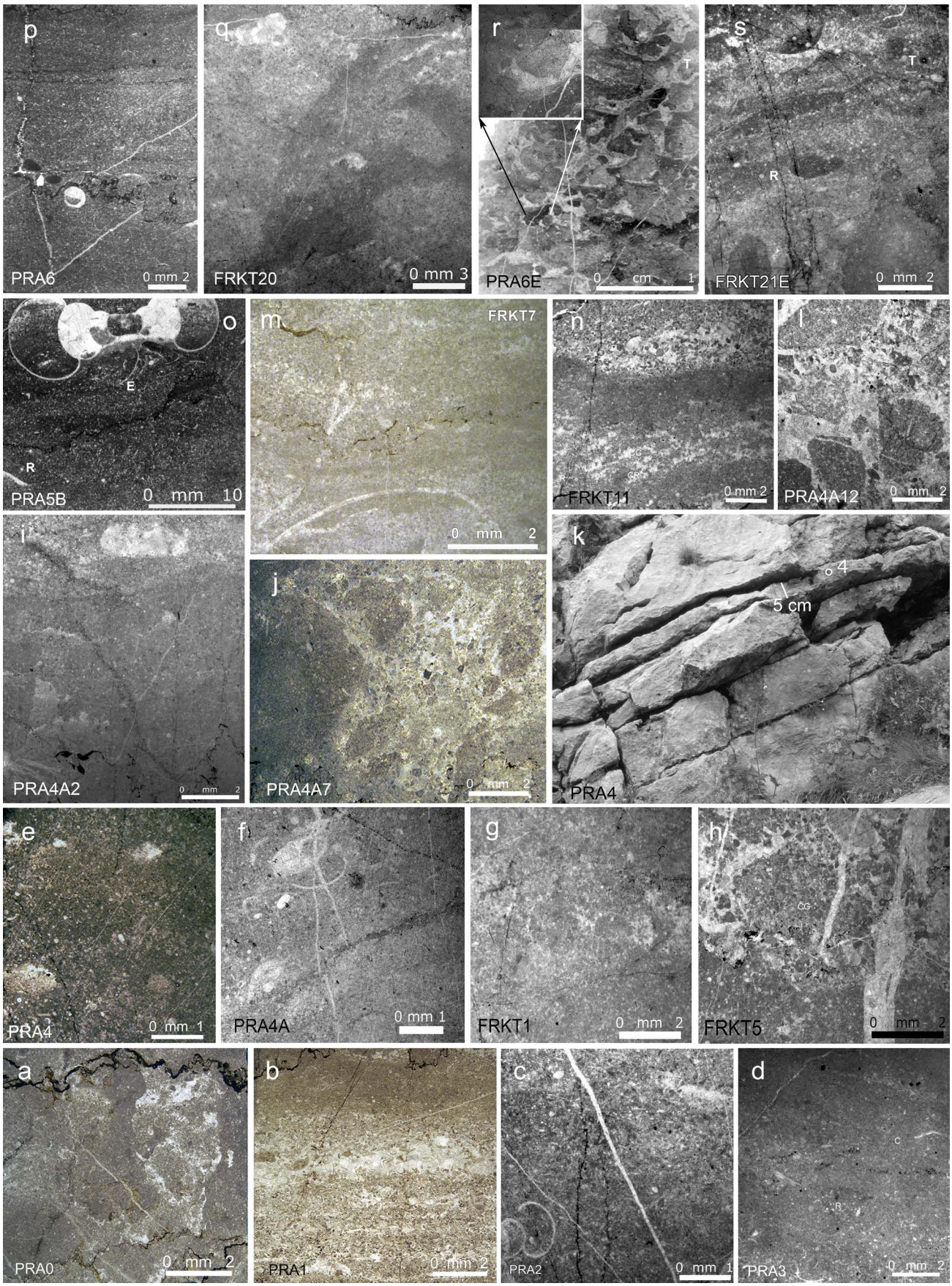
p
PRA6
0 mm 2
q
FRKT20
0 mm 3
r
T
PRA6E
0 cm 1
s
T
R
FRKT21E
0 mm 2
o
E
R
PRA5B
0 mm 10
m
FRKT7
0 mm 2
n
CG
CG
FRKT11
0 mm 2
l
PRA4A12
0 mm 2
i
PRA4A2
0 mm 2
j
PRA4A7
0 mm 2
k
4
5 cm
PRA4
e
PRA4
0 mm 1
f
PRA4A
0 mm 1
g
FRKT1
0 mm 2
h
CG
FRKT5
0 mm 2
a
PRA0
0 mm 2
b
PRA1
0 mm 2
c
PRA2
0 mm 1
d
C
R
PRA3
0 mm 2

grainstone bed-sets; abundances are more than 3000 P_1 elements (the highest value detected in this study), 1000 and ca 1500 per kg respectively. Conversely, the content of conodonts in the Freikofel T section is less than 100 P_1 elements per kg. *Polygnathus* continues to be the dominant genus in both sections except at the base and top of facies E in the Pramosio A section where *Palmatolepis* becomes dominant. It is noteworthy that these two peaks of *Palmatolepis* align perfectly with two peaks (first and last) in conodont-abundances (Fig. 6). The coeval tract of the Freikofel T section displays a comparable but much smoother trend. Icriodids are present in the second part of the biozone in facies E of the Pramosio A section and in facies K and L in the Freikofel T section. *Icriodus* shows a peak in sample PRA6 corresponding with the second peak in conodont abundance. Regarding the depositional environment, this interval in the Pramosio A section is more readily characterized as pelagic.

The $\delta^{18}O$ of conodont apatite of facies E shows two pronounced minima: at the base and at the top respectively of this biostratigraphic interval. They align with two minima in $\delta^{13}C$. Two marked positive peaks in $\delta^{13}C$ correspond with two rudstone bed-sets (1.5 and 2.5‰, respectively) (Fig. 6).

Facies of the Frasnian Zone 13c

This interval consists of the uppermost part of facies E and facies F in the Pramosio A section and the middle part of facies L in the Freikofel T section.

The uppermost part of facies E (sample PRA6C) is free of ammonoids but nevertheless retains its pelagic character.

Facies F (samples PRA6D1-PRA7) consists predominantly of microbialites alternating with subordinate, cross-laminated grey grainstones and packstones. Pelagic components are scarce, mostly radiolarians. Many of the ostracod shells are tightly closed. The mm-cm, rounded-subrounded clasts in the upper part seem to have been produced by disruption and transport of early-lithified microbialites (Figs 6, 7r). Bioturbation ranges from scarce to absent.

Facies L (samples FRKT21D-FRKT23) consists entirely of microbialitic limestones with parallel planar, undulating and domed bedding (Figs 6, 7s). The pelagic components consist of trilobites, radiolarians and dacryoconarids with ammonoids (at the base); they are associated with crinoid ossicles and armoured balls. Bioturbation is frequent. The beige colour at the base passes upward to grey. Elongate stromatactis-type and globular cavities are frequent.

The conodont abundance is generally quite low. *Palmatolepis* becomes dominant and *Icriodus* increases significantly in both sections within facies E, F and L correlated with the Upper Kellwasser Event.

The $\delta^{18}O$ of conodont apatite and $\delta^{13}C$ from the top of facies E and facies F increases upwards from 18.2 to 18.8‰ and 2.5 to 4.0‰, respectively. The peak of $\delta^{13}C$ in facies F is aligned with the peak of relative frequency of *Icriodus* (Fig. 6).

Facies of the Palmatolepis subperlobata *Zone*

This interval consists of facies G, the lowermost part of facies H (Fig. 8a) in the Pramosio A section and the upper part of facies L in the Freikofel T section.

Facies G (PRA7A-PRA7B) consists of microbialitic limestones rich in radiolarians, ammonoids, thin-shelled ostracods and some shallow-water components. Bioturbation is absent.

Facies H is described below.

The upper part of facies L (samples FRKT21F-FRKT23) consists of grey microbialitic limestones, similar to the lower part of the same facies described above (Figs 6, 8b-c).

Conodont abundances are generally low, even though in facies G in the Pramosio A section it appears high, possibly as consequence of condensation. *Palmatolepis* continues to dominate up-section and the abundance of icriodids remains relatively high.

The $\delta^{18}O$ of conodont apatite increases at the base of the *Palmatolepis subperlobata* Zone reaching 19‰ after tending to decrease. The $\delta^{13}C$ value (4.0‰) measured on the total rock of Facies G continues to be high like in the biozone below (Fig. 6).

Facies of the Palmatolepis triangularis *Zone*

This interval consists of the lower part of facies H in the Pramosio A section, facies M, and the lower part of facies N in the Freikofel T section.

The lowest part of facies H (PRA7Bis-PRA8B), starting in the *Pa. subperlobata* Zone, consists of microbialitic grey limestones rich in radiolarians and thin-shelled ostracods. Packstones and wackestones are rare. Shallow-water components are rare; bioturbation ranges from frequent to very frequent (Figs 6, 8a, d). Viewed in toto, it appears to be a variant of the facies B.

Facies M (samples FRKT25-FRKT29) consists of red-brick-coloured microbialitic limestones alternating with rare thin-bedded and very fine to very coarse packstones and grainstones. The pelagic components are ammonoids and radiolarians. The upper part of facies M (samples FRKT28-FRKT29) is similar to its lower part but lacks ammonoids (Figs 6, 8e).

The entire facies N (samples FRKT32-FRKT50) consists of reddish microbialitic limestone with grey rudstone bed-sets with a fine-grained grainstone matrix and clasts up to 4 cm in diameter (Figs 6, 8f-g). The conodont abundance is low; *Palmatolepis* still dominates.

Facies M of the Freikofel T section displays the lowest $\delta^{18}O$ value (18.8 ‰ sample FRKT25) for the biozone; it coincides with increase of *Palmatolepis* and *Icriodus* and re-appearance of frequent ammonoids. $\delta^{18}O$ and $\delta^{13}C$ values decrease upwards (from 19 to 18.2 and 4.0-3.6‰, respectively) (Fig. 6).

Facies of the Palmatolepis delicatula platys *Zone*

This interval consists of the middle part of facies H in the Pramosio A section, and the middle part of facies N in the Freikofel T section.

Facies H p.p. (PRA8C-PRA9A) consists of microbialitic grey limestones containing radiolarians, thin-shelled ostracods and trilobites mixed with minor shallow water elements such as coated grains, crinoid ossicles, bivalves and brachiopods. Packstones and wackestones are rare. Bioturbation ranges from frequent to very frequent with some burrows (Figs 6, 8h). Overall, it could be regarded as a variant of facies B.

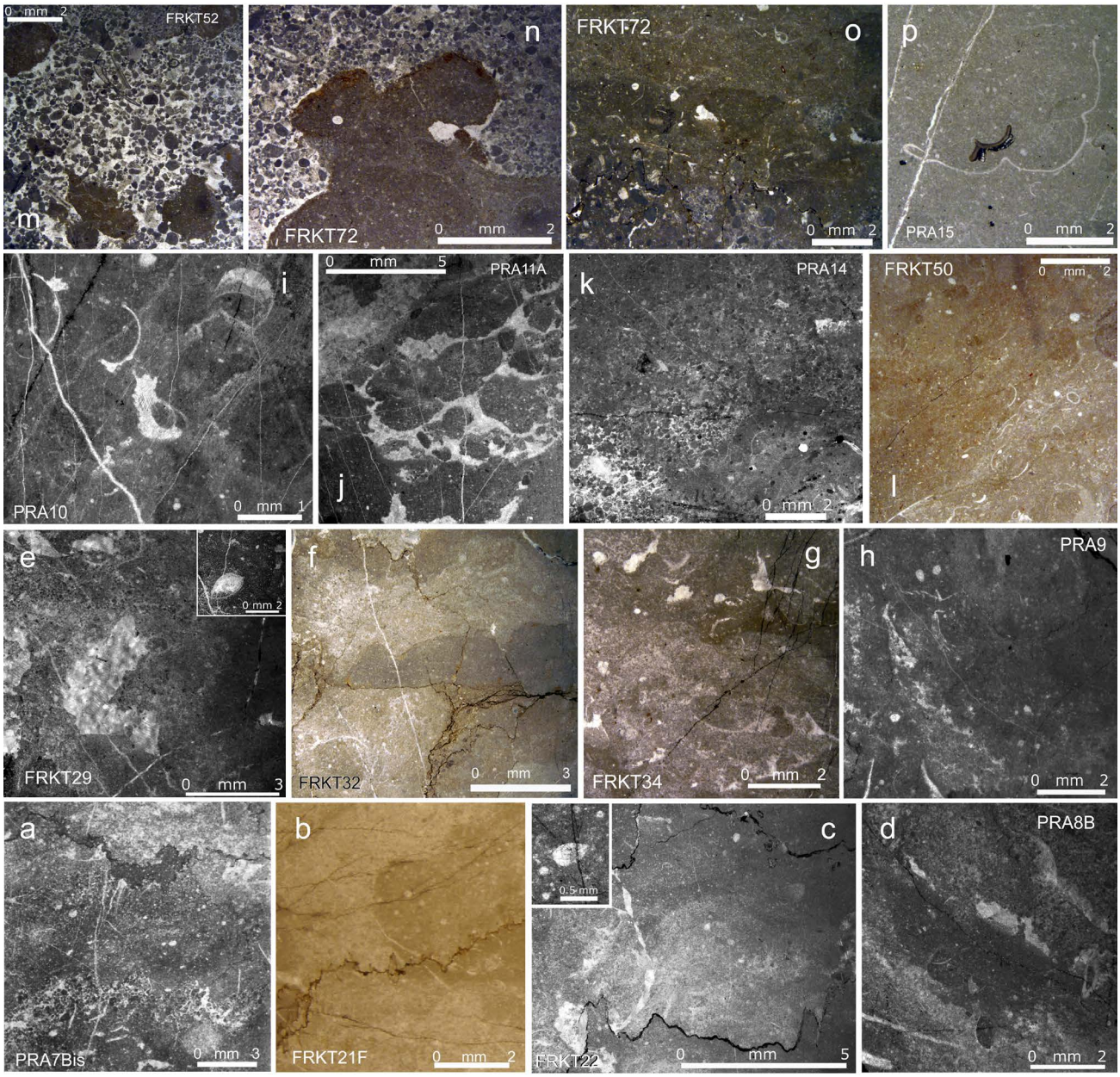

Fig. 8 - Microfacies of Famennian beds from the Pramosio A and Freikofel T sections grouped according to conodont biozones. a) Facies H, PRA7Bis, bioturbated microbialitic limestone alternating with wackstone to packstone intervals rich in radiolarians; *Palmatolepis subperlobata* Zone. b) Facies L, FRKT21F, bioturbated microbialitic limestone; *Palmatolepis subperlobata* Zone. c) Facies L, FRKT22, microbialitic limestone, in the small square some calcisphaerae and a tiny brachiopod; *Palmatolepis subperlobata* Zone. d) Facies H, PRA8B, microbialitic limestone; *Pa. triangularis* Zone. e) Facies M, FRKT29, microbialitic limestone passing upward to packstone, in the small square a tiny, geopetally filled brachiopod; *Pa. triangularis* Zone. f) Facies N, FRKT32, bioturbated, reddish microbialitic limestone; *Pa. triangularis* Zone. g) Facies N, FRKT34, bioturbated, reddish microbialitic limestone; *Pa. triangularis* Zone. h) Facies H, PRA9, microbialitic limestone with radiolarians; *Pa. delicatula platys* Zone. i) Facies H, PRA10, bioturbated microbialitic limestone with an ammonoid, radiolarians, thin shelled ostracods and bivalves; *Pa. minuta minuta* Zone. j) Facies H, PRA11A, rudstone consisting of rounded lithoclasts; *Pa. minuta minuta* Zone. k) Facies I, PRA14, microbialitic limestone alternating with wackestone-grainstone; *Pa. minuta minuta* Zone. l) Facies N, FRKT50, bioturbate reddish microbialitic limestone rich in radiolarians, ostracods and brachiopods; *Pa. minuta minuta* Zone. m) Facies O, FRKT52, grainstone, the largest pebbles consist of red-brick-coloured microbialitic limestone; *Pa. minuta minuta* Zone. n) Facies O, FRKT72, red-brick-coloured microbialitic limestone in sharp contact with grainstone; *Pa. minuta minuta* Zone. o) Facies O, FRKT72, microbialitic reddish limestone passing to fine-grained packstone; *Pa. minuta minuta* Zone. p) Facies I, PRA15, wackestone with a trilobite and a conodont fragment; *Pa. crepida* Zone.

Facies N (samples FRKT41-FRKT48) consists of reddish microbialitic limestone.

Conodont abundance is very low in facies H of the Pramosio A section, whereas in facies N the only conodont sample (FRKT41) referred to this biozone from the Freikofel T section has an appreciable abundance of conodonts (more than 400 P_1 elements per kg) with *Palmatolepis* continuing to be dominant.

Both the $\delta^{18}O$ of conodont apatite and the $\delta^{13}C$ of whole-rock samples change little up-section (less

than 0.5‰). The increased sedimentation rate (2×) in the Freikofel T section is believed to reflect the rapid deposition of the rudstones (Fig. 6).

Facies of the Palmatolepis minuta minuta *Zone*

This interval consists of the upper part of facies H and the lower part of facies I in the Pramosio A section, and the very top of facies N and facies O in the Freikofel T section.

The upper part of facies H (samples PRA10-PRA11A) consists of microbialitic grey limestones (Figs 6, 8i-j). These differ from the lower part of the facies described above in having scattered angular and rounded lithoclasts (samples PRA11-PRA11A).

Facies I (samples PRA11B-PRA15) consists mainly of grey microbialitic limestone alternating with wackestones-grainstones. Shallow water components (oolites, corals, bryozoans and rounded clasts) are present in both lithologies whereas ammonoids and radiolarians characterize the middle part. Bioturbation ranges from frequent to very frequent (Figs 6, 8k). Its upper part, Facies N (sample FRKT50) consists of reddish microbialitic limestone similar to that already described in the *Palmatolepis delicatula platys* Zone (Figs 6, 8l).

Facies O (FRKT52-FRKT72) consists primarily of thin, very fine to fine grey packstones and red-brick-coloured microbialitic limestones (Figs 6, 8m-o). Additional components of the microbialites are frequent pelagic trilobites and radiolarians mixed with occasional shallow water clasts (mostly coated grains, pellets and calcispheres, as well as rounded lithoclasts). The grainstone-wackestone components are almost exclusively shallow-sea-derived (coated grains, calcispheres, pellets and crinoid ossicles), apart from some radiolarians. Bioturbation is highly variable, ranging from absent to frequent.

In both sections, the conodont abundance increases up-section with peaks up to ca 500 P_1 elements per kg in facies I of the Pramosio A section and up to about 1200 in facies O of the Freikofel T section, but the two peaks are not aligned. In both sections *Palmatolepis* is still dominant and *Icriodus* shows high peaks of abundance. In the Pramosio A section the highest value of icriodids aligns with the peak of conodont abundance. Freikofel T section displays the highest peaks of icriodid abundance of the two sections (up to 350 P_1 elements per kg) but these highest values do not align with those of highest conodont abundance. The $\delta^{18}O$ of conodont apatite shows little change up-section (ca 0.5 ‰) (Fig. 6).

Facies of the Palmatolepis crepida *Zone*

This interval consists, in part, of facies I (sample PRA15) in the Pramosio A section, already described in the *Palmatolepis minuta minuta* Zone (Figs 6, 8p). Conodont abundance is significant; *Icriodus* is very abundant, but *Palmatolepis* dominates. The value of $\delta^{18}O$ of conodont apatite is 18.4‰ (Fig. 6).

CONODONT DATA

Material and methods

Conodonts were extracted from limestones by leaching in 10% acetic acid and the insoluble residues then separated into light and heavy fractions using a solution of sodium polytungstate as the heavy liquid. Picking included all complete and broken conodont elements found in the > 125 μ fraction. Identifications have focused primarily on elements in the P_1 position in the conodont feeding apparatus. Ramiform elements, referable to species for which a reconstruction of the apparatus has been presented in the literature, have been recognized in the sample associations but were not listed and counted. Ramiforms, incidentally, seemed always to be lower in number than anticipated. Their discrimination nevertheless confirmed the occurrence of the species identified on the basis of P_1 elements. Taxonomic identifications focused on complete as well as broken P_1 elements that could be unequivocally identified at species and subspecies level. These were counted and are listed in the distribution table for each sample along with the weight of leached rock (Tabs 1, 2). Broken P_1 elements, whose genus could be identified confidently, have been listed under their generic name followed by sp. Juvenile P_1 elements are grouped under the generic name followed by sp. juv. These too were counted and are listed in the distribution tables (Tabs 1, 2).

Conodonts are figured in Pls 1-16. Abbreviations of generic names used in the text, tables and figure captions are: *Al.* = *Alternognathus*, *Anc.* = *Ancyrodella, Ang.* = *Ancyrognathus*, *Br.* = *Branmehla*, *Ic.* = *Icriodus*, *Me* = *Mehlina*, *Pa.* = *Palmatolepis*, *Pel.* = *Pelekysgnathus*, *Po.* = *Polygnathus.* Repository: Museo "Giovanni Capellini", Dipartimento di Scienze Biologiche, Geologiche e Ambientali, Via Zamboni 67, I-40136 Bologna, Italy.

Biostratigraphy

The two studied sections were intensively sampled for conodonts for determining biostratigraphic ranges across the Frasnian-Famennian boundary (FFB): 54 samples from the Pramosio A (PRA) section and 21 from the Freikofel T (FRKT) section. The PRA section ranges from Frasnian Zone 12 to the Famennian *Pseudopolygnathus granulosus* Zone, the FRKT section from Frasnian Zone 13a to Famennian *Palmatolepis termini* Zone. The Colour Alteration Indices (CAI; Epstein et al., 1977) on the conodont organic metamorphism scale is 4.5 in the PRA section and 4 in the FRKT section.

One of our goals was to test applicability in the Carnic Alps of the method for the recognition of the Frasnian-Famennian boundary proposed by Klapper et al. (2004) and modified by Klapper (2007b): specifically, the flood occurrence of *Palmatolepis ultima* Ziegler, 1958 immediately above the Fr-Fm extinction event and, additionally, the lowest occurrence of *Pa. subperlobata* Branson & Mehl, 1934.

Our approach to the Frasnian of the Carnic Alps uses the Frasnian biozonation proposed by Klapper (1985, 1989), Feist & Klapper (1985), and Klapper (1997) based on the Montagne Noire sequence and subsequently applied globally (Klapper & Foster, 1993; Klapper et al., 1996, 2004; Girard et al., 2005; Klapper, 2007a; Hillbun et al., 2015; Klapper & Kirchgasser, 2016), aligned with the widely applied "Standard Conodont Zonation" inferred for Upper Devonian pelagic environments by Ziegler & Sandberg (1990). Klapper's approach was first to establish biozones using traditional methods, then to add evidence for the equivalence of the zones at different localities

through graphic correlation (Klapper et al., 1995, 1996; Klapper, 1997, 2007a), shape analysis (Klapper & Foster, 1986, 1993) and multi-element taxonomy (e.g., Klapper, 2007a). Species so defined may be easily discriminated using the traditional method based solely on identification of the P_1 elements using a binocular microscope.

The two Frasnian biozonations (of Ziegler & Sandberg, and of Klapper) are based on different concepts of species of *Ancyrognathus* and especially of *Palmatolepis*. Ranges and taxonomic concepts of species, especially *Pa. hassi* Müller & Müller, 1957, *Pa. rhenana* Bischoff, 1956 and *Pa. triangularis* Sannemann, 1955, differ from author to author. Re-sampling the section at Martenberg in the Rhenish Slate Mountains of Germany, one of the reference sections basis for the Frasnian zonation of Ziegler & Sandberg (1990), coupled with the taxonomic concepts underlying the zonation proposed on the basis of conodont data from the Frasnian of the Montagne Noire, enabled Klapper & Becker (1999) to align the two biozonations and to easily and consistently integrate even older reports on Frasnian conodont biozonations from elsewhere including North America and Australia.

Defining the Fr-Fm boundary has a long and complicated history. The first appearance datum (FAD) of *Palmatolepis triangularis* was selected as the sole criterion for defining the base of the Lower *triangularis* Zone by Ziegler (1962) and Ziegler & Sandberg (1990). The Subcommission on Devonian Stratigraphy (SDS) decided (1989) that the Global Boundary Stratotype Section and Point (GSSP) for the Famennian Stage had to be sought in relation to the base of the Lower *triangularis* conodont Zone. The SDS in 1991 decided to have this coincide precisely with the lower boundary of the Lower *triangularis* Zone (Klapper et al., 1994). This decision was ratified (January 1993) by the International Commission on Stratigraphy (ICS) and the International Union of Geological Sciences (IUGS), with a specific level in a section at Coumiac, in the Montagne Noire of southern France, designated as the Global Boundary Stratotype Section and Point (GSSP). This level coincides with the base of bed 32a in the Upper Coumiac Quarry. Klapper et al. (1994, imprint December 1993, p. 437) suggested using the flood occurrence of *Palmatolepis triangularis* to "the virtual exclusion of other species of the genus, stratigraphically *above* the fauna dominated by the characteristic upper Frasnian species" so as to exclude "the extremely rare occurrences of *Palmatolepis triangularis* a few centimetres lower, within the uppermost (Frasnian) conodont zone". "The introduction of *Pa. praetriangularis* Ziegler & Sandberg, 1988 (in Sandberg et al., 1988), a species closely related to *Palmatolepis triangularis*, made the taxonomy complicated because some authors treated it as a discrete species, whereas others regarded it as a junior synonym of *Pa. triangularis*" (Klapper, 2007b, p. 67).

According to Klapper et al. (2004, p. 383) and Klapper (2007b), *Palmatolepis praetriangularis* is a junior synonym of *Pa. ultima* Ziegler, 1958 because the two are within the range of intraspecific variation. The latter name had been largely overlooked because the important monograph of Ziegler (1962) had regarded *Pa. ultima* as a junior synonym of *Pa. triangularis.*

Palmatolepis ultima (= *Pa. praetriangularis*) occurs first in the uppermost Frasnian Zone 13c (Girard et al., 2005) and extends into the lowermost Famennian. It is the only species of *Palmatolepis* to have survived the biological crisis at the end of the Frasnian. Klapper et al. (2004) considered *Pa. ultima* to be a discrete species and thus restricted the taxonomic concept of *Pa. triangularis* in accord with the original diagnosis of the holotype of Sannemann (1955). This revision was in contrast not only to Ziegler (1962) but also to Schülke (1995), who had included both *Pa. ultima* and *Pa. praetriangularis* as synonyms of *Pa. triangularis*. Because the latter species as thus restricted enters slightly higher in the Lower *triangularis* Zone, a need for adjustment of the definition of the base of that zone became apparent.

Klapper et al. (2004) proposed defining the base of the Lower *triangularis* Zone by the flood occurrence of *Pa. ultima* immediately above the Fr-Fm extinction event. Klapper (2007b) also drew attention to the potentially important, stratigraphically lowest occurrence of *Pa. subperlobata* at the base of the Lower *triangularis* Zone. Spalletta et al. (2017), building on Klapper et al. (2004) and Klapper (2007b), proposed a *Pa. subperlobata* Zone for the discrete, brief interval between the first occurrence of *Pa. subperlobata* and the entry of *Pa. triangularis* (sensu Klapper et al., 2004). It equates with the lower part of the Lower *triangularis* Zone of Ziegler & Sandberg (1990).

For the Famennian sequence of the Carnic Alps we use the zonation proposed by Spalletta et al. (2017), basically similar and correlatable to the Famennian part of the Upper Devonian "Standard Conodont Zonation" proposed by Ziegler & Sandberg (1990). Spalletta et al. (2017) made modifications of the Ziegler and Sandberg zonation with the aim of defining each biozone by the first appearance of species that are widely distributed and well known by Famennian conodont researchers, eliminating a few zones based on last appearance data (LADs). All biozones are named after the species whose FAD defines its lower boundary. Most the same zonal markers of Ziegler & Sandberg (1990) are used primarily for maintaining stability after about 50 years of investigations. The revised biozonation eliminates the group-zones, Early/Lower, Middle, Late/Upper, etcetera.

Analysis of the PRA and FRKT sections permits recognition in the Carnic Alps of the sequence of conodont bioevents discriminated by Klapper and co-authors cited above (and in the references) in the Montagne Noire, Germany, North America and Australia as well as high-precision identification of the Fr-Fm boundary in these regions. Biostratigraphic notes are given below. Complete conodont numerical data for the two sections are presented on Tables 1, 2.

Frasnian Zone 12 - The zone has been aligned with the upper part of the Lower *rhenana* Zone and the lower interval of the Upper *rhenana* Zone of Ziegler & Sandberg (1990). Co-occurrence of *Ancyrodella ioides* Ziegler, 1958 and *Pa. orlovi* Khrustchevae & Kuz'min, 1996 entering at and near the base of Zone 12, respectively in the Composite Standard (Klapper et al., 1995; Klapper, 1997, 2007a) allowed assigning the base of the PRA section (PRA0-PRA1) to Zone 12. The zonal marker *Pa. winchelli* (Stauffer, 1938) occurs higher in the subsequent biozone.

Pramosio A section (PRA)

Conodont zones	FZ 12		FZ 13a					FZ 13b													FZ 13c			*Pa. subperl.*		*Pa. triang.*	
Samples	PRA0	1	2	3	4	4A	5	5A	5B	5C	5D	6	6A	6AA	6BA	6BB	6BC	6B1A	6B1B	6C	6D	6E	7A	7B	8A	8B
Weights (gr)	1725	2075	1050	1550	1700	2100	2075	1000	2450	1100	200	2050	1660	1125	1025	700	1200	1730	1950	1820	1940	420	2975	4470	2410	2225
Anc. loides	3																									
Anc. hamata	184	6	11	8	4		4		1	2		18	1	1												
Ic. alternatus alternatus	8	28	1	2					5			171	5	1	3	1	10	8	14	11	51	2	62	35		2
Pa. cf. *anzhelae*	1																									
Pa. hassi	11	1	6	5	1																					
Pa. jamieae	18	4																								
Pa. nasuta	1																									
Pa. orlovi	6	2																								
Pa. uyenoi	10			1																						
Po. decorosus	11	1	161	166	19	21	250	393	1703	1597	12	877	60	38	66	33	197	276	75							
Po. lodinensis	1	2			2				11	5	2	4					4	28								
Po. praepolitus	10								47						2											
Po. zinaidae	2			1																						
Ang. amana		1								1		3							1							
Ang. triangularis		1										1														
Po. politus		1							1		1															
Pa. bogartensis			10	4	3		2	33	204	22		54	3	2	2	4	26	40	5	8	60	5				
Ang. asymmetricus				1					2	2		2	2													
Pa. boogaardi				4	3	1	3	25	60	27		17	3			3	15	21			1	2				
Pa. juntianensis				3			2	7	128	116	1	55	2		1	2				2						
Po. brevis				1					1																	
Po. webbi				1	1		8	7	60	10		8	2				11	30	1	11	12	1				
Anc. curvata					1			7	68	18		20	1			2	28	32	3	2	7	2				
Po. aequalis					3			12		2		14				1	2			4	2	1				
Pa. winchelli							4	5	69	15		21		1	1		2	24	1	12	3	2				
Pa. beckeri								1																		
Pa. linguiformis								23	129	44		83	2		1		81	58	1	3	5	1				
Pa. rhenana								7	29	32		16	1				2	19	1							
Pa. klugi									45	18		6														
Pel. planus									2	1							46	20			2		1			
Po. brevilaminus									15	28								10	1	4	13	4	105	121	6	14
Pa. n. sp. A									17								3	3								
Po. cf. *Po. procerus* Klapper, 2007a										4																
Ic. alternatus helmsi												7					1				7	1	3	5	1	1
Po. n. sp. B												22				1			1			1				
Po. maximovae																	2									
Po. cf. *Po. churkini*																		1								
Pa. ultima																				19	34	9	122	120	17	29
Po. macilentus																				2						
Ic. deform. asymmetricus																					2		1			
Ic. alternatus mawsonae																						2	1			
Pa. subperlobata																							14	28	8	3
Po. praecursor																							5	4		
Ic. deformatus deformatus																								1		
Pa. delicatula delicatula																								2	1	
Po. n. sp. E																								1		
Pa. triangularis																									7	5
Po. angustidiscus																									1	
Pa. delicatula platys																										
Pa. perlobata perlobata																										
Pa. protorhomboidea																										
Pa. clarki																										
Pa. lobicornis																										
Pa. minuta minuta																										
Pa. tenuipunctata																										

Tab. 1 - (upper part) Distribution of P_1 conodont elements, Pramosio A section. *Al.* = *Alternognathus*, *Anc.*= *Ancyrodella*, *Ang.* = *Ancyrognathus*, *Br.* = *Branmehla*, *Ic.* = *Icriodus*, *Me.* = *Mehlina*, *Pa.* = *Palmatolepis*, *Pel.* = *Pelekysgnathus*, *Po.* = *Polygnathus*. In red biozonal markers and first presence of species utilized for identifying some biozones in absence of marker.

Pa. delicatula platys				*Pa. minuta minuta*							*Pa.crep*	*Pa.ter.*	*Pa. gl.prima*		*Pa. gl.pect.*		*Pa. rhomb.*		*Pa. gr. gracil.*		*Pa. mar.*	*Pa. mar. utahensis*			*Sc. v. vel.*	*Pa. r. tr.*	*Ps. gra.*	
8C	8C1	8D	9	10	11	11A	11B	12	13	14	15	16	17	18	19	20	21	22	23	24	25	26	27	28	29	30	31	Tot.
1430	700	1065	2925	3875	3250	2120	1925	3575	1500	2450	2200	2150	2350	4800	2300	1900	2300	2650	1600	2250	1800	3850	2610	1190	2475	1680	2425	
																												3
																												240
3	1	1	11	10	4	7	25	53	89	33	130	77		3	3	7												877
																												1
																												24
																												22
																												1
																												8
																												11
																												5956
																												59
																												59
																												3
																												6
																												2
																												3
																												487
																												9
																												185
																												319
																												2
																												163
																												191
																												41
																												160
																												1
																												431
																												107
																												69
					1		4	2	12	7	2	1	4															105
6	2		6	6	10	10	47	4	33	16	38																	499
																												23
																												4
							1	9	8	7	18	3																72
																												25
																												2
																												1
9	2	2	11																									374
																												2
																												3
2							1	2	9	7	13	8			1													46
3	1	2		2		2	48	68	20	18	7	10	1	3	3	4	20	20	5	1							291
	1	1			1			87	4	12		1																116
							2	2	2	2																		9
3	3	3		4	3	3	13	19	4	10	4																	72
				1				7	6																			15
22	7	4	16	29	28	10	15	54	40	58	39																	334
2				1	1	1						1																7
1	2			3	5	2	16	20	2	2	6																	59
3	1		1		1							6			1													13
3	2	1	3	3	10	1	16	12	3	8	3																	65
			3	9	15	3	13	28	4	15	13																	103
				2	1		2	9	3	5	9		2	4	3		1											41
				1		1	1	1		4	2	6	23	24	14	19	15	16	11	12	3	1		1	3	3	2	163
				3			1					10	13	36	8	2												73

Tab. 1 - (upper part) Continuation.

Pramosio A section (PRA)

Conodont zones	FZ 12		FZ 13a					FZ 13b													FZ 13c			*Pa. subperl.*		*Pa. triang.*	
Samples	PRA0	1	2	3	4	4A	5	5A	5B	5C	5D	6	6A	6AA	6BA	6BB	6BC	6B1A	6B1B	6C	6D	6E	7A	7B	8A	8B
Weights (gr)	1725	2075	1050	1550	1700	2100	2075	1000	2450	1100	200	2050	1660	1125	1025	700	1200	1730	1950	1820	1940	420	2975	4470	2410	2225
Po. eoglaber																										
Po. n. sp. D																										
Pa. spathula																										
Ang. sinelaminus																										
Ic. cornutus																										
Pa. regularis																										
Pa. robusta																										
Ic. iowaensis iowaensis																										
Pa. crepida																										
Po. procerus																										
Pa. quadrantinodosalobata																										
Pa. termini																										
Pa. glabra prima																										
Pa. minuta loba																										
Po. semicostatus trend 1																										
Po. semicostatus trend 8																										
Pa. glabra ssp.																										
Pa. perlobata ssp.																										
Po. glaber glaber																										
Po. nodocostatus																										
Ic. olivierii																										
Pa. glabra glabra																										
Pa. glabra pectinata																										
Pa. glabra ssp. juv.																										
Pa. poolei																										
Pa. rhomboidea																										
Pa. glabra acuta																										
Pa. klapperi																										
Pa. inflexa																										
Pa. perlobata schindewolfi																										
Pa. marginifera marginifera																										
Pa. minuta ssp. juv.																										
Po. glaber bilobatus																										
Br. werneri																										
Pa. gracilis gracilis																										
Pa. marginifera utahensis																										
Al. beulensis																										
Pa. glabra lepta																										
Pa. rugosa trachythera																										
Al. regularis																										
Me. strigosa																										
Pa. gracilis sigmoidalis																										
Pa. minuta schleizia																										
Po. granulosus																										
Po. marginvolutus																										
Anc. sp.									12	5							8	19	1		1					
Anc. sp. juv.	66								5	7					3				1							
Ang. sp.																					1					
Ang. sp. juv.												1														
Ic. sp.																					2			1		
Pa. sp.	48	13	47	27	1	2	28	160	871	496	1	264	18	6	15	10	650	783	8	31	75	14	170	137	18	9
Pa. sp. juv.	249	12	38	101	20	6	25	357	1825	674	8	229	22	1	23	6	424	394	15	16	25	10	292	235	24	11
Po. sp.	4		8	14	6		5	152	59	323		90	9		3	3	172	164	3	3	13	2	16	6		3
Po. sp. juv.																				2			2			
Tot.	633	72	282	339	64	30	331	1189	5369	3449	25	1983	131	50	120	66	1684	1930	132	130	316	59	794	696	83	77

Tab. 1 - (lower part) Distribution of P_1 conodont elements, Pramosio A section. *Al.* = *Alternognathus*, *Anc.*= *Ancyrodella*, *Ang.* = *Ancyrognathus*, *Br.* = *Branmehla*, *Ic.* = *Icriodus*, *Me.* = *Mehlina*, *Pa.* = *Palmatolepis*, *Pel.* = *Pelekysgnathus*, *Po.* = *Polygnathus*. In red biozonal markers and first presence of species utilized for identifying some biozones in absence of marker.

Pa. delicatula platys				*Pa. minuta minuta*							*Pa.crep*	*Pa.ter.*	*Pa. gl.prima*		*Pa. gl.pect.*		*Pa. rhomb.*		*Pa. gr. gracil.*		*Pa. mar.*	*Pa. mar. utahensis*			*Sc. v. vel.*	*Pa. r. tr.*	*Ps. gra.*	
8C	8C1	8D	9	10	11	11A	11B	12	13	14	15	16	17	18	19	20	21	22	23	24	25	26	27	28	29	30	31	Tot.
1430	700	1065	2925	3875	3250	2120	1925	3575	1500	2450	2200	2150	2350	4800	2300	1900	2300	2650	1600	2250	1800	3850	2610	1190	2475	1680	2425	
				1				2		4	6																	13
				1																								1
					1		11		10	4	3																	29
								2																				2
								1	10	14	4	5	5	2	2													43
									1		4	5	3		11													24
										3																		3
											1					1												2
											1	1	2	25	4		1	2										36
											10	2	36	4														52
												5	1	3	3	16	15											43
												3	4	4														11
													1	1	14	17	18	13		7								71
													1															1
														7	2		1	4	1	3								18
														48	9		1											58
																11				15		8			1		10	45
																1												1
																1	25	6	1	33	3	23						92
																6	12	4		3	1					1		27
																	138											138
																	3			3								6
																	11	15	32	26	2	7	1	1				95
																	19	4	10	17	18	25	1				8	102
																	1	3										4
																	1			4								5
																		2		2								4
																			4									4
																				1								1
																				5		5			1		10	21
																					10	36						46
																					2							2
																					2			1				3
																						5	1		1	5	8	20
																						5			1	1	6	13
																						2						2
																									2		6	8
																									1		3	4
																										1	1	2
																											2	2
																											1	1
																											1	1
																											7	7
																											4	4
																											1	1
																												46
																												82
																												1
																												1
								2	20	6	22	35			1		6											95
47	5		27	12	24	28	64	154	175	138	60	38	15	10	28	7	36		1	13	2	1			3	4	2	4796
14	5	5	37	23	27	25	59	177	250	302	93	49	15	12		14	9						1					6159
3	1			2		6	4	17		3	7	8	15	14	1	2		9		5	1				1			1157
								6	8	17	6	2	14														2	59
121	33	19	115	113	132	99	343	738	713	695	501	276	155	200	108	108	333	98	65	150	44	118	4	3	14	15	74	25421

Tab. 1 - (lower part) Continuation.

Conodont biodiversity of Zone 12 is relatively high due to the presence of several species of *Palmatolepis, Ancyrodella*, *Polygnathus* and *Icriodus* including *Palmatolepis anzhelae* Khrustchevae & Kuz'min, 1996, *Pa. hassi* Müller & Müller, 1957*, Pa. jamieae* Ziegler & Sandberg, 1990, *Pa. nasuta* Müller, 1956, *Pa. orlovi*, *Pa. uyenoi* Klapper, 2007 (in Klapper, 2007a), *Ancyrodella hamata* Ulrich & Bassler, 1926*, Anc. ioides*, *Polygnathus decorosus* Stauffer, 1938, *Po. lodinensis* Pölsler, 1969, *Po. praepolitus* Kononova, Alekseev, Barskov & Reimers, 1996*, Po. zinaidae* Kononova, Alekseev, Barskov & Reimers, 1996, *Po. politus* Ovnatanova, 1969*, Icriodus alternatus alternatus* Branson & Mehl, 1934 and a few elements of *Ancyrognathus amana* Müller & Müller, 1957 and *Ang. triangularis* Youngquist, 1945. In the section, *Palmatolepis nasuta* disappears within the biozone. *Palmatolepis jamieae, Pa. orlovi* and *Ancyrodella ioides* became extinct within the biozone (Tab. 1).

Frasnian Zone 13a - The zone has been aligned with the upper part of the Upper *rhenana* Zone of Ziegler & Sandberg (1990). In the PRA section the entry of the marker *Palmatolepis bogartensis* (Stauffer, 1938) (Klapper & Kirchgasser, 2016) has been utilized for defining the lower limit of the zone (PRA2). In the PRA section the biozone lasts up to sample PRA5 (Tab. 1). The presence of the marker in the lowest sample of the FRKT section allows referring its basal part (FRKT2-FRKT18) to Zone 13a (Tab. 2). *Palmatolepis boogaardi* Klapper & Foster, 1993*, Pa. juntianensis* Han, 1987*, Pa. nicolli* Klapper, 2007a*, Pa. rhenana* Bischoff, 1956, whose FADs are within the biozone, co-occur with *Pa. hassi*, *Pa. ederi* Ziegler & Sandberg, 1990, *Pa. uyenoi*, *Pa. winchelli*, *Ancyrodella curvata* (Branson & Mehl, 1934), *Ancyrognathus asymmetricus* (Ulrich & Bassler, 1926), *Pelekysgnathus planus* Sannemann, 1955, *Polygnathus aequalis* Klapper & Lane, 1985, *Po. brevis* Miller & Youngquist, 1947, *Po. krestovnicovi* Ovnatanova, 1969 and *Po. webbi* Stauffer, 1938. Only one sample has produced *Palmatolepis nicolli* (FRKT13). The following species range through the biozone: *Ancyrodella hamata*, *Polygnathus decorosus*, *Po. lodinensis*, *Po. zinaidae* and *Icriodus alternatus alternatus*. *Polygnathus decorosus* appears as a flood occurrence starting at the base of Zone 13a and persisting to the top of Zone 13b where the species becomes extinct. *Palmatolepis hassi*, whose LAD is at the top the biozone, and *Pa. uyenoi* become extinct. The last was described by Klapper (2007a) from the Canning Basin in Western Australia where it ranges through Frasnian zones 11 and 12.

Frasnian Zone 13b - This biozone, aligned with the *linguiformis* Zone of Ziegler & Sandberg (1990), is defined by the FAD of *Palmatolepis linguiformis* Müller, 1956 (Sandberg et al., 1988). Zone 13b should coincide with the total range of *Pa. linguiformis*. Intervals PRA5A-PRA6B1B of the PRA section and FRKT19-FRKT21D of the FRKT section are referred to this zone, noteworthy for its high biodiversity and abundance (Tabs 1, 2). *Palmatolepis linguiformis* co-occurs with *Pa. klugi* Klapper, 2007 (in Klapper, 2007a), *Pa. beckeri* Klapper, 2007 (in Klapper, 2007a), *Polygnathus brevilaminus* Branson & Mehl, 1934, *Po.* cf. *Po. churkini* Savage & Funai, 1980, *Po. maximovae* Ovnatanova & Kononova, 1996, *Po*. cf. *Po. procerus* Sannemann, 1955 sensu Schülke, 1999 (in Klapper, 2007a, fig. 7.4), *Icriodus alternatus helmsi* Sandberg & Dreesen, 1984 and *Ic. deformatus deformatus* Han, 1987. The last enters during this zone. We have identified and listed the subspecies of *Icriodus alternatus* (Tabs 1, 2, S5, S6), having they slightly different stratigraphic ranges in the studied sections, even though by a biologic point of view they could be intraspecific variations as suggested by Girard et al. (2022). In the Canning Basin, Klapper (2007a) found *Palmatolepis klugi* in Zone 13b and *Pa. beckeri* was found in the upper part of Zone 13a and at the base of Zone 13b.

Species persisting from the previous biozone include *Palmatolepis bogartensis* (with its three morphotypes) as well as *Pa. boogaardi*, *Pa. juntianensis*, *Pa. rhenana*, *Pa. winchelli*, *Polygnathus aequalis*, *Po. brevis*, *Po. decorosus*, *Po. krestovnicovi*, *Po. lodinensis*, *Po. politus*, *Po. praepolitus*, *Po. webbi*, *Ancyrodella curvata*, *Anc. hamata*, *Ancyrognathus amana*, *Ang. asymmetricus*, *Ang. triangularis* and *Icriodus alternatus alternatus. Ancyrognathus asymmetricus*, whose LAD is in Zone 13c, disappears in our sections within the zone. *Ancyrodella hamata*, *Ancyrognathus triangularis*, *Palmatolepis beckeri*, *Pa. klugi*, *Polygnathus brevis*, *Po.* cf. *Po. churkini*, *Po. lodinensis*, *Po. maximovae*, *Po. politus* and *Po. praepolitus* become extinct within the zone. *Po. decorosus* and *Ancyrognathus amana* persist to the end of the zone.

Frasnian Zone 13c - This zone equates with the Late *linguiformis* Zone of Sandberg et al. (2002). The first occurrence datum (FAD) of *Palmatolepis ultima* falls close to the base of this zone (Klapper, 2007b). We have used its entry as an approximation for identifying the lower limit of the biozone. The interval PRA6C-PRA6E of the PRA section and sample FRKT21E of the FRKT section have been referred to the biozone (Tabs 1, 2).

Palmatolepis ultima co-occurs with *Pa. bogartensis* that, in the second half of the zone, becomes dominant compared with elements of *Pa. winchelli* and very rare elements of *Pa. rhenana.* In both sections, a few elements of *Palmatolepis linguiformis*, *Pa. juntianensis*, *Pa. boogaardi* and *Ancyrodella curvata* still occur in association with elements of *Pelekysgnathus planus*, *Polygnathus aequalis*, *Po. brevilaminus*, *Po. krestovnikovi*, *Po.* cf. *Po. morgani* Klapper & Lane, 1985, *Po. webbi*, *Icriodus alternatus alternatus*, *Ic. alternatus helmsi. Icriodus deformatus asymmetricus* Ji, 1989 and *Ic. alternatus mawsonae* Yazdi, 1999 enter within the biozone. *Mehlina gradata* Youngquist, 1945, *Polygnathus angustidiscus* Branson & Mehl, 1934 and *Po. macilentus* Kuz'min, 1993 (in Obukhovskaya & Kuz'min, 1993) occur in our sections. *Icriodus deformatus asymmetricus* and *Ic. alternatus mawsonae* have been reported previously only from the Famennian. *Palmatolepis bogartensis*, *Pa. boogaardi*, *Pa. juntianensis*, *Pa. linguiformis*, *Pa. rhenana*, *Pa. winchelli*, *Ancyrodella curvata*, *Polygnathus aequalis*, *Po. krestovnikovi*, *Po. macilentus*, *Po.* cf. *Po. morgani* and *Po. webbi* become extinct within this biozone.

Palmatolepis subperlobata Zone - First biozone of the Famennian. Spalletta et al. (2017) used the first

Freikofel T section (FRKT)

Conodont zones	FZ 13a				FZ 13b			FZ13c	*Pa. subperlobata*			*Pa. triang.*		*Pa.d.pl.*	*Pa. minuta minuta*				*Pa. crep*	*Pa. termini*		
Samples	FRKT2	5	13	18	19	20	21D	21E	21F	22	23	25	28	41	50	55	72	87	100	119	132	
Weights (gr)	1719	1983	1519	1322	2695	2020	6190	4505	1525	2120	988	1340	1250	1231	1628	1092	1755	1057	773	1007	1290	Tot.
Pa. bogartensis	12	16	3	2	5	8	29	12														87
Anc. hamata	1	18		1																		20
Pa. boogaardi	1	22	1	3	1	5	14															47
Pa. ederi	1																					1
Pa. rhenana	2			1	1	2	8	1														15
Po. decorosus	58	620	117	50	26	106	98															1075
Po. lodinensis	1			4	4	9	10	1														29
Po. webbi	1			1	3	3	28															36
Anc. curvata		10				2	14	4														30
Ang. asymmetricus		2	1				2															5
Pa. juntianensis		2	2	1		3																8
Pa. winchelli		1				2	2	3														8
Po. n. sp. A		2																				2
Pa. nicolli			1																			1
Po. n. sp. C			7																			7
Ic. alternatus alternatus				6		1	10	13	6		1	7	4	14	144	42	488	18	75			829
Pe. planus				1					1					2	6	1	4	4				19
Po. aequalis				3				2														5
Po. krestovnikovi				1	1			1														3
Pa. linguiformis					2	3	38	2														45
Po. brevilaminus					3		31	25	5	7	5	19	5	35	54	29	22		1			241
Po. praepolitus						1	2															3
Ic. alternatus helmsi							4	7		1	1	4			8	7						32
Ic. deformatus deformatus							1	3									4					8
Pa. n. sp. A							4															4
Po. brevis							1															1
Ic. alternatus mawsonae								1		1		2	1	2	15	7	43		16			88
Me. gradata								2		6			1									9
Pa. ultima								55	15	18	15	28	22	47								200
Po. angustidiscus								10	3	2	1	3	1									20
Po. cf. *Po. morgani*								2														2
Pa. subperlobata									8	3	6	15	3	16	27	18	12		8		1	117
Po. praecursor									1	1					3	1	1					7
Pa. delicatula delicatula											2	4	4	10	4	19						43
Pa. n. sp. B												2										2
Pa. protorhomboidea												3		19	4	16						42
Pa. triangularis												2	2	4	27	22	35					92
Pa. clarki														1	10	26	58					95
Pa. delicatula platys														19	4	16						39
Ic. cornutus															2		25	1	3	4	3	38
Pa. lobicornis															2	11	28	4				45
Pa. minuta minuta															1	9	3	6	14	4	11	48
Pa. spathula															2	19						21
Po. n. sp. E															1	2						3
Pa. sandbergi																7	2	1	3			13
Pa. regularis																	2	2	5	1	2	12
Pa. robusta																	1					1
Po. eoglaber																	3	3	4		5	15
Po. procerus																	11			82	299	392
Pa. tenuipunctata																		4	27	5	11	47
Pa. crepida																			1			1
Pa. quadrantinodosalobata																			10	2	1	13
Pa. termini																				4	3	7
Ic. multicostatus lateralis																					2	2
Me. strigosa																					1	1
Pa. perlobata perlobata																					1	1
Anc. sp.	1	12																				13

Tab. 2 - Numerical distribution of P_1 conodont elements in the Freikofel T section. *Anc.* = *Ancyrodella*, *Ang.* = *Ancyrognathus*, *Ic.* = *Icriodus*, *Me.* = *Mehlina*, *Pa.* = *Palmatolepis*, *Pel.* = *Pelekysgnathus*, *Po.* = *Polygnathus*. In red biozonal markers and first presence of species utilized for identifying some biozones in absence of marker.

Conodont zones	FZ 13a				FZ 13b			FZ13c	*Pa. subperlobata*			*Pa. triang.*		*Pa.d.pl.*	*Pa. minuta minuta*				*Pa. crep*	*Pa. termini*		
Samples	FRKT2	5	13	18	19	20	21D	21E	21F	22	23	25	28	41	50	55	72	87	100	119	132	
Weights (gr)	1719	1983	1519	1322	2695	2020	6190	4505	1525	2120	988	1340	1250	1231	1628	1092	1755	1057	773	1007	1290	Tot.
Anc. sp. juv.		4	1																			5
Ic. sp.												4		4	50	9	55		19	3	1	145
Ic. sp. juv.										1												1
Me. sp.															1							1
Pa. sp.	18	19	3	1	11	7	47	31	23	35	8	62	13	145	229	128	162	11	13	12	15	993
Pa. sp. juv.	25	109	32	10	18	37	85	76	20	25		27	18	196	428	833	446	45	62	7	22	2521
Po. sp.		5	20	5	4	7	3	2		3	2	3	4		6	12	8		10	12	110	216
Po. sp. juv.															5	15	14	1		23	115	173
Tot.	121	842	188	90	79	196	431	253	82	103	41	185	78	514	1033	1249	1427	100	271	159	603	8045

Tab. 2 - Continuation.

appearance of *Palmatolepis subperlobata*, coinciding with the flood of *Palmatolepis ultima* immediately above the Frasnian extinction, for defining the base of the zone following Klapper et al. (2004) and Klapper (2007b). Intervals PRA7A-PRA7B in the PRA section and FRKT21F-FRKT23 in the FRKT section are referred to this biozone (Tabs 1, 2).

In the Carnic Alps immediately above the drastic drop in biodiversity, coincident with extinction of all Frasnian species of *Ancyrodella, Ancyrognathus* and *Palmatolepis*, is the flood occurrence of *Pa. ultima* and the entry of *Pa. subperlobata* marking the base of the Famennian (Fig. 9). P_1 elements identified as *Palmatolepis ultima* double in number and juvenile P_1 elements of *Palmatolepis* quadruple their abundance in comparison with the preceding sample (Tabs 1, 2, S5, S6). In the FRKT section, increase in abundance of *Palmatolepis ultima* is less apparent, possibly masked by reduced sedimentation during Frasnian Zone 13c. *Icriodus alternatus* (with subspecies *alternatus*, *helmsi* and *mawsonae*), *Ic. deformatus* (with subspecies *deformatus* and *asymmetricus*), *Polygnathus angustidiscus*, *Po. brevilaminus*, *Pelekysgnathus planus*, *Mehlina gradata* and *Palmatolepis ultima*, the last representative of Frasnian species of the genus *Palmatolepis*, survived the biological extinction at the top of the Frasnian, extending their ranges into the lower Famennian. *Palmatolepis delicatula delicatula* Branson & Mehl, 1934 as reported globally and *Polygnathus praecursor* Matyja, 1993 enter the biozone.

Palmatolepis triangularis Zone - The lower limit of the *Palmatolepis triangularis* Zone has been identified in both sections by the entry of *Pa. triangularis* sensu Klapper et al. (2004) and Klapper (2007b) (Fig. 9). The intervals PRA8A-PRA8B of the PRA section and FRKT25-FRKT28 of the FRKT section are referred to this biozone (Tabs 1, 2). *Palmatolepis delicatula delicatula*, *Pa. protorhomboidea* Sandberg & Ziegler, 1973, *Pa. subperlobata*, *Pa. ultima*, *Polygnathus angustidiscus*, *Po. brevilaminus*, *Mehlina gradata* (this last disappears within the biozone), *Icriodus alternatus* (with subspecies *alternatus*, *helmsi* and *mawsonae*) are constituents of the conodont faunas. *Palmatolepis protorhomboidea* enters the biozone globally; Ziegler & Sandberg (1990) report its entry in the upper part of their Lower *triangularis* Zone.

Palmatolepis delicatula platys Zone - The lower limit of the zone has been identified by the entry of the biozonal marker *Palmatolepis delicatula platys* Ziegler & Sandberg, 1990. The interval PRA8C-PRA9 of the PRA section and sample FRKT41 of the FRKT section have been assigned to this biozone (Tabs 1, 2). *Palmatolepis clarki* Ziegler, 1962 enters within the biozone globally. Representatives of *Palmatolepis delicatula delicatula*, *Pa. protorhomboidea*, *Pa. triangularis*, *Pa. subperlobata*, *Pa. ultima* (becoming extinct at the top of the biozone), *Polygnathus angustidiscus*, *Po. brevilaminus*, *Po. praecursor*, *Pelekysgnathus planus* and *Icriodus alternatus* (with subspecies *alternatus* and *mawsonae*) make up the association.

Palmatolepis minuta minuta Zone - The lower limit is identified by the entry of *Palmatolepis minuta minuta* Branson & Mehl, 1934. The intervals PRA10-PRA14 of the PRA section and FRKT50-FRKT87 of the FRKT section are referred to this biozone (Tabs 1, 2). Several species whose first appearances are within the biozone, testify to increasing biodiversity and recovery. *Palmatolepis tenuipunctata* Sannemann, 1955 and *Polygnathus eoglaber* Ji & Ziegler, 1993 enter at the base of the biozone as well as *Pa. lobicornis* Schülke, 1995. Making their first appearance within this biozone are *Palmatolepis perlobata perlobata* Ulrich & Bassler, 1926, *Pa. regularis* Cooper, 1931, *Pa. robusta* Schülke, 1995 (present only in this biozone in both sections), *Pa. sandbergi* Ji & Ziegler, 1993, *Pa. spathula* Schülke, 1995, *Polygnathus procerus* Sannemann, 1955 and *Icriodus cornutus* Sannemann, 1955.

Palmatolepis lobicornis, described by Schülke (1995) from the Lower and Middle *crepida* Zone (*Palmatolepis crepida-Palmatolepis termini* zones) and reported by Klapper et al. (2004) from the Lower *crepida* Zone (*Palmatolepis crepida* Zone) to possibly the Lower *marginifera* Zone (*Palmatolepis marginifera marginifera* Zone), has been found in our sections from the *Palmatolepis minuta minuta* Zone up to the *Palmatolepis rhomboidea* Zone; this range has been cited in Spalletta et al. (2017) as unpublished datum.

It is noteworthy that we identified *Polygnathus procerus* following the original diagnosis of Sannemann (1955) who described the species from levels referred to toIIα (*Palmatolepis crepida-Palmatolepis termini* zones). In our opinion the elements figured by Schülke (1999, Pl. 13, figs 12-18) do not fit the diagnosis of the species. *Palmatolepis clarki, Pa. delicatula delicatula, Pa. delicatula platys, Pa. protorhomboidea, Pa. subperlobata, Pa. triangularis, Polygnathus angustidiscus, Po.*

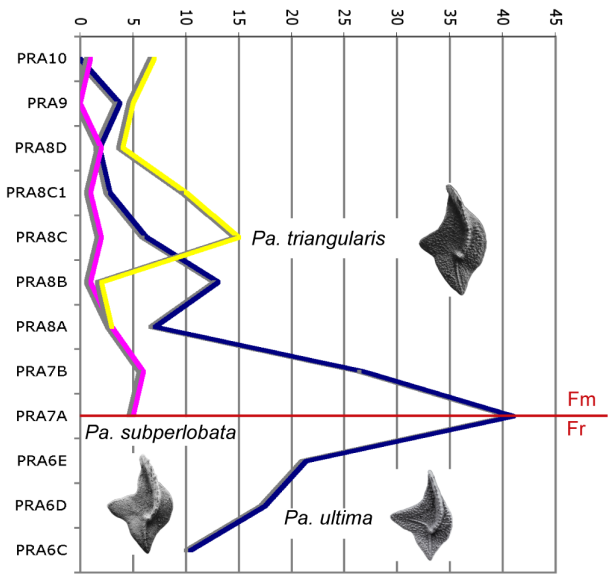

Fig. 9 - Vertical distribution and abundance of *Palmatolepis ultima*, *Pa. subperlobata* and *Pa. triangularis* across the Frasnian-Famennian boundary in Pramosio A section. Numbers across the top of the figure are quantities of P_1 elements that could be identified at species-level per kg of rock (Tab. S5).

brevilaminus, Po. praecursor, Pelekysgathus planus and *Icriodus alternatus* (with subspecies *alternatus, helmsi* and *mawsonae*) co-occur. *Ancyrognathus sinelaminus* Branson & Mehl, 1934 is known only in the PRA section. *Icriodus deformatus deformatus* became extinct at the top of this zone.

Palmatolepis crepida Zone - The lower limit is defined by the entry of *Palmatolepis crepida* Sannemann, 1955. Samples PRA15 of the PRA section and FRKT100 of the FRKT section are referred to this zone (Tabs 1, 2). *Palmatolepis quadrantinodosalobata* Sannemann, 1955 first enters, globally, in this biozone. *Icriodus iowaensis iowaensis* Youngquist & Peterson, 1947 first occurs in the PRA section. *Palmatolepis lobicornis*, *Pa. minuta minuta*, *Pa. regularis*, *Pa. subperlobata*, *Pa. tenuipunctata*, *Polygnathus eoglaber*, *Po. procerus*, *Pelekysgnathus planus*, *Icriodus alternatus* (with subspecies *alternatus*, *helmsi* and *mawsonae*) and *Icriodus cornutus*, range through the biozone. *Palmatolepis protorhomboidea*, *Pa. spathula*, *Pa. triangularis* and *Polygnathus brevilaminus* disappear in our sections within the biozone. *Palmatolepis clarki*, *Pa. delicatula delicatula*, *Pa. delicatula platys* and *Pa. sandbergi* became extinct within the biozone. Ziegler & Sandberg (1990) reported the range of *Palmatolepis delicatula platys* and *Pa. clarki* as ending in the Upper *triangularis* Zone (*Palmatolepis minuta minuta* Zone of Spalletta et al., 2017). Here we extend their ranges to the *Palmatolepis crepida* Zone, these data have been cited in Spalletta et al. (2017) as unpublished.

Palmatolepis termini Zone - The lower limit is defined by the entry of *Palmatolepis termini* Sannemann, 1955. Sample PRA16 of the PRA section and the interval FRKT119-FRKT132 of the FRKT section are referred to this zone (Tabs 1, 2). *Icriodus multicostatus lateralis* Ji & Ziegler, 1993 and *Mehlina strigosa* (Branson & Mehl, 1934) enter within the biozone. The first appearance datum for the last species was reported stratigraphically higher by Ziegler & Sandberg (1984) within the Lower *marginifera* Zone. The datum of the range extension of *Mehlina strigosa* has been cited in Spalletta et al. (2017) as unpublished. *Palmatolepis crepida*, *Pa. minuta minuta*, *Pa. perlobata perlobata*, *Pa. quadrantinodosalobata*, *Pa. regularis*, *Pa. subperlobata*, *Pa. tenuipunctata*, *Polygnathus procerus*, *Pelekysgnathus planus*, *Icriodus alternatus* (with subspecies *alternatus* and *mawsonae*) and *Ic. cornutus* co-occur. In our sections, the last occurrence of *Polygnathus eoglaber* is within this zone. *Polygnathus angustidiscus*, *Po. praecursor* and *Icriodus alternatus helmsi* became extinct within this zone.

Palmatolepis glabra prima Zone - The lower limit is identified by the entry of *Pa. glabra prima* Ziegler & Huddle, 1969. Conodont data reported for the *Palmatolepis glabra prima* to the *Pseudopolygnathus granulosus* zones are only from the PRA section. The interval PRA17-PRA18 has been referred to this biozone (Tab. 1). Data are scarce compared with data derived from the same stratigraphic interval of other sections in the Carnic Alps. *Po. semicostatus* Branson & Mehl, 1934 (morphologic trend 1 and 8 sensu Dreesen & Dusar, 1974) occur in this zone. *Palmatolepis minuta loba* Helms, 1963 has been found in only one sample referred to this biozone. *Palmatolepis crepida*, *Pa. lobicornis*, *Pa. minuta minuta*, *Pa. quadrantinodosalobata* and *Pa. subperlobata* range through the biozone. *Polygnathus procerus* disappeared in our section within this interval. *Palmatolepis termini* and *Pelekysgnathus planus* became extinct, as globally.

Palmatolepis glabra pectinata Zone - The interval PRA19-PRA20 has been referred to this biozone (Tab. 1). In PRA section *Palmatolepis glabra pectinata* Ziegler, 1962 enters in association with *Pa. rhomboidea* Sannemann, 1955 in sample PRA21 referred to the *Palmatolepis rhomboidea* Zone. The *Palmatolepis glabra pectinata* Zone has been discriminated as the interval between the extinction of *Palmatolepis termini* and the entry of *Pa. rhomboidea*. *Polygnathus glaber glaber* Ulrich & Bassler, 1926 and *Po. nodocostatus nodocostatus* Branson & Mehl, 1934 enter within the biozone; *Palmatolepis perlobata perlobata*, *Pa. regularis*, *Pa. tenuipunctata*, *Icriodus alternatus alternatus*, *Ic. cornutus* and *Ic. iowaensis iowaensis* disappeared in our section within this interval. Here we extend the range of *Icriodus alternatus mawsonae* to this biozone where it became extinct.

Palmatolepis rhomboidea Zone - The lower limit of this zone is identified by the entry of *Palmatolepis rhomboidea.* Interval PRA21-PRA22 is referred to the *Palmatolepis rhomboidea* Zone (Tab. 1). *Palmatolepis poolei* Sandberg & Ziegler, 1973, whose global distribution is limited to this biozone, enters at the base and becomes extinct close the top of the zone. *Palmatolepis glabra acuta* Helms, 1963, *Pa. glabra pectinata*, and *Icriodus olivierii* Corradini, 1998 occur within the biozone. *Palmatolepis glabra prima*, *Pa. minuta minuta*, *Pa. subperlobata*, *Polygnathus glaber*

glaber, *Po. nodocostatus nodocostatus*, *Po. semicostatus* (morphologic trend 1) range through the biozone. *Palmatolepis quadrantinodosalobata* and *Polygnathus semicostatus* (morphologic trend 8) disappear within this zone. *Palmatolepis crepida* and *Pa. lobicornis* became extinct.

Palmatolepis gracilis gracilis Zone - The lower limit is defined by the first appearance of *Palmatolepis gracilis gracilis* Branson & Mehl, 1934. The biozone has been identified by the entry of *Palmatolepis quadrantinodosa inflexa* Müller, 1956 (PRA24) because the marker *Palmatolepis gracilis gracilis* has been found only in higher levels and by extinction of *Pa. poolei* occurring in statigraphically lower samples referred to the *Pa. rhomboidea* Zone. The interval PRA23-PRA24 has been referred to this biozone (Tab. 1). *Palmatolepis klapperi* Sandberg & Ziegler, 1973 and *Pa. quadrantinodosa inflexa* are spot records in this zone. *Pa. perlobata schindewolfi* Müller, 1956 occurs within the biozone. *Palmatolepis glabra pectinata*, *Pa. minuta minuta*, *Polygnathus glaber glaber* and *Po. nodocostatus nodocostatus* range through the biozone. In our section, *Palmatolepis glabra acuta*, *Pa. glabra prima*, *Pa. rhomboidea*, *Pa. subperlobata* and *Polygnathus semicostatus* (morphologic trend 1) have their last occurrence within the zone.

Palmatolepis marginifera marginifera Zone - The lower limit is identified by the entry of the zonal marker *Palmatolepis marginifera marginifera* Helms, 1959. Sample PRA25 has been assigned to the zone (Tab. 1). *Palmatolepis glabra pectinata*, *Pa. minuta minuta*, *Polygnathus glaber bilobatus* Ziegler, 1962 (entering the biozone globally), *Polygnathus glaber glaber* and *Po. nodocostatus nodocostatus* are associated species.

Palmatolepis marginifera utahensis Zone - The lower limit is identified by the entry of *Palmatolepis marginifera utahensis* Ziegler & Sandberg, 1984. The interval PRA26-PRA28 has been referred to this zone (Tab. 1). *Palmatolepis gracilis gracilis* and *Branmehla werneri* (Ziegler, 1962) make their appearance within this biozone. *Palmatolepis minuta minuta* and *Pa. perlobata schindewolfi* range through the biozone. *Palmatolepis marginifera marginifera*, *Polygnathus glaber bilobatus* and *Po. glaber glaber* disappear. *Pa. glabra pectinata* became extinct, as globally.

Scaphignathus velifer velifer Zone - In the absence of the marker *Scaphignathus velifer velifer* Helms, 1959, extremely rare in the Southern Alps, its lower limit was identified by the entry of *Alternognathus beulensis* Ziegler & Sandberg, 1984. Sample PRA29 has been assigned to this zone (Tab. 1). *Palmatolepis glabra lepta* Ziegler & Huddle, 1969 occurs first within the biozone; *Pa. gracilis gracilis*, *Pa. minuta minuta*, *Pa. perlobata schindewolfi* and *Branmehla werneri* range through it.

Palmatolepis rugosa trachytera Zone - The entry of *Palmatolepis rugosa trachytera* Ziegler, 1960 defines its lower limit. Sample PRA30 has been assigned to this zone (Tab. 1). *Palmatolepis gracilis gracilis, Pa. minuta minuta, Polygnathus nodocostatus nodocostatus* and *Branmehla werneri* are among the few species associated with *Palmatolepis rugosa trachytera.*

Pseudopolygnathus granulosus Zone - The lower limit is defined by the first appearance of *Pseudopolygnathus granulosus* Ziegler, 1962. In the PRA section, in the absence of the marker, the zone has had to be identified by the entry of *Palmatolepis gracilis sigmoidalis* Ziegler, 1962 though its first appearance is in the middle of the zone. Sample PRA31 has been referred to this zone (Tab. 1). *Palmatolepis minuta schleizia* Helms, 1963, *Polygnathus granulosus* Branson & Mehl, 1934, *Po. marginvolutus* Gedik, 1969 and *Alternognathus regularis* Ziegler & Sandberg, 1984 make their first appearance within this zone. *Palmatolepis glabra lepta*, *Pa. gracilis gracilis*, *Pa. minuta minuta*, *Pa. perlobata schindewolfi*, *Pa. rugosa trachytera*, *Alternognathus beulensis*, *Branmehla werneri* and *Mehlina strigosa* also occur in this interval.

Percentages of Genera

Data obtained from our taxonomic and biostratigraphic investigations have been used for generating the diagram showing variations in genera-percentages along our sections. Variation of the relative percentages of the genera, so called conodont biofacies analysis, has been historically utilized for indirectly approximating variation of seawater depth. This method could be only approximate as species of the same genus can live in different habitats. That was considered by Lüddecke et al. (2017) proposing a conodont biofacies model for groups of species. In Fig. 10 the equivalent biozonal intervals have been aligned for highlighting similarities in the genera-percentage distributions. Conodont species, identified in our sections belong to nine genera (*Alternognathus*, *Ancyrodella*, *Ancyrognathus*, *Branmehla*, *Icriodus*, *Mehlina*, *Palmatolepis*, *Pelekysgnathus* and *Polygnathus*). Variations in frequency of these reflect differences in environmental/ecological preferences. In both sections, the most frequent genera are *Palmatolepis*, *Polygnathus* and *Icriodus.* Following criteria used by Ziegler & Sandberg (1990), samples with high percentages of *Palmatolepis* and *Polygnathus* are assigned to the palmatolepid-polygnathid biofacies. In both sections, most of the samples have been assigned to that biofacies (Tabs S1-S2). In the Frasnian 13a and 13b zones the high frequency of *Polygnathus*, higher than that of palmatolepids, is noteworthy. In both sections the top of Zone 13a displays a significant dominance of *Polygnathus* (PRA4A, PRA5, FRKT13, FRKT19). The decrease in percentage of *Polygnathus* at the top of Zone 13b persisted during the lower Famennian up to the *Palmatolepis crepida* Zone in the FRKT section and to the *Palmatolepis delicatula platys* Zone in PRA section. Peaks of high frequency occur again within the *Palmatolepis delicatula platys* and *Palmatolepis minuta minuta* zones. From the uppermost part of Zone 13b (with the exception for the last sample referred to this biozone in the PRA section), *Palmatolepis* reaches high percentages. The high frequency of *Palmatolepis* continued during Zone 13c, the top of the Frasnian and the lower part of the Famennian (*Palmatolepis subperlobata* to *Palmatolepis minuta minuta* zones) (Fig. 10). *Palmatolepis* increases in both sections within Zone 13c with values averaging

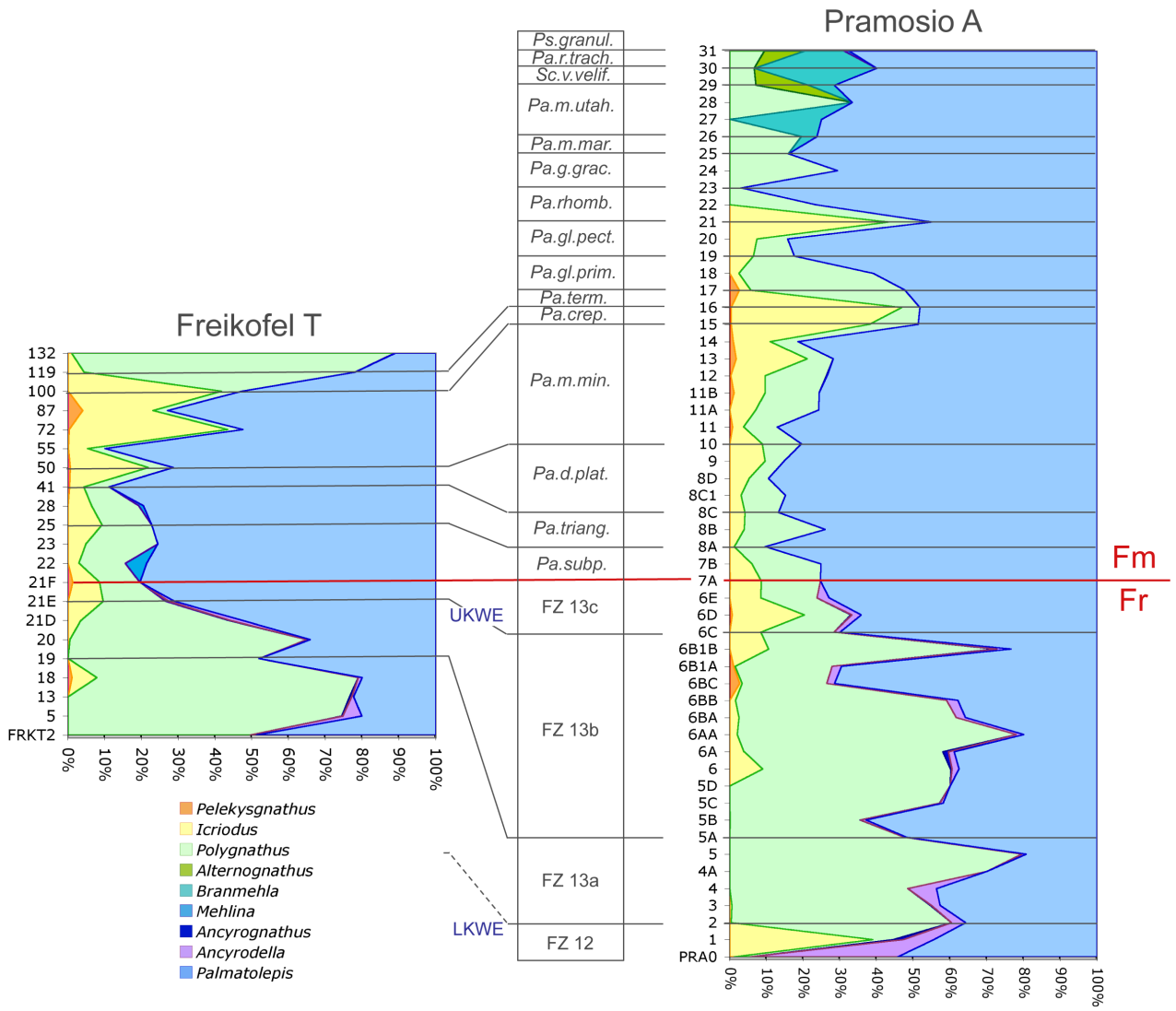

Fig. 10 - Conodont genera-percentage variation up-sequence in the Pramosio A and Freikofel T sections. Equivalent biozonal intervals have been aligned. FZ 12: Frasnian conodont Zone 12; FZ 13a: Frasnian conodont Zone 13a; FZ 13b: Frasnian conodont Zone 13b; FZ 13c: Frasnian conodont Zone 13c; *Pa. subp.*: *Palmatolepis subperlobata* Zone; *Pa. triang.*: *Palmatolepis triangularis* Zone; *Pa. d. plat.*: *Palmatolepis delicatula platys* Zone; *Pa. m. min.*: *Palmatolepis minuta minuta* Zone; *Pa. crep.*: *Palmatolepis crepida* Zone; *Pa. term.*: *Palmatolepis termini* Zone; *Pa. gl. prim.*: *Palmatolepis glabra prima* Zone; *Pa. gl. pect.*: *Palmatolepis glabra pectinata* Zone; *Pa. rhomb.*: *Palmatolepis rhomboidea* Zone; *Pa. g. grac.*: *Palmatolepis gracilis gracilis* Zone; *Pa. m. mar.*: *Palmatolepis marginifera marginifera* Zone; *Pa. m. utah.*: *Palmatolepis marginifera utahensis* Zone; *Sc. v. velif.*: *Scaphignathus velifer velifer* Zone; *Pa. r. trach.*: *Palmatolepis rugosa thachytera* Zone; *Ps. granul.*: *Pseudopolygnathus granulosus* Zone.

70-80%; this persisted during the Famennian *Palmatolepis subperlobata-Palmatolepis minuta minuta* zones, declining significantly in the FRKT section during the *Palmatolepis termini* Zone, and slightly in the PRA section during the interval *Palmatolepis crepida* Zone-basal part of the *Palmatolepis glabra prima* Zone.

Most of the lower Famennian samples have been referred to the palmatolepid biofacies and only two samples to the polygnathid biofacies, at the top of the Frasnian Zone 13a (PRA5) and in the *Palmatolepis termini* Zone (FRKT 132) (Tabs S1-S2).

The shallow-water genus *Icriodus* persists in low percentages to the middle of Zone 13b up to the *Palmatolepis rhomboidea* Zone. It peaks at the top of the Zone 12 (PRA1), in Zone 13c, in the *Palmatolepis minuta minuta* and *Palmatolepis crepida* zones in both sections, and in the *Palmatolepis termini* Zone (PRA16) (Tabs S1-S2). The increase in percentage of *Icriodus* is often associated with an increase of *Palmatolepis* but not of *Polygnathus*, as we would expect for a polygnathid-icriodid biofacies (see Ziegler & Sandberg, 1990). The shallow-water *Pelekysgnathus* co-occurs with *Icriodus*.

Ancyrodella occurs in abundance in PRA1 (Zone 12) but for the remainder of the Frasnian its percentage is low in both sections. No sample could be referred to the polygnathid-ancyrodellid biofacies of Sandberg et al. (1988). The genus *Ancyrognathus* as well as *Mehlina* and *Branmehla* are poorly represented. *Alternognathus* enters only at the top of the PRA section. A few samples have been assigned to mixed biofacies.

Abundance

Conodont abundance, estimated as the total number of P_1 elements per kg of rock, is variable along the two examined sections (Tabs S3-S4). Equivalent biozonal intervals of the graphics of the total abundance and of the three most frequent genera, *Palmatolepis*, *Polygnathus* and *Icriodus* in both sections, have been aligned (Figs 11-12). In the PRA section, the abundance is higher than in the FRKT section. In the former, highest values are reached in the Frasnian interval. Samples exceeding 300 P_1 elements/kg occur in the Frasnian Zone 13b where five of them have values between 1,000 and more than 3,000 P_1 elements/kg (3135 PRA5C). Abundance decreases in the Zone 13c and persists low to the *Palmatolepis minuta minuta* Zone where it starts to increase until reaching an important peak (475 P_1 elements/kg in PRA13) in the upper part of the zone. The relatively high abundance in the lowest Famennian sample (267/kg in PRA7A) referred to the *Palmatolepis subperlobata* Zone is noteworthy (Tabs S3-S4). In the FRKT section, one peak occurs in Zone 13a (Figs 11-12). Zone 13b does not present peaks of abundance as high as those in the PRA section. Abundance decreases at the end of the Frasnian and remains low during the basal part of the Famennian. Maximum abundance in the FRKT section is reached in the *Palmatolepis minuta minuta* Zone and also in the PRA section where the first peak in abundance during the Famennian occurs, but in the FRKT section the increase starts within the *Palmatolepis delicatula platys* Zone, before that in the PRA section, reaching its maximum peak (1144 P_1 elements/kg in FRKT 55) in the *Palmatolepis minuta minuta* Zone. Conodont abundances differ in the two sections even though the percentage ratios of genera up-sequence are very similar for intervals referred to the same conodont zone (see Fig. 10).

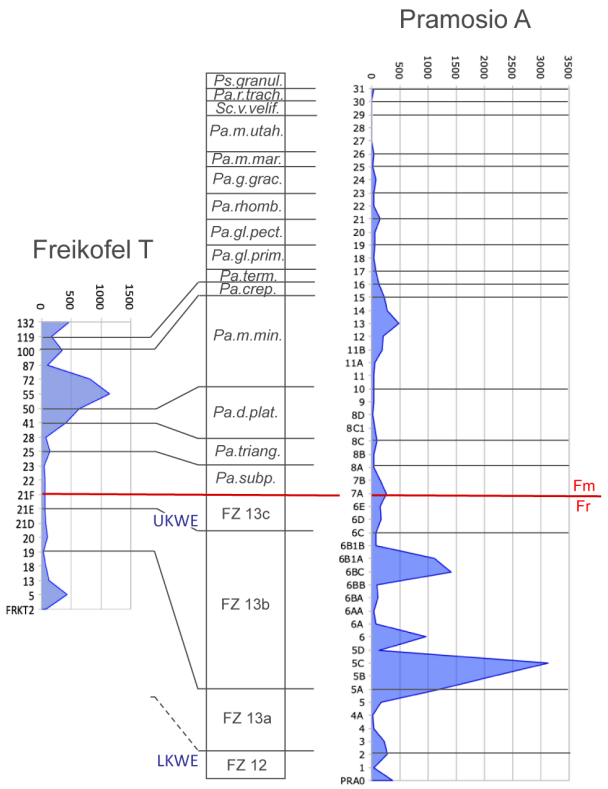

Fig. 11 - Conodont total abundance variation up-sequence in the Pramosio A and Freikofel T sections. Equivalent biozonal intervals have been aligned. For abbreviations of biozone names, see caption of Fig. 10.

Conodont biodiversity and genera abundance

Conodont biodiversity, expressed as total number of species and subspecies occurring per sample, displays fluctuating values up-sequence in the two sections (Tabs S5, S6, lowest line). Conodont generic biodiversity, corresponding to the number of species and subspecies belonging to the same genus, calculated per sample, may or may not be dependent on the genus percentage value and its relative abundance (Tabs S5, S6 third line from the top). In Tabs S5 and S6, for each sample genus biodiversity (left column in bold black) is matched with genus abundance per kg of rock (right column in blue), given by the total of P_1 elements including the elements listed as sp. and sp. juv. (Tabs S3, S4), and with only the P_1 elements identified at specific and subspecific level (central column in green).

In Fig. 13, equivalent biozonal intervals of the diagrams of conodont biodiversity variations up-sequence in the PRA and FRKT sections have been aligned.

Icriodus diversity ranges between one and five taxa co-occurring in the same sample (Tabs S5-S6). It increases within the uppermost Frasnian to basal Famennian and in the *Palmatolepis minuta minuta-Palmatolepis crepida* zones up to the *Palmatolepis termini* Zone in the PRA section, concurrently with increase in relative abundance. Vice versa, the peak of relative abundance at PRA21, in the *Palmatolepis rhomboidea* Zone, corresponds with a low diversity value. In addition to the peak at PRA1, where the conodont abundance is lower, it relates to low diversity of *Icriodus*, possibly reflecting the biological crisis connected with the Lower Kellwasser extinction event (Tab. S5). *Icriodus* diversity is relatively constant from the Frasnian Zone 12 up to the Famennian *Palmatolepis rhomboidea* Zone, except for a few samples referred in both sections to the 13a and lower part of the 13b zones, corresponding with very high peaks in *Polygnathus decorosus* (Fig. 13). The *Icriodus* occurrence almost corresponds with the vertical distribution of *Icriodus alternatus alternatus*, the most abundant species of *Icriodus* in the two sections. The relative abundance of other *Icriodus* species and subspecies is low. *Icriodus alternatus alternatus* is responsible for the high peaks of icrodid abundance in PRA1 (top of Zone 12), PRA6 (Zone 13b), PRA6D (Zone 13c), PRA7A (base of the Famennian), PRA13, FRKT50, FRKT55, FRKT72 (*Palmatolepis minuta minuta* Zone), PRA15 (*Palmatolepis crepida* Zone) and PRA16 (*Palmatolepis termini* Zone). One species occurring in high abundance, even though limited only to one sample, is *Icriodus olivierii* appearing within the PRA section in the *Palmatolepis rhomboidea* Zone immediately above the disappearance of *Icriodus alternatus alternatus* and determining the peak of frequency of icriodids in PRA21.

Polygnathus diversity ranges from one to seven taxa co-occurring in a single sample and is independent of generic abundance (Tabs S5-S6) with highest values occurring in the Frasnian zones 13b-13c and decreasing in the *Palmatolepis subperlobata-Palmatolepis delicatula*

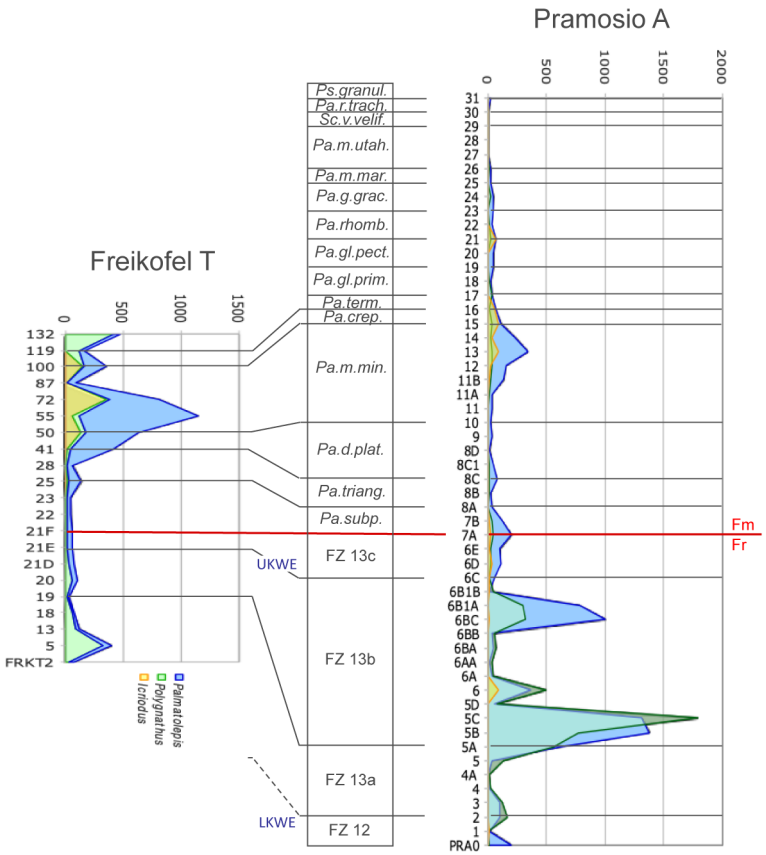

Fig. 12 - Abundance variation of genera *Icriodus*, *Palmatolepis* and *Polygnathus* up-sequence in the Pramosio A and Freikofel T sections. Equivalent biozonal intervals have been aligned. For abbreviations of biozone names, see caption of Fig. 10.

platys zones, rising again slightly in the *Palmatolepis minuta minuta* Zone (Fig. 13). The relative abundance of polygnathids drops at the top of Zone 13b and continues decreasing through the uppermost Frasnian into the basal Famennian. Low values persist through the remainder of the PRA section as well as in the FRKT section where, however, a peak occurs in the *Palmatolepis termini* Zone (FRKT132) (Fig. 12). *Polygnathus decorosus* is responsible for the peaks of relative abundance present in the lower part of Zone 13a in the PRA section (PRA2, PRA3, PRA5) and in the FRKT section (FRKT5), as well as in the most important peaks in Zone 13b of the PRA section (PRA5A, PRA5B, PRA5C, PRA6, PRA6BC, PRA6B1A). In both sections, *Po. decorosus* displays sudden flood occurrence in zones 13a and 13b, becoming extinct at the top of Zone 13b where the abundance of polygnathids drops suddenly.

At generic level, *Palmatolepis* displays persistent high diversity in both sections with one to 11 taxa present per sample (Tabs S5, S6). In only three of 75 examined samples, PRA4A (Zone 13a), PRA5D (Zone 13b) and PRA27 (*Palmatolepis marginifera utahensis* Zone), *Palmatolepis* is represented by only one species. Substantial reduction of palmatolepid biodiversity is confined to the *Palmatolepis subperlobata* Zone. Values of biodiversity as high and also higher than those in Zone 13b were reached in the upper part of the *Palmatolepis minuta minuta* Zone and *Palmatolepis crepida* Zone (Fig. 13).

Lower and Upper Kellwasser Extinction Events and Recovery in the Carnic Alps

In the Carnic Alps, there is no evidence of anoxic black-shale bituminous layers and/or black limestones, the Lower and Upper Kellwasser Horizons (Walliser, 1981, 1996; Sandberg et al., 1988; Walliser et al., 1989; Schindler, 1990, 1993) identified in Germany, southern France (including the GSSP for the Famennian Stage in the Upper Quarry at Coumiac), Morocco, North America and China. Two biotic extinction events, the Lower and Upper Kellwasser events, are connected with the two Kellwasser horizons. The Lower Kellwasser extinction event (LKWE) was located by Girard & Renaud (2007) at the top of Frasnian Zone 12, correlating with the lower third of the Upper *rhenana* Zone (Ziegler & Sandberg, 1990; Klapper & Becker, 1999); the Upper Kellwasser extinction event (UKWE) corresponds to the top of Zone 13b and to Zone 13c, the uppermost part of the *linguiformis* Zone (Ziegler & Sandberg, 1990; Joachimski & Buggisch, 1993, 2002).

The PRA sequence accumulated in oxic environments. Notwithstanding this, the Lower Kellwasser extinction event was determinable at the top of Frasnian Zone 12 (sample PRA1) by coincidence of various data, especially: 1) similar values of conodont biodiversity up-biozone but sharp decreasing abundance at the top; 2) low conodont abundance of 35 P_1 elements/kg, followed by an increase to 269 associated with decrease in biodiversity in the next sample up-sequence, referred to Zone 13a; 3) extinction of palmatolepids and ancyrodellids; 4) dominance of

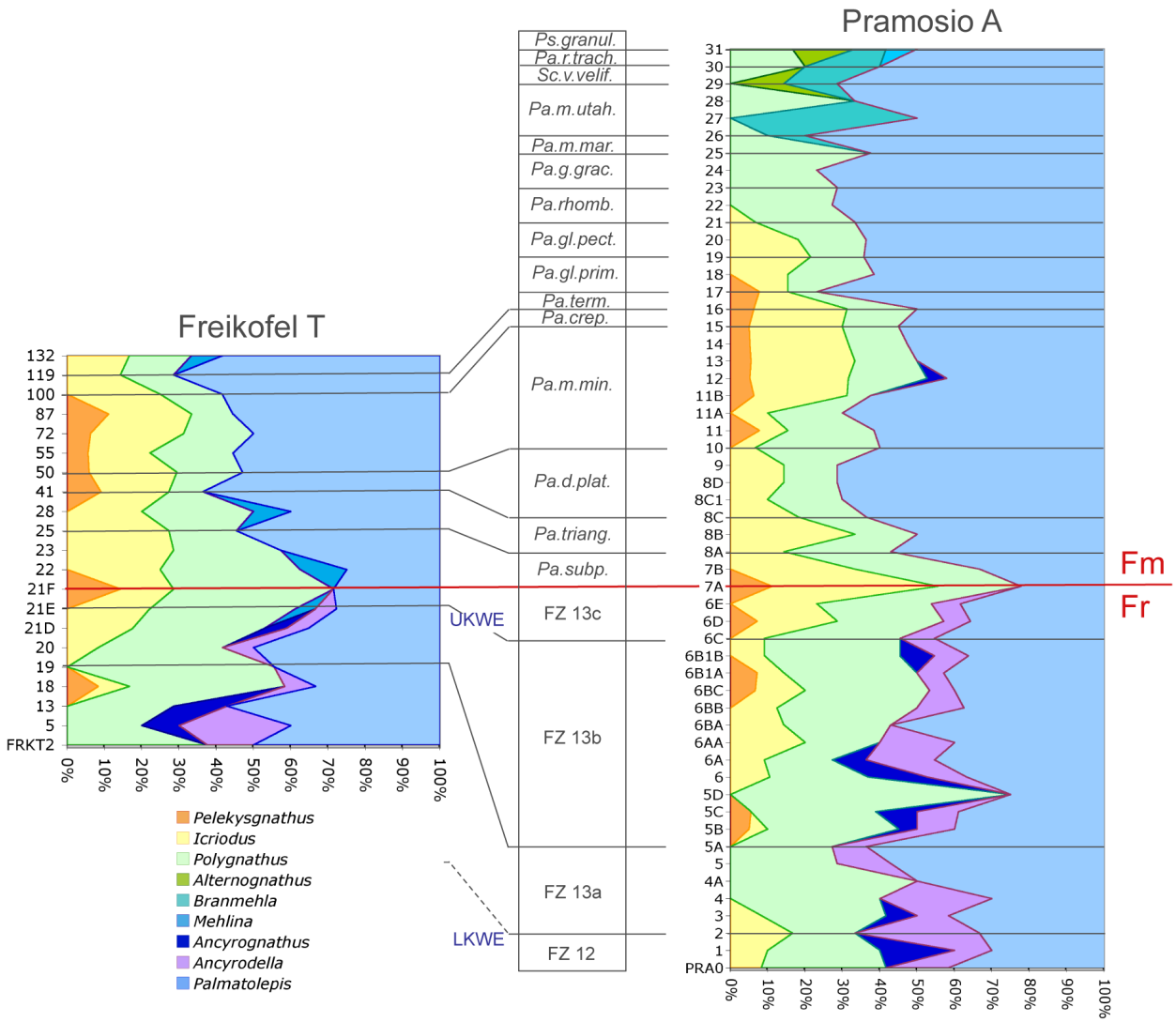

Fig. 13 - Conodont biodiversity variation up-sequence in the Pramosio A and Freikofel T sections. Equivalent biozonal intervals have been aligned. For abbreviations of biozone names, see caption of Fig. 10.

palmatolepids over polygnathids; 5) peak in abundance of icriodids; and, 6) decrease in sea water temperatures reconstructed from $\delta^{18}O$ from conodont apatite in the upper part of Zone 12 to base of Zone 13a (Tabs S5, S8; Figs 10-14).

The Upper Kellwasser extinction event (LKWE), connected with the biologic crisis at the end of Frasnian, has been identified in both of our sections in samples referred to the uppermost Frasnian Zone 13b and to Zone 13c. It is characterized by: 1) conodont biodiversity continuing to high in the event; 2) decreasing conodont abundance; 3) extinction of the genus *Ancyrodella*, Frasnian palmatolepids, numerous polygnathids and ancyrognathids; 4) palmatolepids becoming dominant relative to polygnathids; 5) increasing abundance of icriodids up-sequence; and, 6) decrease in reconstructed temperatures to the very base of the Famennian (Tabs S5, S6, S8, S9; Figs 10-15). In the FRKT section, the decreasing conodont abundance at the top of the Frasnian is partly masked by condensed sedimentation. It is noteworthy to underline that the above-mentioned conodont data characterizing both the Lower and Upper Kellwasser extinction events are perfectly comparable. Two phases of the Upper Kellwasser extinction event have been discriminated in our sections. The first phase (UKWE1), the most dramatic, at the top of Zone 13b, is where 16 species in the PRA section (three *Palmatolepis,* eight *Polygnathus,* two *Ancyrodella,* three *Ancyrognathus*) and seven species in the FRKT section (three *Pa.,* three *Po.,* one *Ang.*) became extinct. The second phase (UKWE2) occurred at the top of Zone 13c where the genus *Ancyrodella* as well as nine species of other genera became extinct in the PRA section (five *Pa.,* four *Po.,* one *Anc.*) and eight in the FRKT section (four *Pa.,* four *Po.,* one *Anc.*). It is worth highlighting that in Zone 13c *Palmatolepis linguiformis*, *Pa. juntianensis*, *Pa. boogaardi* and *Ancyrodella curvata* persist, though with only a few elements; they are reported in the literature as having become extinct at the top of Zone 13b (Sandberg et al., 1988, 2002; Girard et al., 2005; Klapper, 2007a, b). Lithologic data do not indicate reworking. A possibility is that the Carnic basin could have been a refugium for those

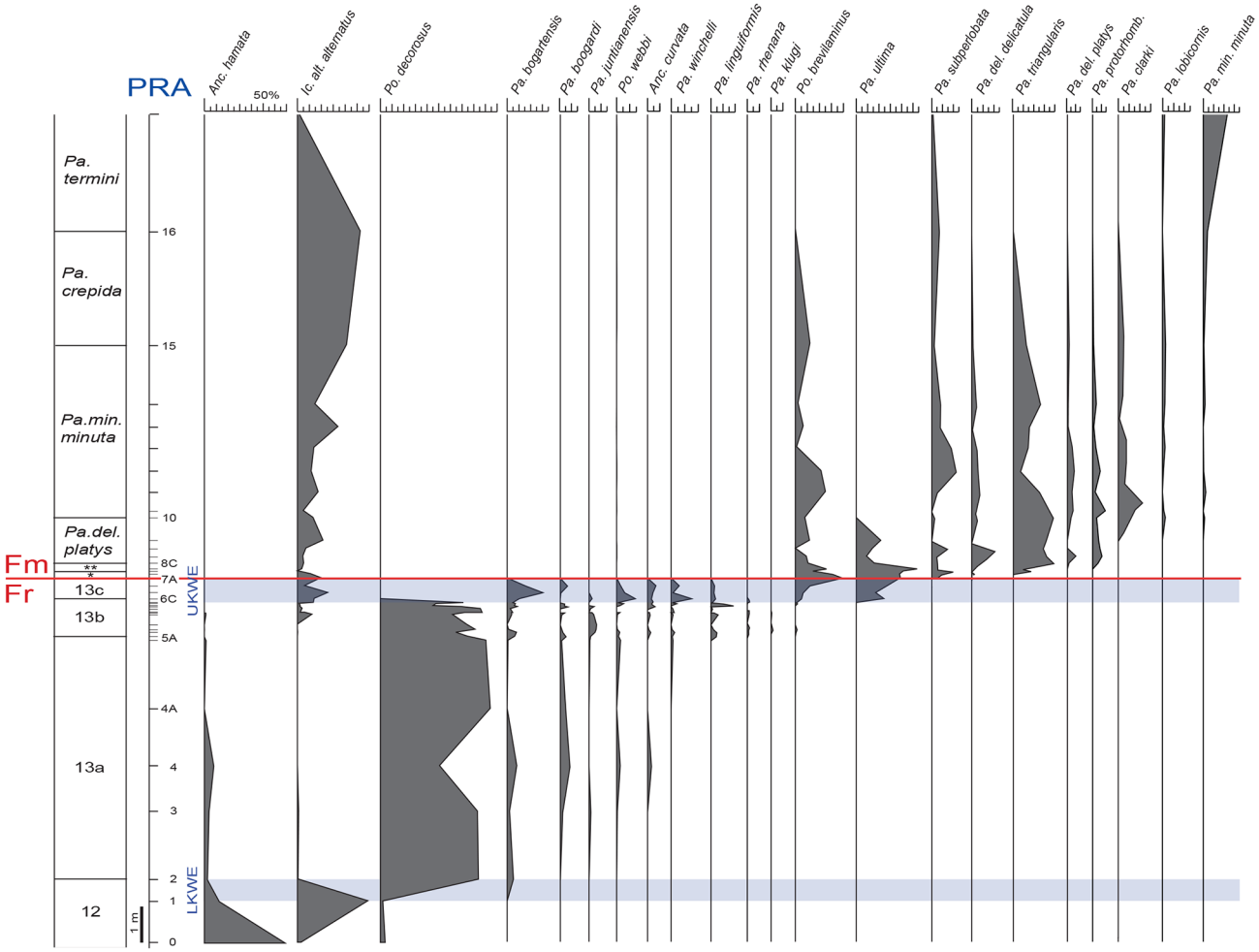

Fig. 14 - Vertical distribution and percentage of selected conodont species and subspecies across the Frasnian-Famennian boundary in the Pramosio A section. LWKE Lower Kellwasser Event, UKWE Upper Kellwasser Event. In the conodont biozone column: * *Palmatolepis subperlobata* Zone, ** *Palmatolepis triangularis* Zone.

species, whereas *Palmatolepis* dominated remarkably during the entire end-Frasnian (top of Zone 13b and Zone 13c). In our sections, peaks of elements of *Icriodus* characterize both the Lower and Upper Kellwasser events, as occurs globally (Sandberg et al., 1988, 2002; Schindler et al., 1998; Schülke, 1998, 1999; Girard et al., 2005, 2017; Girard & Renaud, 2007).

In the Carnic Alps, *Palmatolepis ultima*, *Polygnathus angustidiscus*, *Po. brevilaminus*, *Icriodus alternatus alternatus*, *Ic. alternatus helmsi*, *Ic. alternatus mawsonae*, *Ic. deformatus asymmetricus* and *Pelekysgnathus planus* survived the extinction. Once the crisis had receded, the recovery of conodonts started immediately without any Lilliput effect in the associations (Figs 14-15).

Recovery was swift, lasting through the *Palmatolepis subperlobata* to *Palmatolepis minuta minuta* zones. Low conodont diversity characterized the base of the Famennian. Substantial reduction of palmatolepid biodiversity is confined to the *Pa. subperlobata* Zone, related to their extinction at the top of the Frasnian. Rapid evolution of palmatolepids connected with vacant ecological niches developed by extinction of the Frasnian species is reflected in the appearance of new species (Figs 14-15). The high number of P_1 elements of unidentifiable *Palmatolepis* in juvenile stages of growth characterizes the lowermost Famennian conodont associations. A succession of 14 first appearances of *Palmatolepis* species rapidly followed each other during the *Pa. subperlobata*-*Pa. minuta minuta* zones (Tabs 1-2; Figs 14-15). Values of biodiversity and abundance returned to being as high and also higher than they were in the Frasnian Zone 13b; this situation occurred in the *Palmatolepis minuta minuta*-*Palmatolepis crepida* zones when the recovery, mainly concerning this genus, had already taken place.

Discussion of conodont data

Viewed in detail, conodont data from the two sampled sections display inhomogeneities thought to be linked to slight differences in the oxic depositional environments (see discussion of facies analysis). In previous chapters, we stressed that conodont abundances were higher in the PRA section than in the FRKT section, with exceptional values occurring in Frasnian Zone 13b. Peaks of abundance coincide with pelagic environments (conodonts associated with other pelagic biota, especially ammonoids and radiolarians). Low abundances often coincide with rudstone levels; those in the early Famennian obviously reflect events during the worldwide end-Frasnian mass

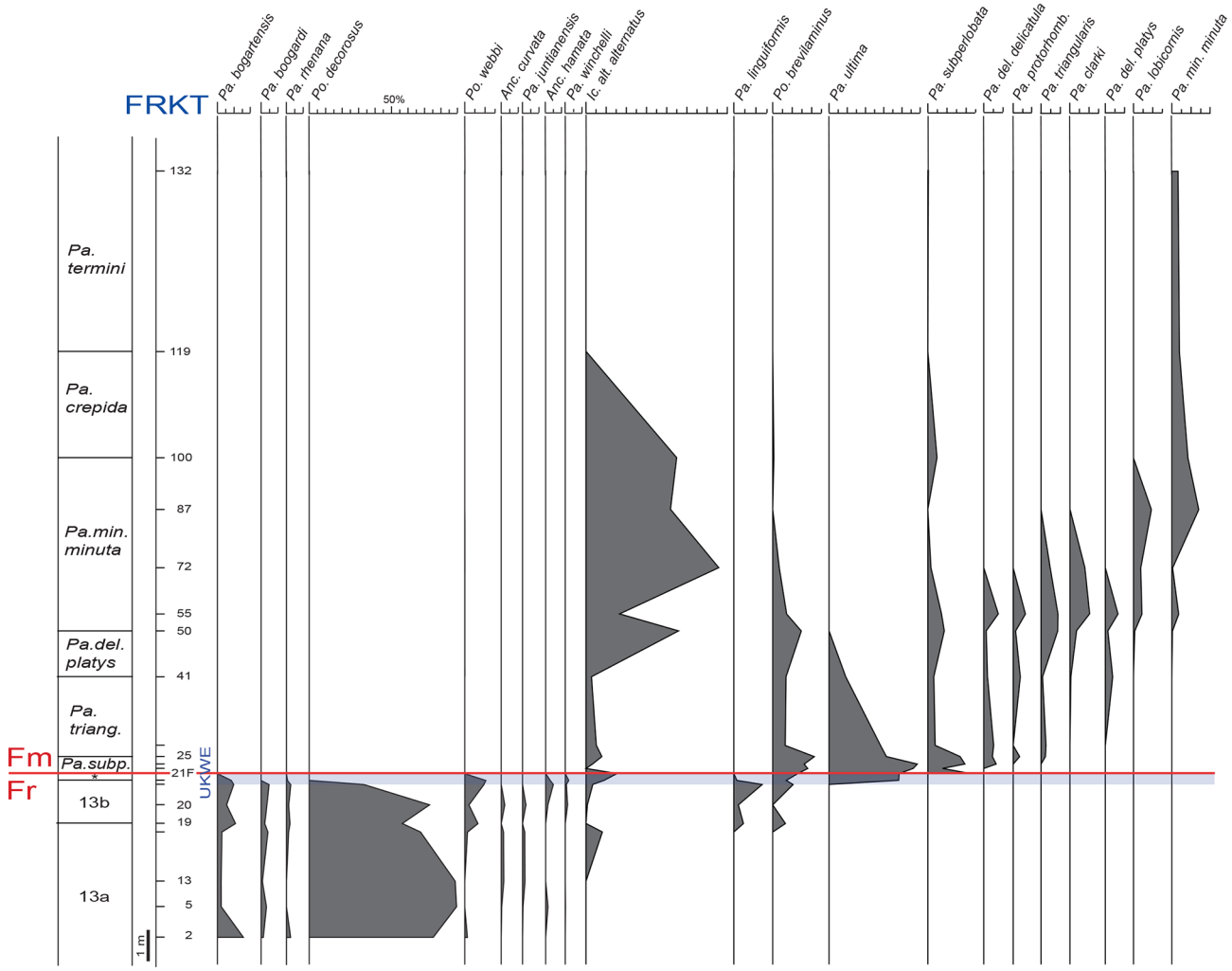

Fig. 15 - Vertical distribution and percentage of selected conodont species and subspecies across the Frasnian-Famennian boundary in the Freikofel T section. UKWE Upper Kellwasser Event. In the conodont biozone column: * Frasnian Zone 13c.

extinction. Viewed on a broad scale, the conodont data display comparable trends (see Figs 10, 13). Polygnathids dominate until the upper part of Frasnian Zone 13b when palmatolepids become prevalent. Their dominance was maintained during Frasnian Zone 13c into the lower Famennian. Icriodids increased contemporaneously with the onset of palmatolepid dominance, persisting into the *Palmatolepis rhomboidea* Zone.

During the Late Devonian, due to the absence of ice caps until the latest Famennian, oceanic waters were generally warmer than today. The Carnic microplate seems to have occupied a more distal position with respect to land than other microplates (Germany, southern France, Morocco, North America; Fig. 1) where black shales reflect anoxia that affected sea waters during the late Frasnian. The extinction events seem to be related to a transgressive episode followed by a rapid and strong regression at the top of the Frasnian (Johnson et al., 1985; Johnson & Sandberg, 1989). A pronounced, rapid sea-level fall, reflected in the curves presented by Johnson et al. (1985) and Johnson and Sandberg (1989), resulted in a corresponding swift regression generating an increased influx of nutrients from intensified terrestrial erosion with consequent growth of enormous quantities of phytoplankton. In areas close to land, the effect would have been a reduction of O_2 content in the seawater. The enhanced burial of organic matter would have resulted in black shale horizons.

In that part of the Carnic basin where our sections have been sedimented, oxygen levels were higher, not allowing deposition of black shales. In fact, microfacies analysis indicates the presence of extensive bioturbation. Sea water was sufficiently oxygenated to support substantial infaunal activity. Although sea water was oxygenated, death of a large quantity of biota is recorded clearly by, for example, conodonts having undergone significant extinction.

Burial of organic matter is evidenced by the increase of $\delta^{13}C$ measured on whole-rock carbonates in the PRA section at the top of Zone 13b and during Zone 13c, coincident with the Upper Kellwasser extinction event (UKWE), and in the lowermost part of *Pa. subperlobata* Zone with an excursion of ca +2.5‰ (Tab. S7). The $\delta^{13}C$ trend is comparable with those reported from other countries (Joachimski et al., 1994, 2002). The UKWE took place during a rapid regressive event. Lithologic and biologic data support this (see Ch. General discussion).

During rapid regression, species stressed thereby are compelled to migrate due to decreasing habitats and isolation of populations. Survival or extinction of a species depends on the ability and speed of migration and on their capacity to overpower species in neighbouring environments with which they come into competitive contact. Palmatolepids living farther offshore than icriodids and polygnathids are assumed to have been sufficiently numerous to migrate rapidly seaward. Polygnathids, possibly less able to migrate rapidly, could have been disadvantaged compared with predators that may have included palmatolepids. This would explain the dominance of palmatolepids over polygnathids during the UKWE in the Carnic basin. Icriodids and pelekysgnathids, inhabitants of shallow water, display a conspicuous increase in abundance during the Lower and Upper Kellwasser extinction events in the Carnic Alps, as well as in other areas, exemplified by the Montagne Noire of southern France, Germany, Belgium, Morocco, U.S.A. (Nevada, Utah), northwest Australia, and South China (Sandberg et al., 1988, 2002; Schindler et al., 1998; Schülke, 1998, 1999; Girard et al., 2005, 2017; Girard & Renaud, 2007). In our sections, the conspicuous increase in those two genera, recorded in associations with dominant pelagic palmatolepids, have been interpreted as having been due to short down-slope transport of shallow-marine components during sea-level falls. Supporting evidence comes from the presence of calcarenite and rudstone levels with carbonate particles interpreted as having formed in shallow water and lagoonal environments (see Ch. General discussion).

In our opinion, conodonts swam in superfice seawaters, as already suggested by Joachimski & Buggisch (2002), based on comparable $\delta^{18}O$ data for icriodids and palmatolepids, with possible very short excursions perpendicularly within the water column. In the Carnic basin, the dominance of *Palmatolepis* in the latest Frasnian would accord with representatives of that genus having had high-quality environmental conditions for life. But all Frasnian palmatolepids underwent extinction in the Carnic basin as well as globally with the exception of *Palmatolepis ultima*, the only species to survive the crisis. This last species may have been evolving during Frasnian Zone 13c in an environment that was already undergoing profound change. We cannot confidently assume the cause of the extinction of the palmatolepids being anoxia; other causes may well have been involved. For instance, erosion of land during a rapid regression may have been associated with variations in seawater chemistry on an oceanic scale, not just connected with an excessive influx of nutrients hither and thither, associated with mixing by marine currents, though the latter may have played an important role in grand-scale water mixing, as occurs within and between oceans at present.

Conodont data from the two studied sections indicate that during the end-Frasnian and beginning of the Famennian, dwellers in the Carnic basin lived in stressed environments. The high relative abundance of one genus may be connected with the demographic explosion of single species dominating over others of the same genus, acting ecologically as an opportunistic (r-selected) species in unstable environments. We noted the constant presence, regardless of genera, of one or two opportunistic species. During Frasnian zones 13a and 13b, the dominance of polygnathids involved the flood occurrence of *Polygnathus decorosus*; it in fact was numerically the most common conodont species regardless of genus. *Po. decorosus* may have been an opportunistic taxon with high reproductive capacity dominating over other polygnathids. *Palmatolepis bogartensis* reached its greatest abundance in the second part of Frasnian Zone 13c. *Palmatolepis ultima* too could be considered an opportunistic species. It became the most abundant species at the base of the Famennian and was thus probably the only palmatolepid tolerating the changed environment. Other opportunistic taxa may have been *Icriodus alternatus alternatus* and *Icriodus olivierii*. The last species is morphologically very close to *Ic. alternatus alternatus*; it seems to substitute for it in the ecosystem, entering and being present in only one sample (with a high number of elements) immediately after the disappearance of *Ic. alternatus alternatus.*

STABLE ISOTOPE STRATIGRAPHY

Methods

Carbon and oxygen isotopes were analysed by Anita Andrew on whole-rock powders by reaction in evacuated Exutainer tubes with 104% phosphoric acid for about 24 hours at 25 °C. A subsample of the produced CO_2 was extracted using a gas syringe and the C and O isotope values were analysed by injection into a He stream and separated from other gases by a GC attached to a Finnigan MAT 252 mass spectrometer via a Conflo III. The internal laboratory carbonate standards CSIRO ($\delta^{13}C$ = -13.46 VPDB; $\delta^{18}O$ = -5.26 VPDB) and PRM-2 ($\delta^{13}C$ = 1.15 VPDB; $\delta^{18}O$ = -17.63 VPDB) were used to correct the data. The laboratory standards have been calibrated against international standards NBS19 and LSVEC (Coplen, 1995; Coplen et al., 2006). Replicate analysis of the standard calcites is generally better than ± 0.1 for C and O. Carbon isotope values are reported in permil (‰) relative to VPDB but oxygen isotope values were affected by alteration and are not reported with the oxygen data from conodonts considered more robust.

Oxygen isotopes analyses on conodont apatite were provided by Michael Joachimski. Conodont samples analysed consisted of mixed polygnathids, palmatolepids and ramiform elements. The analyses were based on 0.3 to 1.0 mg of conodont apatite weighed into small polyethylene beakers and dissolved by adding 5 ml 2 M HNO_3. The phosphate group was precipitated as Ag_3PO_4 (as described by Joachimski et al., 2009). The Ag_3PO_4 crystals thus obtained were washed intensively, ground to fine powder using an agate mortar, and 0.2 to 0.3 mg of it weighed into silver foil and transferred to the sample carousel of a TC-EA (thermally coupled elemental analyzer) coupled online with a Thermo Fisher Delta V Plus isotope-ratio mass spectrometer. Samples and internal standards were generally analysed in triplicate (Helium flow rate was 80 ml/s, reactor temperature was set to 1450 °C, column temperature was 90 °C). Conodont apatite oxygen isotope values are reported in ‰ relative to VSMOW. The oxygen isotope composition of the standard NBS 120c was measured as 21.7 ± 0.09‰ (1 sd; n = 14). Reproducibility of triplicate sample

measurements was between ± 0.08 and 0.33‰ (average ± 0.14‰; 1sd).

Results from conodont apatite

In the PRA section oxygen isotope values of conodont apatite from samples PRA2-PRA15 range from 18.0 to 19.1‰ (Tab. S8; Figs 6, 16). Relatively high values of 18.7 and 19‰ were obtained at the base of the Frasnian Zone 13a. Up-section, $\delta^{18}O$ values decrease and are between 18.5 and 18.0‰. At the top of Zone 13b, values increase again (except for 18.2‰ from PRA6C) to 18.8‰ and reach a maximum of 19.0‰ at the base of the *Palmatolepis subperlobata* Zone (lower part of the Lower *triangularis* Zone). Values between 18.4 and 18.7‰ and 18.2 and 18.7‰ were found in the *Pa. delicatula platys* and *Pa. minuta minuta* zones, respectively.

In the FRKT section, relatively high oxygen isotope ratios of 18.6 and 18.9‰ are measured in the upper part of Zone 13a (Tab. S9; Figs 6, 16). Following, $\delta^{18}O$ decreases to 18.3‰ and increases again to values around 19‰ in the *Palmatolepis superlobata* Zone and 19.2‰ in *Palmatolepis triangularis* Zone. $\delta^{18}O$ values in the *Palmatolepis delicatula platys* to *Palmatolepis termini* zones are between 18.1 and 18.5‰ with one higher value of 19.1‰ measured in the base of the *Pa. minuta minuta* Zone.

Discussion of stable isotope data

Oxygen isotope analyses that are unaffected by alteration can be used to evaluate variations in climatic conditions and temperature related to a mass extinction event. On the other hand, variations in carbon isotope values indicate global changes in carbon reservoirs that can occur because of changes in ocean mixing that will release organic matter stored in the deep ocean (negative shifts in $\delta^{13}C$) or increase production or preservation of organic matter in the deep ocean (negative shifts in $\delta^{13}C$).

Joachimski & Buggisch (2002) first described positive excursions in $\delta^{18}O$ of 1 to 1.5‰ from two German Fr-Fm sections. The positive $\delta^{18}O$ excursions coincide with the Lower and Upper Kellwasser horizons as well as with positive excursions in carbonate $\delta^{13}C$. The excursions in $\delta^{18}O$ have been confirmed by studies on sections in southern France as well as in China (Balter et al., 2008; Le Houedec et al., 2013; Huang et al., 2018a). The positive excursions in $\delta^{13}C$ were interpreted as reflecting enhanced deposition of organic material, lowering of atmospheric CO_2 and may thus have resulted in climate cooling as documented in the positive $\delta^{18}O$ excursions. The conodont oxygen record of the PRA section also shows two intervals with relatively high $\delta^{18}O$ values. The first maximum is observed in the lowermost Zone 13a, in an interval immediately post-dating the Lower Kellwasser extinction event. The second positive excursion is at the top of Zone 13b and in Zone 13c, correlating with the Upper Kellwasser extinction event, with the peak of $\delta^{18}O$ value observed in the *Palmatolepis subperlobata* Zone. While the general pattern is comparable to the pattern described by Joachimski & Buggisch (2002), the positive shifts in $\delta^{18}O$ are smaller. At the transition of zones 12-13a as well as across the Frasnian-Famennian boundary, there is a +0.8‰ change. If explained solely by temperature, this positive shift in $\delta^{18}O$ would translate into 3.5° C cooling and thus less than the 5 to 7° C cooling observed by Joachimski & Buggisch (2002).

The positive $\delta^{18}O$ excursion at the Fr-Fm transition in the PRA section correlates with a positive excursion in carbonate $\delta^{13}C$. In Zone 13b, $\delta^{13}C_{carb}$ values start increasing to values of around 1.8‰ with maximum values around +4‰ in Zone 13c at the base of the *Palmatolepis subperlobata* Zone. Thus, the positive shift in $\delta^{13}C_{carb}$ clearly pre-dates the shift in $\delta^{18}O$ (Fig. 16). This positive 2-3‰ increase in $\delta^{13}C_{carb}$ values suggests that ocean circulation has decreased with cooling of the ocean enhancing organic matter preservation in the deep ocean. Such stratifications have been identified in isotopic profiles across many events.

GENERAL DISCUSSION

Our discussion is focused on the interval across the Frasnian-Famennian boundary connected with the Lower and Upper Kellwasser extinction events and the post-event recoveries. We do not discuss higher horizons of the two sections that inter alia were sparsely sampled or are characterized by conodont abundances that were too sparse.

The facies and depositional environments connected with Frasnian conodont Zone 12 and the very base of Zone 13a were based on a short tract of the PRA section. This tract consists of grey rudstone passing to packstone and microbialites. Absence of positive grading and sorting of the rudstone beds seems to indicate mass-flow depositional processes near the upper margin of a reef/fore-reef setting, presumed to be at no great depth. The 0.8‰ increase in $\delta^{18}O$ of conodont apatite translates into a decrease in palaeotemperature of 3.5 °C. The abundance of conodonts decreases up-section (366 to 35 P_1 elements per kg) in the upper part of Zone 12. This decrease may be connected with a rapid increase of carbonate clastic input (grainstones and rudstones), implying a rapid increase in sedimentation rate during a sea-level fall. It may also be linked with the biological crisis at the top of Zone 12 detected worldwide. The abundance of the shallow-water and peri-reefal conodont genus *Ancyrodella* decreases rapidly up-section from 40% to 8%. In parallel, the shallow-water conodont genus *Icriodus* increases significantly from 1% to about 40% in the microbialite bed-sets capping the rudstones whereas *Palmatolepis,* considered a pelagic conodont genus, decreases slightly. The strong increase of *Icriodus* compared with substantial stability in abundance of *Palmatolepis* leads us to hypothesize that the former suffered modest transport down-slope during sea-level fall. The sudden decrease of *Icriodus* and increase of *Polygnathus* at the very base of Zone 13a concomitantly with the reappearance of ammonoids (sample PRA2) may mark the onset of steady low-stand conditions. Facies developed in the upper part of Zone 12-base of Zone 13a are interpreted as having been deposited in shallow-marine oxic waters during a significant cooling of sea water linked to rapid sea-level fall followed by a low-stand. These facies are aligned with black carbonates/shales rich in organic matter present in other areas worldwide typifying the dysoxic or anoxic environments of the Lower Kellwasser (LKW) horizons. In the oxic sequence of the PRA section,

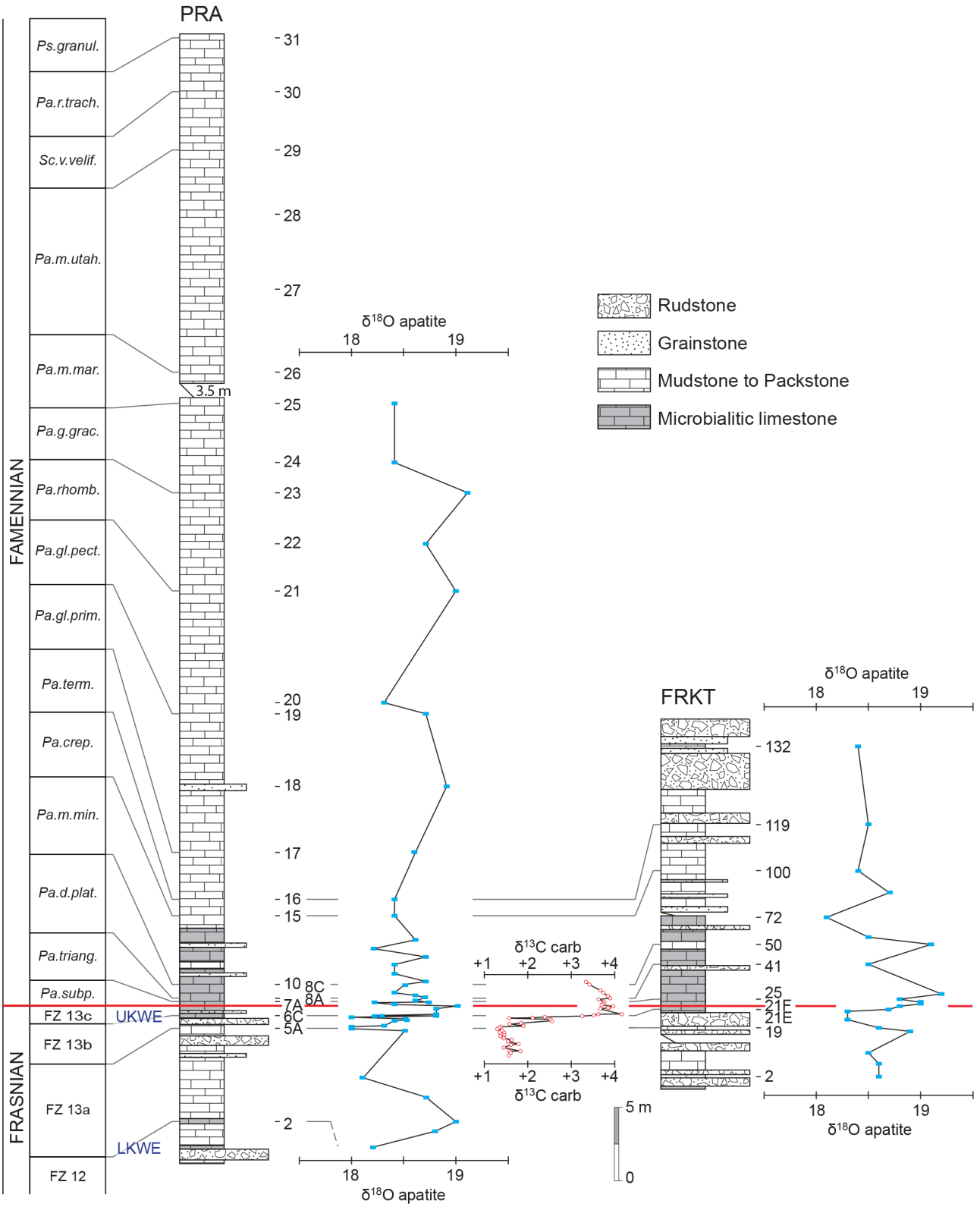

Fig. 16 - Curves of $\delta^{18}O$ of conodont apatite in Pramosio A and Freikofel T sections and of $\delta^{13}C$ of total rock in Pramosio A section aligned with lithostratigraphic columns and conodont biozones. Analysis of oxygen isotopes on conodont apatite were provided by Michael Joachimski and those for carbon isotopes on whole-rock by Anita Andrew. For abbreviations of biozone names, see caption of Fig. 10.

our conodont data display the extinction of palmatolepids and ancyrodellids at the top of Zone 12, associated with the Lower Kellwasser extinction event (LKWE) (see Ch. Conodont data).

The middle part of Zone 13a in the Pramosio A section is characterized by bioturbated pack- and wackestones rich in shallow-water components such as calcisphaeres, pellets, algae and corals mixed with pelagic fossils such

as radiolarians and ammonoids. Conodont abundances tend to be slightly reduced; icriodids tend to disappear, and there is a minor decrease in $\delta^{18}O$ of conodont apatite. Our data seem consistent with a faint transgressive trend.

Rudstone bed-sets in the upper part of Zone 13a are broadly aligned with those of the Freikofel T section. In both sections the shallow-water icriodids are almost absent and the more offshore polygnathids dominate, increasing in percentage up-section. Red-stained alternating with grey intervals occur in the Freikofel T section (e.g., sample FRKT9). Van der Kooij et al. (2007) interpreted these facies of early-diagenetic origin produced by alternating maximum flooding (red) and relative low-stand (grey) on the peri-reefal upper surface of the marine platform and slope, to several dozens of metres depth. Grey clasts of rudstone present in both sections are interpreted as derived from a nearby depositional system consisting in part of a dismantling reef surrounded by shallow-marine and lagoonal facies. Red-stained clasts in the rudstones of bed FRKT15 testify to dismantling of the top of the reef slope, probably during a relative sea-level fall.

The $\delta^{13}C$ values of whole rock carbonates in the PRA section decrease slightly up-section with some faint high-frequency fluctuations (< 0.6‰). Positive excursions in $\delta^{13}C$ are interpreted as reflecting enhanced deposition of organic material; these mostly align with rudstone bed-sets. In both sections, a weak shallowing upward trend seems to be confirmed by the gradual increase of the *Polygnathus*-percentage coupled with a slight decrease in the percentage of *Palmatolepis*. $\delta^{18}O$ values during the middle and upper part of Zone 13a vary from 18.1 (PRA4) to 18.5‰ (PRA5) in the PRA section and 18.5 (FRKT13) to 18.9‰ (FRKT18) in the FRKT section (Tabs S8, S9).

Zone 13b shows the highest variability of data. The rudstone bed-sets, well aligned between the two sections, are organized in a thickening-upwards sequence. In the FRKT section, there is double the amount of rudstone compared with that in the Pramosio A section, probably reflecting a higher rate of sedimentation.

In the PRA section, the conodont abundances display three maxima with 1000-3000 P_1 elements/kg separated by two minima. The peaks correspond to high percentages of palmatolepids associated with other pelagic fossils, especially ammonoids and radiolarians. The peaks of conodont abundance are mostly aligned with low values of $\delta^{18}O$ of apatite and $\delta^{13}C$ of total rock (Fig. 6). These matching results in the PRA section, representing a relatively deep-water setting, are consistent with marine warming and, probably, with the transgressive trend indicated by the increase of pelagic components, especially ammonoids and palmatolepids. Contrastingly, the minima in conodont abundances are aligned with marine cooling and, probably, with sea-level fall and low-stand with increase of polygnathids. Moreover, the thicker rudstone bed-set seems aligned with the second minimum of conodont abundance. The ammonoids enclosed in the rudstone clasts at the top of this biozone in Pramosio A section may be explained by a rather rapid sea-level fall.

The up-section increase in $\delta^{13}C$ slightly pre-dates the increase in conodont apatite $\delta^{18}O$. It could be that C_{org} burial started first, whereas the climate of this shallow sub-tropical sea along the margin of the western Palaeotethys underwent cooling some tens of thousands of years later.

In the shallower marine FRKT section, the conodont abundance is generally lower. Pelagic organisms are represented mainly by radiolarians, with ammonoids occurring only in the uppermost sample FRKT21D accompanied by a pronounced increase in abundance of *Palmatolepis*. The red- and beige-stained "transgressive" samples FRKT19 and FRKT21B-FRKT21D can be correlated with the lowermost and uppermost transgressions in the Pramosio A section. In the FRKT section, ratio of *Palmatolepis* to *Polygnathus* changes gradually up-section with *Palmatolepis* becoming increasingly dominant. The signal of the intermediate transgression identified in the PRA section is missing, probably due to the presence of rudstones combined with the non-systematic distribution of samples collected. Ultimately, the positive $\delta^{18}O$ shift of 0.5‰ in the Pramosio A section would translate into ≤ 2°C cooling. This minor temperature change does not explain the intense first phase of the Upper Kellwasser extinction event (UKWE1), most dramatic at the top of Zone 13b where, in the PRA section, 16 conodont species became extinct (three *Palmatolepis,* eight *Polygnathus,* two *Ancyrodella,* three *Ancyrognathus*), and in the FRKT section seven species became extinct (three *Palmatolepis,* three *Polygnathus,* one *Ancyrognathus*). Consequently, other environmental factors, such as widespread anoxic events and other possible changes in the oceans may have played a role in the extinction. The top of Zone 13b and the whole of Zone 13c are considered coeval with the Upper Kellwasser extinction event at the end of the Frasnian.

Zone 13c in both sections is characterized by microbialites. In the PRA section they alternate with thin rudstone beds; the abundance of conodonts is medium to low. In both sections, *Icriodus* increases up-section showing significant peaks of abundance concurrently with the rise of pelagic *Palmatolepis* that prevails over *Polygnathus.* We highlighted the persistence during this biozone of a few species of *Palmatolepis* that could have become extinct within Zone 13b but did not, hypothesizing that the Carnic basin could have been a refugium particularly for those species and for all palmatolepids. The *Icriodus* peaks may be interpreted as being caused by down-slope transport of shallow-marine components during a sea-level fall. Transport processes in such environments are common, proven by the presence of carbonate particles formed in lagoonal and shallow-water environments. In the PRA section, both the $\delta^{18}O$ measured on apatite and the $\delta^{13}C$ measured on whole-rock increase up-section.

The strongly condensed sedimentation of the FRKT section may be due to lack of rudstone deposition but also to the impact of regression reflecting a shallower water interval in this section. Decrease of sedimentation rate may, in part, have resulted from extinction of reef builders, expressed by a decrease of productivity of the shallow-marine carbonate-factories, mostly represented by small microbialitic reefs. The top of Zone 13c coincides with the final stage of the biologic crisis at the end of the Frasnian identified by us as the second phase of the Upper Kellwasser extinction event (UKWE2) in which the conodont genus *Ancyrodella* as well as nine species of other genera became extinct in the PRA section (five *Palmatolepis,* four *Polygnathus,* one *Ancyrodella*) and eight in the FRKT section (four *Palmatolepis,* four *Polygnathus,* one *Ancyrodella*) as was the case globally.

The *Palmatolepis subperlobata* Zone is mainly represented by microbialites in both sections. Ammonoids and radiolarians indicate a pelagic environment consistent with a transgressive trend. The thickness of the Freikofel T section is twice that of the PRA section. The higher sedimentation rate in the FRKT section may be due to horizontal transport of shallow-sea components as armoured balls. The conodont abundance is medium to low in both sections, pelagic palmatolepids continue to be dominant associated with a peak of icriodids at the very base of the Famennian. Conodont biodiversity is low due to the post-extinction effect. Values of $\delta^{18}O$ in conodont apatite increase in both sections (up to 19‰); whole rock $\delta^{13}C$ values in the PRA section slightly decrease upwards (from 3.96 to 3.71‰).

The *Palmatolepis triangularis* Zone is represented by microbialites in the PRA section and by microbialites interbedded with packstones overlain by a rudstone bed in the FRKT section. The thickness of the biozone in the FRKT section is ten times that in the PRA section, possibly due to the higher rate of sedimentation indicated by the presence of packstones and rudstones. Conodont abundance is low to medium with palmatolepids dominating over polygnathids. The presence of frequent ammonoids and the red-stained interval of the Freikofel T section are believed to corroborate the presence of the same transgressive trend. Whole rock $\delta^{13}C$ values are constant; $\delta^{18}O$ values of conodont apatite show a positive shift of ca 0.5‰ in both sections at the top of the biozone.

The *Palmatolepis delicatula platys* Zone in the PRA section consists of grey microbialitic limestones containing pelagic elements mixed with minor shallow-sea-derived elements. The FRKT section consists mostly of red-stained microbialites and packstone with pelagic components. In the PRA section conodont abundance is low, whereas in the FRKT section it is higher, reaching a peak of more than 400 P_1 elements/kg. Palmatolepids are still dominant, icriodids increase and polygnathids decrease significantly. Data from both sections are consistent with a general transgressive trend (or high-stand conditions). $\delta^{18}O$ values of conodont apatite are between 18.4 and 18.7‰ in both sections; $\delta^{13}C$ values measured by whole-rock range between 3.6 and 3.9‰.

During the *Palmatolepis minuta minuta* Zone the depositional environment in the PRA section seems to be more pelagic than that of the FRKT section. Both sections consist of microbialitic limestones with minor input of shallow-water-derived components, alternating with rare thin rudstone beds. The red-brick-coloured microbialitic limestone in the FRKT section accords with the persisting transgressive trend. The abundance of conodonts increases up-section; in the FRKT section, the peak of ca 1200 P_1 elements/kg coincides with the highest value of pelagic *Palmatolepis*. In both sections, the relative abundance of palmatolepids, always dominant, tends to increase associated with a significant increase in icriodids, whereas polygnathids are scarce. The high numbers of icriodids in the biozone is amazing. They present high peaks of abundance in the PRA section (sample PRA13) and in the FRKT section (samples FRKT50 and FRKT72) where they reach a maximum of 350 P_1 elements/kg (Fig. 12). Abundance of conodonts, in particular of *Palmatolepis* and the coeval increase of pelagic character evidenced by ammonoids, seems to accord with a persisting transgressive trend of the sequence. This contrasts with our previous interpretation of icriodid peaks, even though, doubtfully, we suggested the stratigraphically lower peaks of icriodids along both sections may have been linked to lateral transport during regressive phases of the sequence, attested to by the presence of calcarenites and rudstones. Here the significant increases in *Icriodus* seem not to be firmly linked to lateral transpost, not coinciding with layers of calcarenite and rudstone. Moreover, they seem not to be linked to temperature variations, the peak in sample FRKT50 is aligned with a $\delta^{18}O$ value of 19.1‰; that in sample FRKT72 corresponds with a $\delta^{18}O$ value of 18.1‰. Perhaps they relate to minor regressive pulses not linked with lithology.

INTERPRETATION OF DEPOSITIONAL ENVIRONMENTS, CLIMATE AND RELATIVE SEA-LEVEL CHANGES

In this chapter we compare and interpret the main lithologic, sedimentologic, biologic and stable isotope data, as well as facies and microfacies architectures in the context of a robust conodont biostratigraphy.

Carbonate breccia bed-sets in the upper part of Frasnian biozones 13a and 13b of the two stratigraphic sections can be correlated almost perfectly. Clasts with calcispheres, foraminifers and coated grains are usually interpreted as indicating that a lagoonal setting was prevalent; clasts with corals consistent with shallow marine environments and associated with clasts and matrix containing open-marine taxa, particularly radiolarians, are rare. Additionally, occurrences of breccia bed-sets, where identifiable, correspond well with positive fluctuations in $\delta^{13}C$ based on whole rock and with positive fluctuations in $\delta^{18}O$ of conodont apatite. Conodonts are sparse in rudstones of Zone 13b compared with those in associated packstones and grainstones by a factor of more than 1 to 10. Monomictic breccias (e.g., sample PRA5E) seem to have accumulated during the early stages of shallowing, whereas polymictic ones seem more characteristic of the final stages of regression and the low stand tracts.

Sediments intercalated between rudstone bed-sets typically have abundant pelagic taxa such as radiolarians and/or ammonoids, and have the highest yields of conodonts (cf. Fig. 6). In the PRA section, the peaks of conodont abundance match well with increase in pelagic palmatolepids; this is consistent with transgressive and high-stand phases. The scarcity of samples from the FRKT section does not allow these peaks to be discriminated but nevertheless shows only the relative increase of *Palmatolepis* at the top of the Frasnian. In both sections the increase to dominance of *Palmatolepis* over *Polygnathus* begins suddenly from the top of the Zone 13b, then persists through Zone 13c and up-sequence into the Famennian. It is noteworthy that the peaks in abundance of conodonts always correspond to paucity of microbial matter. That the rudstones and microbialites are mutually exclusive can be linked with erosional processes generated by rapid marine currents. Microbialites were generated in both warm and cool periods (reflected in variations in stable isotopes).

Additionally, in the absence of true dysoxic/anoxic conditions the mucilaginous carpets on the sea floor would have impacted on ostracods (nektonic breathers), in many cases encountered with their valves tightly closed as though having died imprisoned in organic matter. Other factors, for example the cooler water temperature, are not necessarily implicated.

That the frequency of shallow water conodonts, such as some species of *Icriodus*, increases simultaneously to that of more open-sea conodonts (*Palmatolepis*) during periods of high stand, sometimes devoid of microbialites, is suggested as having been probably due to minor regressive pulses not indicated by lithology or to a combination of factors: temperature, salinity, pH, changes in water currents (such as increased/decreased energy), changes in spatial distribution of habitats, and inhabitants. We cannot discriminate which may have been the primary, or even subtle factors involved in particular extinctions. It seems unlikely that rudstones were produced and prograded during stable, high-stand conditions. Lack of chaotic and slump deposits makes it likely that the PRA succession was deposited along the middle to upper part of a slightly inclined ramp, sloping probably < 2° and certainly much less than the 6° angle of equilibrium of submarine carbonate mud. According to actual geographic schemes, the depositional environment should equate with a lower shore face or an inner shelf.

In the FRKT section the rudstone bed-sets are coarser, thicker and more frequent than in the PRA section. Usually, they are grey and intercalated with slightly nodular to brecciated pink-brown, thin-bedded carbonates. Not counting the thickness of rudstones, the sedimentation rate is taken to have been similar to that in the PRA section, with the exception of the interval corresponding to the profoundly more condensed Zone 13c. We interpret the FRKT section as having been deposited along or at the base of a well oxygenated, metastable carbonate ramp, sloping less than 6°, but not necessarily much shallower than the PRA section.

If it is accepted that the soft carpets of microbes grow below the level of the base of low energy waves, other factors need to be taken into account if one wishes to arrive at an estimate of the approximate maximum depth at which deposition took place. It is certain that most of the well-sorted coated grains and fossils in the grainstones were derived from lagoons, ruling out deposition on a deep bathyal to epibathyal sea floor. This can be satisfactorily explained if the transport was made by storm currents, which by their nature do not promote the sorting of particles during transport, rather than by turbidity currents. The overall picture led us to favour deposition close to the storm-wave base (ca 40 m) with eustatic sea-level changes of metres to dozens of metres, causing the sea floor to be alternately at and below the mean sea level. Its clearest expression is in the FRKT section, but it can also be discriminated in the PRA section (cf. high-stand intervals in the *Palmatolepis minuta minuta* Zone).

Finally, the presence of numerous stromatactis-type early-diagenetic cavities has led us to interpret the microbialites as repeated mud-mound deposits on decimetric to metric scale (the thickness of a bed-set). Under conditions of favorable energy and climate during transgressive and high-stand intervals, roofs of mud mounds were colonized by bivalves, brachiopods and algae (with associated pelagic organisms). During periods of low stand, tops of mud mounds were frequently eroded by exceptionally strong wave action producing rudstones or were covered by packstone and grainstone bed-sets generated by storm currents. During such high-energy phases, development of microbe carpets was inhibited.

Three transgressive-regressive cycles are discriminated during Frasnian Zone 13b in the Carnic Alps. The regressive trend of the last cycle persisted throughout all of Frasnian Zone 13c when the basin reached a low-stand condition that was followed by a transgressive phase at the base of the Famennian, immediately above the Fr-Fm boundary. De Vleeschouwer et al. (2017) reported that their time-scale indicates that 600 kyr separate the lower and upper Kellwasser positive $\delta^{13}C$ excursions - equivalent to the interval embracing uppermost Frasnian Zone 12 to uppermost Zone 13c. Consequently, the T-R cycles were of high frequency and possibly of fourth order. Values of the same order of magnitude but slightly different are reported by Da Silva et al. (2020) and Racki (2020). According to Percival et al. (2022) the UKW began ~ 150 kyr before the end of the Frasnian.

SUPPLEMENTARY ONLINE MATERIAL

Supplementary data of this work are available on the BSPI website at: https://www.paleoitalia.it/bollettino-spi/bspi-vol-622/

ACKNOWLEDGEMENTS

This contribution owes much to the impetus provided by Enzo Farabegoli, our late, amazingly versatile friend, co-author and former professor at the Università di Bologna. Unique to him was an otherworldliness of genius that came across in everything he did. No matter what role he played, whether as a team member or as a hyperproductive loner, he was always himself, unique. We have lost an inimitable friend.

For helpful comments and suggestions, we thank Gilbert Klapper, formerly of the University of Iowa and mentor of many, a researcher of unique intelligence who greatly raised the standards of conodont biostratigraphy including the interval through the Late Devonian Kellwasser extinction events, the focus of this paper. We are grateful to John Alfred Talent of the Macquarie University in Sydney for conspicously improving of the manuscript, helpful suggestions and patient help. We thank Andrew Simpson of the Macquarie University in Sydney who provided a first useful and positive review of the manuscript. Beniamino Costantini, one of Enzo's former students, assisted in the field, slicing and sampling the rock sequences using a heavy electric cutting machine. Fabio Gamberini (Università di Bologna) produced the large-format thin sections. Our Bologna colleagues, Marco Del Monte and Stefano Claudio Vaiani produced photomicrographs of thin sections. Stefano Claudio patiently helped us for realizing Figs 14 and 15. Paolo Ferrieri (Università di Bologna) and Agostino Rizzi (CNR, Università di Milano) took SEM photos of conodonts. Giuseppe Onorevoli, one of Enzo's former PhD students, meticulously corrected Fig. 6. We thank our reviewers Gilbert Klapper (University of Iowa) and Carlo Corradini (Università di Trieste) for the extremely meticulous review and fruitfull suggestions. We are grateful to our Università di Bologna students for help in the field, acid-leaching rocks and picking acid-insoluble residues for

conodonts. Financial support came from the Università di Bologna (Grants ex 60% 1990-2001 to Maria Cristina Perri, RFO 2007-2009 to Enzo Farabegoli and Maria Cristina Perri, RFO 2007-2011 to Claudia Spalletta).

REFERENCES

Balter V., Renaud S., Girard C. & Joachimski M.M. (2008). Record of climate-driven morphological changes in 376 Ma Devonian fossils. *Geology*, 36: 907-910.

Becker R.T., Feist R., Flajs G., House M.R. & Klapper G. (1989). Frasnian-Famennian extinction events in the Devonian at Coumiac, southern France. *Comptes Rendus de l'Academie des Sciences Paris*, Series II, 309: 259-266.

Becker R.T., Marshall J.E.A. & Da Silva A.-C. (with contributions by Agterberg F.P., Gradstein F.M. & Ogg J.G.) (2020). Chapter 22 - The Devonian Period. *In* Gradstein F.M., Ogg J.G., Schmitz M.D. & Ogg G.M. (eds). The Geologic Time Scale, 2. Elsevier, Amsterdam: 733-810.

Belka Z. & Wendt J. (1992). Conodont biofacies patterns in the Kellwasser Facies (upper Frasnian/lower Famennian) of the eastern Anti-Atlas, Morocco. *Palaeogeography, Palaeoclimatology, Palaeoecology*, 91: 143-173.

Bischoff G. (1956). Oberdevonische Conodonten (to I delta) aus dem Rhenischen Schiefergebirge. *Notizblatt des Hessischen Landesamtes für Bodenforschung zu Wiesbaden*, 84: 115-137.

Bond D. & Wignall P.B. (2005). Evidence for Late Devonian (Kellwasser) anoxic events in the Great Basin, western United States. *In* Over D.J., Morrow J.R. & Wignall P.B. (eds), Understanding Late Devonian and Permian-Triassic Biotic and Climatic Events: Towards an Integrated Approach. *Developments in Palaeontology and Stratigraphy*, 20, Elsevier, Amsterdam: 225-262.

Bond D.P.G. & Wignall P.B. (2008). The role of sea-level change and marine anoxia in the Frasnian-Famennian (Late Devonian) mass extinction. *Palaeogeography, Palaeoclimatology, Palaeoecology*, 263: 107-118.

Bond D.P.G. & Wignall P.B. (2014). Large igneous provinces and mass extinctions: An update. *In* Keller G. & Kerr A.C. (eds), Volcanism, Impacts, and Mass Extinctions: Causes and Effects. *Geological Society of America, Special Paper*, 505: 29-55.

Bond D., Wignall P.B. & Racki G. (2004). Extent and duration of marine anoxia during the Frasnian-Famennian (Late Devonian) mass extinction in Poland, Germany, Austria and France. *Geological Magazine*, 141: 173-193.

Branson E.B. & Mehl M.G. (1934). Conodonts from the Grassy Creek shale of Missouri. *Missouri University Studies*, 8: 171-259.

Bratton J.F., Berry W.B.N. & Morrow J.R. (1999). Anoxia pre-dates Frasnian-Famennian mass extinction horizon in the Great Basin, U.S.A. *Palaeogeography, Palaeoclimatology, Palaeoecology*, 154: 275-292.

Buggisch W., Rabien A. & Hühner G. (1978). Biostratigraphische Parallelisierung und Faziesvergleich von oberdevonischen Becken- und Schwellen- Profilen E Dillenburg. *Geologisches Jahrbuch Hessen*, 106: 53-115.

Carmichael S.K., Waters J.A., Suttner T.J., Kido E. & DeReuil A.A. (2014). A new model for the Kellwasser Anoxia Events (Late Devonian): Shallow water anoxia in an open oceanic setting in the Central Asian Orogenic Belt. *Palaeogeography, Palaeoclimatology, Palaeoecology*, 399: 394-403.

Chang J., Bai Z., Sun Y., Peng Y., Qin S. & Shen B. (2019). High resolution bio- and chemostratigraphic framework at the Frasnian-Famennian boundary: Implications for regional stratigraphic correlation between different sedimentary facies in South China. *Palaeogeography, Palaeoclimatology, Palaeoecology*, 531: 108-299.

Chen D. & Tucker M.E. (2003). The Frasnian-Famennian mass extinction: insights from high-resolution sequence stratigraphy and cyclostratigraphy in South China. *Palaeogeography, Palaeoclimatology, Palaeoecology*, 193: 87-111.

Claeys P., Kyte F.T., Herbosch A. & Casier J.-G. (1996). Geochemistry of the Frasnian-Famennian boundary in Belgium: Mass extinction, anoxic oceans and microtektite layer, but not much iridium. *Geological Society of America, Special Paper*, 307: 491-504.

Cooper C.L. (1931). New conodonts from the Woodford Formation of Oklahoma. *Journal of Paleontology*, 5: 230-243.

Coplen T.B. (1995). Reporting of stable hydrogen, carbon, and oxygen isotopic abundances. *Geothermics*, 24: 707-712.

Coplen T.B., Brand W.A., Gehre M., Groening M., Meijer H.A.J., Toman B. & Verkouteren R.M. (2006). New Guidelines for $\delta^{13}C$ Measurements. *Analytical Chemestry*, 78: 2439-41.

Copper P. (1998). Evaluating the Frasnian-Famennian mass extinction: comparing brachiopod faunas. *Acta Palaeontologica Polonica*, 43: 137-154.

Copper P. (2002). Reef development at the Frasnian-Famennian mass extinction boundary. *Palaeogeography, Palaeoclimatology, Palaeoecology*, 181: 27-66.

Corradini C. (1998). New Devonian (Famennian) taxa of Polygnathids and Icriodids (Conodonts) from Sardinia. *Giornale di Geologia*, 60, Special Issue: 89-92.

Corradini C. & Pondrelli M. (2021). The Pre-Variscan Sequence of the Carnic Alps (Italy and Austria). *Geological Field Trips and Maps*, 13: 1-72.

Corradini C. & Suttner T.J. (eds) (2015). The pre-Variscan sequence of the Carnic Alps (Austria and Italy). *Abhandlungen der Geologischen Bundesanstalt*, 69: 1-158.

Corradini C., Suttner T.J., Ferretti A., Pohler S.M.L., Pondrelli M., Schönlaub H.P., Spalletta C. & Venturini C. (2015). The Pre-Variscan sequence of the Carnic Alps - an introduction. *In* Corradini C. & Suttner T.J. (eds), The Pre-Variscan sequence of the Carnic Alps (Austria and Italy). *Abhandlungen der Geologischen Bundesanstalt*, 69: 7-15.

Corradini C., Kido E., Suttner T.J., Simonetto L., Pondrelli M., Corriga M.G. & Spalletta C. (2019). Devonian reefs of the Carnic Alps and related environments. 13th International Symposium on Fossil Cnidaria and Porifera, Modena, 3-6 September 2019. Pre-Conference field Trip. 24 pp. Modena.

Corradini C., Pondrelli M., Simonetto L. & Corriga M.G. (2020). Geology of Mount Zermula Massif (Carnic Alps, Ne Italy). *Gortania*, 42: 5-24.

Courtillot V. & Olson P. (2007). Mantle plumes link magnetic superchrons to Phanerozoic mass depletion events. *Earth Planetary Science Letters*, 260: 495-504.

Da Silva A.-C., Sinnesael M., Claeys P., Davies J.H.F.L., deWinter N.J., Percival L.M.E., Schaltegger U. & De Vleeschouwer D. (2020). Anchoring the Late Devonian mass extinction in absolute time by integrating climatic controls and radio-isotopic dating. *Scientific Reports*, 10: 12940.

De Vleeschouwer D., Da Silva A.-C., Sinnesael M., Chen D., Day J.E., Whalen M.T., Guo Z. & Claeys P. (2017). Timing and pacing of the Late Devonian mass extinction event regulated by eccentricity and obliquity. *Nature Communications*, 8, 2268: 1-11.

Dreesen R. & Dusar M. (1974). Refinement of conodont-biozonation in the Famenne area. *In* Bouckaert J.P. & Street M. (eds), International Symposium on Belgian Micropalaeontological Limits, Namur 1974. *Geological Survey of Belgium*, 13: 1-38.

Ellwood B.B., Benoist S.L., El Hassani A., Wheeler C. & Crick R.E. (2003). Impact ejecta layer from the mid-Devonian: Possible connection to global mass extinctions. *Science*, 300: 1734-1737.

Epstein A.G., Epstein J.B. & Harris L.D. (1977). Conodont color alteration – An index to organic metamorphism. *U.S. Geological Survey professional paper*, 995: 1-27.

Feist R. & Klapper G. (1985). Stratigraphy and conodonts in pelagic sequences across the Middle-Upper Devonian boundary, Montagne Noire, France. *Palaeontographica Abteilung A*, 188: 1-18.

Ferrari A. & Vai G.B. (1966). Ricerche stratigrafiche e paleoecologiche al Monte Zermula (Alpi Carniche). *Giornale di Geologia*, 33[1965]: 389-415.

Ferrari A. & Vai G.B. (1973). Revision of the Famennian Rhynchonellid genus *Plectorhynchella*. *Giornale di Geologia*, Serie 2, 39: 163-220.

Ferretti A., Corriga M.G., Slavík L. & Corradini C. (2022). Running across the Silurian/Devonian Boundary along Northern Gondwana: A Conodont Perspective. *Geosciences*, 12: 43.

Ferretti A., Schönlaub H.P., Sachanski V., Bagnoli G., Serpagli E., Vai G.B., Yanev S., Radonjić M., Balica C., Bianchini L., Colmenar J. & Gutiérrez-Marco J.C. (2023). A global view on the Ordovician stratigraphy of southeastern Europe. *In* Harper D.A.T., Lefebvre B., Percival I.G. & Servais T. (eds), A Global Synthesis of the Ordovician System: Part 1. *Geological Society, London, Special Publications*, 532: 465-499.

Franke W., Cocks L.R.M. & Torsvik T.H. (2017). The Palaeozoic Variscan oceans revisited. *Gondwana Research*, 48: 257-284.

Gereke M. (2007). Die oberdevonische Kellwasser-Krise in der Beckenfazies von Rhenoherzynikum und Saxothuringikum (spätes Frasnium/frühestes Famennium, Deutschland). *Kölner Forum für Geologie und Paläontologie*, 17: 1-228.

Gereke M. & Schindler E. (2012). "Time-Specific Facies" and biological crises - The Kellwasser Event interval near the Frasnian/Famennian boundary (Late Devonian). *Palaeogeography, Palaeoclimatology, Palaeoecology*, 367-368: 19-29.

Girard C. & Lecuyer C. (2002). Variations in Ce anomalies of conodonts through the Frasnian/Famennian boundary of Poland (Kowala - Holy Cross Mountains: Implications for the redox state of seawater and biodiversity. *Palaeogeography, Palaeoclimatology, Palaeoecology*, 181: 209-311.

Girard C. & Renaud S. (2007). Quantitative conodont-based approaches for correlation of the Late Devonian Kellwasser anoxic events. *Palaeogeography, Palaeoclimatology, Palaeoecology*, 250: 114-125.

Girard C., Klapper G. & Feist R. (2005). Subdivision of the terminal Frasnian *linguiformis* conodont Zone, revision of the correlative interval of Montagne Noire Zone 13, and discussion of stratigraphically significant associated trilobites. *In* Over D.J., Morrow J.R. & Wignall P.B. (eds), Understanding Late Devonian and Permian-Triassic Biotic and Climatic Events: Towards an Integrated Approach. *Developments in Palaeontology and Stratigraphy*, 20, Elsevier, Amsterdam: 181-198.

Girard C., Cornee J.-J., Charruault A.-L., Corradini C., Weyer D., Bartzsch K., Joachimski M. & Feist R. (2017). Conodont biostratigraphy and palaeoenvironmental trends during the Famennian (Late Devonian) in the Thuringian Buschteich section (Germany). *Newsletters on Stratigraphy*, 50: 71-89.

Girard C., Charruault A.-L., Gluck T., Corradini C. &. Renaud S. (2022). Deciphering the morphological variation and its ontogenetic dynamics in the Late Devonian conodont *Icriodus alternatus. Fossil Record*, 25: 25-41.

Glikson A.Y., Mory A.J., Iasky R.P., Pirajno F., Golding S.D. & Uysal I.T. (2005). Woodleigh, southern Carnarvon Basin, Western Australia: history of discovery, Late Devonian age, and geophysical and morphometric evidence for a 120 km-diameter impact structure. *Australian Journal of Earth Science*, 52: 545-553.

Golonka J. (2020). Late Devonian paleogeography in the framework of global plate tectonics. *Global and Planetary Change*, 186: 1-19.

Goodfellow W.D., Geldsetzer H., Mclaren D.J., Orchard M.J. & Klapper G. (1989). Geochemical and isotopic anomalies associated with the Frasnian-Famennian extinction. *Historical Biology*, 2: 51-72.

Hallam A. (2004). Catastrophes and Lesser Calamities. The Causes of Mass Extinctions. 274 pp. Oxford University Press, Oxford.

Hallam A. & Wignall P.B. (1997). Mass Extinctions and Their Aftermath. 320 pp. Oxford University Press, New York.

Han Y. (1987). Study on Upper Devonian Frasnian/Famennian boundary in Ma-Anshan, Zhongping, Xiangzhou, Guangxi. *Chinese Academy of Geological Sciences Bulletin*, 17: 171-194.

Helms J. (1959). Conodonten aus dem Saalfelder Oberdevon (Thuringen). *Geologie*, 8: 634-677.

Helms J. (1963). Zur "Phylogenese" und Taxionomie von *Palmatolepis* (Conodontida, Oberdevon). *Geologie*, 12: 449-485.

Hillbun K., Playton T.E., Tohver E., Ratcliffe K., Trinajstic K., Roelofs B., Caulfield-Kerney S., Wray D., Haines P., Hocking R., Katz D., Montgomery P. & Warda P. (2015). Upper Kellwasser carbon isotope excursion pre-dates the F-F boundary in the Upper Devonian Lennard Shelf carbonate system, Canning Basin, Western Australia. *Palaeogeography, Palaeoclimatology, Palaeoecology*, 438: 180-190.

House M.R. (2002). Strength, timing, setting and cause of Mid-Palaeozoic extinctions. *Palaeogeography, Palaeoclimatology, Palaeoecology*, 181: 5-25.

House M.R., Becker R.T., Feist R., Flajs G., Girard C. & Klapper G. (2000). The Frasnian/Famennian boundary GSSP at Coumiac, southern France. *Courier Forschungsinstitut Senckenberg*, 225: 59-75.

Huang C. & Gong J. (2016). Timing and patterns of the Frasnian-Famennian event: Evidences from high-resolution conodont biostratigraphy and event stratigraphy at the Yangdi section, Guangxi, South China. *Palaeogeography, Palaeoclimatology, Palaeoecology*, 448: 317-338.

Huang C., Joachimski M.M. & Gong Y. (2018a). Did climate changes trigger the Late Devonian Kellwasser Crisis? Evidence from a high-resolution conodont $\delta^{18}O_{PO4}$ record from South China. *Earth Planetary Science Letters*, 495: 174-184.

Huang C., Song J., Shend J. & Gong Y. (2018b). The influence of the Late Devonian Kellwasser events on deep-water ecosystems: Evidence from palaeontological and geochemical records from South China. *Palaeogeography, Palaeoclimatology, Palaeoecology*, 504: 60-74.

Ji Q. (1989). On the Frasnian conodont biostratigraphy in the Guilin area Quangxi, South China. *Courier Forschungsinstitut Senckenberg*, 117: 303-319.

Ji Q. & Ziegler W. (1993). The Lali section: an excellent reference section for Late Devonian in south China. *Courier Forschungs-institut Senckenberg*, 157: 1-183.

Joachimski M.M. & Buggish W. (1993). Anoxic events in the Late Frasnian - causes of the Frasnian-Famennian Faunal crisis. *Geology*, 21: 675-678.

Joachimski M.M. & Buggisch W. (2002). Conodont apatite $\delta^{18}O$ signatures indicate climatic cooling as a trigger of the Late Devonian mass extinction. *Geology*, 30: 711-714.

Joachimski M.M., Buggisch W. & Anders T. (1994). Microfazies, Conodontenstratigraphie und Isotopengeochemic des Frasne/Famenne Grenzprofils Wolayer Glitscher (Karnische Alpen). *Abhandlungen der Geologischen Bundesanstalt*, 50: 183-195.

Joachimski M.M., Ostertag-Henning C., Pancost R.D., Strauss H., Freeman K.H., Littke R., Sinninghe-Damsté J.S. & Racki G. (2001). Water column anoxia, enhanced productivity and concomitant changes in $\delta^{13}C$ and $\delta^{34}S$ across the Frasnian -Famennian boundary (Kowala - Holy Cross Mountains/Poland). *Chemical Geology*, 175: 109-131.

Joachimski M.M., Pancost R.D., Freeman K.H., Ostertag-Henning C. & Buggisch W. (2002). Carbon isotope geochemistry of the Frasnian -Famennian transition. *Palaeogeography, Palaeoclimatology, Palaeoecology*, 181: 91-109.

Joachimski M.M., van Geldern R., Breisig S., Buggisch W. & Day J. (2004). Oxygen isotope evolution of biogenic calcite and apatite during the Middle and Upper Devonian. *International Journal of Earth Sciences*, 93: 542 -553.

Joachimski M.M., Breisig S., Buggisch W., Talent J.A., Mawson R., Gereke M., Morrow J.R., Day M.J. & Weddige K. (2009). Devonian climate and reef evolution: Insights from oxygen isotopes in apatite. *Earth Planetary Science Letters*, 284: 599-609.

Johnson J.G. & Sandberg C.A. (1989). Devonian eustatic events in the western United States and their biostratigraphic responses. *Canadian Society Petroleum Geologists*, 14 [1988]: 171-178.

Johnson J.G., Klapper G. & Sandberg C.A. (1985). Devonian eustatic fluctuations in Euramerica. *Geological Society of America Bulletin*, 96: 567-558.

Kaufmann B., Trapp E. & Mezger K. (2004). The numerical age of the Upper Frasnian (Upper Devonian) Kellwasser Horizons: A new U-Pb Zircon date from Steinbruch Schmidt (Kellerwald, Germany). *Journal of Geology*, 112: 495-501.

Khrustchevae N. & Kuz'min A.V. (1996). New upper Frasnian species of *Palmatolepis* (Conodonta) from the Lyaiol Formation of southern Timan. *Paleontological Journal*, 30: 455-458. [Translated from *Paleontologicheskiy Zhurnal*, 1996: 90-93].

Kido E., Pohler S.M.L., Pondrelli M., Schönlaub H.P., Simonetto L., Spalletta C. & Suttner T.J. (2015). Kellergrat Formation. *In* Corradini C. & Suttner T.J. (eds), The Pre-Variscan sequence of the Carnic Alps (Austria and Italy). *Abhandlungen der Geologischen Bundesanstalt*, 69: 101-104.

Klapper G. (1985). Sequence in conodont genus *Ancyrodella* in Lower *asymmetricus* Zone (earliest Frasnian, Upper Devonian) of the Montagne Noire, France. *Palaeontographica Abt A*, 188: 19-34.

Klapper G. (1989). The Montagne Noire Frasnian (Upper Devonian) conodont succession. *In* McMillan N.J., Embry A.F. & Glass D.J. (eds), Devonian of the World, Calgary. *Canadian Society Petroleum Geologists*, 14 [1988]: 449-468.

Klapper G. (1997). Graphic correlation of Frasnian (Upper Devonian) sequences in Montagne Noire, France, and western Canada. *In* Klapper G., Murphy M.A. & Talent J.A. (eds), Paleozoic sequence stratigraphy, biostratigraphy, and biogeography: Studies in Honor of J. Granville ("Jess") Johnson. *Geological Society of America, Special Paper*, 321: 113-129.

Klapper G. (2007a). Frasnian (Upper Devonian) conodont succession at Horse Spring and correlative sections, Canning Basin, Western Australia. *Journal of Geology*, 81: 513-537.

Klapper G. (2007b). Conodont Taxonomy and the recognition of the Frasnian/Famennian (Upper Devonian) Stage Boundary. *Stratigraphy*, 4: 67-76.

Klapper G. & Becker R.T. (1999). Comparison of Frasnian (Upper Devonian) Conodont Zonations. *Bollettino della Società Paleontologica Italiana*, 37: 339-348.

Klapper G. & Foster C.T. Jr (1986). Quantification of outlines in Frasnian (Upper Devonian) platform conodonts. *Canadian Journal of Earth Sciences*, 23: 1214-1222.

Klapper G. & Foster C.T. Jr (1993). Shape analysis of Frasnian species of the Late Devonian conodont genus *Palmatolepis. Journal of Paleontology*, 32: 1-35.

Klapper G. & Kirchgasser W.T. (2016). Frasnian Late Devonian conodont biostratigraphy in New York: graphic correlation and taxonomy. *Journal of Paleontology*, 90: 525-554.

Klapper G. & Lane H.R. (1985). Upper Devonian (Frasnian) Conodonts of the *Polygnathus* biofacies, N.W.T. *Canada Journal of Paleontology*, 59: 904-951.

Klapper G., Feist R., Becker R.T. & House M.R. (1994). Definition of the Frasnian/Famennian Stage boundary. *Episodes*, 16 [1993]: 433-441.

Klapper G., Kirchgasser W.T. & Baesemann J.F. (1995). Graphic correlation of a Frasnian (Upper Devonian) composite standard. *In* Mann K.O. & Lane R.H. (eds), Graphic correlation. *SEPM Special Publication*, 53: 177-184.

Klapper G., Kuz'min A.V. & Ovnatanova N.S. (1996). Upper Devonian conodonts from the Timan-Pechora region, Russia, and correlation with a Frasnian composite standard. *Journal of Paleontology*, 70: 131-152.

Klapper G., Uyeno T.T., Armstrong D.K. & Telford P.G. (2004). Conodonts of the Williams Island and Long Rapids formations (Upper Devonian, Frasnian-Famennian) of the Onakawana B Drillhole, Moose River Basin, northern Ontario, with a revision of Lower Famennian species. *Journal of Paleontology*, 78: 371-387.

Königshof P., Narkiewicz K., Phuong T.H., Carmichael S. & Waters J. (2017). Devonian events: examples from the eastern Palaeotethys (Si Phai section, NE Vietnam). *In* Mottequin B., Slavik L. & Königshof P. (eds), Climate change and biodiversity patterns in the mid-Palaeozoic. Proceedings-Volume IGCP 596/SDS Meeting Brussels (2015). *Palaeobiodiversity and Palaeoenvironments*, 97: 481-496.

Kononova L.J., Alekseev A.S., Barskov J.S. & Reimers A.N. (1996). New species of polygnathid conodonts from the Frasnian of the Moscow syncline. *Paleontological Journal*, 30: 459-465.

Kooij van der B., Immenhauser A., Steuber T., Hagmaier M., Bahamonde J.R., Samankasou E. & Tomé O.M. (2007). Marine red staining of a Pensylvanian carbonate slope: environmental and oceanographic significance. *Journal of Sedimentary Research*, 77: 1026-1045.

Kreutzer L.H. (1990). Mikrofazies, Stratigraphie und Paläogeographie des Zentralkarnischen Hauptkammes zwischen Seewarte und Cellon. *Jahrbuch der Geologischen Bundesanstalt*, 133: 275-234.

Kreutzer L.H. (1992). Photoatlas zu den varizischen Karbonat-Gesteinen der Karnischen Alpen (Österreich/Italien). *Abhandlungen der Geologischen Bundesanstalt*, 47: 1-129.

Le Houdec S., Girard C. & Balter V. (2013). Conodont Sr/Ca and $\delta^{18}O$ record seawater changes at the Frasnian-Famennian boundary. *Palaeogeography, Palaeoclimatology, Palaeoecology*, 376: 114-121.

Lüddecke F., Hartenfels S. & Becker R.T. (2017). Conodont biofacies of a monotonous middle Famennian pelagic carbonate succession (Upper Ballberg Quarry, northern Rhenish Massif). *Palaeodiversity and Palaeoenvironments*, 97: 591-613.

Matyja H. (1993). Upper Devonian of Western Pomerania. *Acta Geologica Polonica*, 43: 27-94.

McGhee G.R. (2005). Testing Late Devonian extinction hypotheses. *In* Over D.J., Morrow J.R. & Wignall P.B. (eds), Understanding Late Devonian and Permian -Triassic biotic and climatic events: towards an integrated approach. *Developments in Palaeontology and Stratigraphy*, 20: 37-50.

Miller A.K. & Youngquist W.L. (1947). Conodonts from the type section of the Sweetland Creek Shale in Iowa. *Journal of Paleontology*, 21: 501-517.

Mottequin B. & Poty E. (2015). Kellwasser horizons, sea-level changes and brachiopod -coral crises during the late Frasnian in the Namur -Dinant Basin (southern Belgium): a synopsis. *In* Becker R.T., Königshof P. & Brett C.E. (eds), Devonian Climate, Sea Level and Evolutionary Events. *Geological Society of London, Special Publications*, 423: 235-250.

Müller K.J. (1956). Zur Kenntnis der Conodonten-Fauna des europaischen Devons, 1; Die Gattung Palmatolepis. *Abhandlunghen and Senckenbergischen Naturforschenden Gesellschaft*, 494: 1-70.

Müller K.J. & Müller E.M. (1957). Early Upper Devonian (Independence) conodonts from Iowa, Pt. 1. *Journal of Paleontology*, 31: 1069-1108.

Obukhovskaya T.G. & Kuz'min A.V. (1993). Spores and Conodonts from the Boundary Beds of the upper Frasnian and lower Famennian of the Ukhta-Tebukskii Region. *Palinologic Method in Geology. Collected papers* (IGiRGI, Institut Geologii i Razrabotki Goryuchih Iskopaemih, Moscow): 35-49 [in Russian].

Olempska E. (2002). The Late Devonian Upper Kellwasser Event and entomozoacean ostracods in the Holy Cross Mountains, Poland. *Acta Palaeontologica Polonica*, 47: 247-266.

Over D.J. (2002). The Frasnian/Famennian boundary in central and eastern United States. *Palaeogeography, Palaeoclimatology, Palaeoecology*, 18: 153-169.

Over D.J. & Schindler E. (2003). Depositional similarities in selected Late Devonian Kellwasser Horizons: Germany, Morocco, and Eastern United States. *Geological Society of America,* Abstracts with programs, 35: 384.

Over D.J., Conaway C.A., Katz D.J., Goodfellow W.D. & Gregoire D.C. (1997). Platinum group element enrichments and possible

chondritic Ru: Ir across the Frasnian-Famennian boundary, western New York State. *Palaeogeography, Palaeoclimatology, Palaeoecology*, 132: 399-410.

Ovnatanova N.S. (1969). New Upper Devonian conodonts from the central regions of the Russian Platform and Timan, *Trudy Vsesoyuznogo Neftianogo Nauchno-Issledovatel'skogo Geologorazvedochnogo Instituta, Novaja Serija*, 93 (Fauna and Stratigraphy of the Paleozoic of the Russian Platform): 139-141.

Ovnatanova N.S. & Kononova L.I. (1996). Some new Frasnian species of *Polygnathus* genus (Conodonta) from the Central part of the Russian Platform. *Paleontologicheskii Zhurnal*, 1: 54-60 [in Russian].

Pas D., Da Silva A.-C., Suttner T.J., Kido E., Bultynck P., Pondrelli M., Corradini C., De Vleeschouwer D., Dojen C. & Boulvain F. (2014). Insight into the development of a carbonate platform through a multi-disciplinary approach: a case study from the Upper Devonian slope deposits of Mount Freikofel (Carnic Alps, Austria/Italy). *International Journal of Earth Science* (Geol Rundsch), 103: 519-538.

Percival L.M.E., Marynowski L., Baudin F., Goderis S., DeVleeschouwer D., Rakociński M., Narkiewicz K., Corradini C., Da Silva A.-C. & Claeys P. (2022). Combined nitrogen-isotope and cyclostratigraphy evidence for temporal and spatial variability in Frasnian-Famennian environmental change. *Geochemistry, Geophysics, Geosystems,* 23: e2021GC010308.

Perri M.C. & Spalletta C. (1998). The Frasnian-Famennian boundary at the Pramosio A section (Carnic Alps, Italy). *In* Perri M.C. & Spalletta C. (eds), Southern Alps Field Trip Guidebook, ECOS VII. *Giornale di Geologia*, Special Issue, 60: 198-205.

Pölsler P. (1969). Conodonten aus dem Devon der Karnischen Alpen (Findenigkofel, Österreich). *Jahrbuch der Geologischen Bundesanstalt*, 112: 399-440.

Pondrelli M., Corradini C., Corriga M.G., Schönlaub H.P., Spalletta C., Pohler S.M.L., Mossoni A., Simonetto L., Suttner T.J., Perri M.C. & Kido E. (2015a). Kellerwand Formation. *In* Corradini C. & Suttner T.J. (eds), The Pre-Variscan sequence of the Carnic Alps (Austria and Italy). *Abhandlungen der Geologischen Bundesanstalt*, 69: 109-112.

Pondrelli M., Pas D., Spalletta C., Schönlaub H.P., Farabegoli E., Corradini C., Suttner T.J., Corriga M.G., Perri M.C., Da Silva A.C., Pohler S.M.L., Simonetto L., Dojen C., Mossoni A., Kido E. & Hüneke H. (2015b). Freikofel Formation. *In* Corradini C. & Suttner T.J. (eds), The Pre-Variscan sequence of the Carnic Alps (Austria and Italy). *Abhandlungen der Geologischen Bundesanstalt*, 69: 121-124.

Pondrelli M., Corradini C., Spalletta C., Simonetto L., Perri M.C., Corriga M.G., Venturini C. & Schönlaub H.P. (2020). Geological map and stratigraphic evolution of the central sector of the Carnic Alps (Austria-Italy). *Italian Journal of Geosciences*, 139: 469-484.

Racki G. (1993). Evolution of the bank to reef complex in the Devonian of the Holy Cross Mountains. *Acta Palaeontologica Polonica*, 37: 87-182.

Racki G. (2005). Towards understanding Late Devonian global events: few answers, many questions. *In* Over D.J., Morrow J.R. & Wignall P.B. (eds), Understanding Late Devonian and Permian-Triassic Biotic and Climatic Events. Towards an Integrated Approach. *Development in Palaeontology and Stratigraphy*, 20: 5-36.

Racki G. (2012). The Alvarez impact theory of mass extinction; limits to its applicability and the "great expectations syndrome". *Acta Palaeontologica Polonica*, 57: 681-702.

Racki G. (2020). A volcanic scenario for the Frasnian-Famennian major biotic crisis and other Late Devonian global changes: More answers than questions? *Global and Planetary Change*, 189: 103174.

Raumer von J.F. & Stampfli G.M. (2008). The birth of the Rheic Ocean - Early Paleozoic subsidence patterns and subsequent tectonic plate scenario. *Tectonophysics*, 461: 9-20.

Sandberg C.A. & Dreesen R. (1984). Late Devonian icriodontid biofacies models and alternate shallow water conodont zonation. *In* Clark D.L. (ed.), Conodont biofacies and provincialism. *Geological Society of America Special Paper*, 196: 143-178.

Sandberg C.A. & Ziegler W. (1973). Refinement of standard Upper Devonian conodont zonation based on sections in Nevada and West Germany. *Geologica et Palaeontologica*, 7: 97-122.

Sandberg C.A., Ziegler W., Dreesen R. & Butler J.L. (1988). Part 3: Late Frasnian mass extinction: conodont event stratigraphy, global changes, and possible causes. *Courier Forschungsinstitut Senckenberg*, 102: 263-307.

Sandberg C.A., Ziegler W., Dreesen R. & Butler J.L. (1992). Conodont biochronology, biofacies, taxonomy, and event stratigraphy around middle Frasnian Lion Mudmound (F2h), Frasnes, Belgium. *Courier Forschungsinstitut Senckenberg*, 150: 1-87.

Sandberg C.A., Morrow J.R. & Ziegler W. (2002). Late Devonian sea-level changes, catastrophic events, and mass extinctions. *In* Koeberl C. & MacLeod K.G. (eds), Catastrophic Events and Mass Extinctions: Impacts and Beyond. *Geological Society of America, Special Paper*, 356: 473-487.

Sannemann D. (1955). Beitrag zur Untergliederung des Oberdevons nach Conodonten. *Neues Jahrbuch für Geologie und Paläontologie, Abhandlungen*, 100: 324-331.

Savage N.M. & Funai C.A. (1980). Devonian conodonts of probable early Frasnian age from the Coronados Islands of southeastern Alaska. *Journal of Paleontology*, 54: 806-813.

Savage N.M., Sardsurd A. & Buggisch W. (2006). Late Devonian conodonts and the global Frasnian-Famennian extinction event, Thong Pha Phum, western Thailand. *Palaeoworld*, 15: 171-184.

Schindler E. (1990). Die Kellwasser-Krise (hohe Frasne-Stufe, Ober Devon). *Göttinger Arbeiten für Geologie und Paläontologie*, 46: 1-115.

Schindler E. (1993). Event-stratigraphic markers within the Kellwasser crisis near the Frasnian/Famennian boundary (Upper Devonian) in Germany. *Palaeogeography, Palaeoclimatology, Palaeoecology*, 104: 115-125.

Schindler E., Schülke I. & Ziegler W. (1998). The Frasnian/Famennian boundary at the Sessacker Trench section near Oberscheld (Dill Syncline, Rheinisches Schiefergebirge, Germany). *Lethaia*, 77: 243-261.

Schönlaub H.P. (1985). Das Palaozoikum der Karnischen Alpen. *In* Schönlaub H.P. (ed.), Arbeitstagung der Geologischen Bundesanstalt 1985 Kötschach-Mauthen, Gailtal. *Abhandlungen der Geologischen Bundesanstalt*, Wien: 34-52.

Schönlaub H.P. (1992). Stratigraphy, Biogeography and Paleoclimatology of the Alpine Paleozoic and its Implications for Plate Movements. *Abhandlungen der Geologischen Bundesanstalt*, 135: 381-418.

Schönlaub H.P. (1998). Review of the Paleozoic Paleogeography of the Southern Alps. The Perspective from the Austrian Side. *In* Perri M.C. & Spalletta C. (eds), Southern Alps field-trip guide-book, ECOS VII. *Giornale di Geologia*, Special Issue, 60: 59-68.

Schönlaub H.P. & Histon K. (2000). The Palaeozoic Evolution of the Southern Alps. *Mitteilungen der Österreichische Geologische Gessellschaft,* 92: 15-34.

Schülke I. (1995). Evolutive Prozesse bei *Palmatolepis* in der frühen Famenne-Stufe (Conodonta, Ober-Devon). *Göttinger Arbeiten für Geologie und Paläontologie*, 67: 1-108.

Schülke I. (1998). Conodont community structure around the Kellwasser mass extinction event (Frasnian/Famennian boundary interval). *Lethaia*, 77: 87-99.

Schülke I. (1999). Conodont multielement reconstructions from the early Famennian (Late Devonian) of the Montagne Noire (southern France). *Geologica et Palaeontologica*, 3: 1-123.

Scotese C.R. (1997). Continental Drift Flip Book, 7th edition. 80 pp. University of Texas, Arlington, Texas.

Scotese C.R. (2001). Atlas of Earth History, PALEOMAP Project. 52 pp. University of Texas, Arlington, Texas.

Selli R. (1963). Schema geologico delle Alpi Carniche e Giulie occidentali. *Giornale di Geologia*, 30: 1-136.

Song H., Song H., Algeo T.J., Tong J., Romaniello S.J., Zhu Y., Chu D., Gong Y. & Anbar A.D. (2017). Uranium and carbon isotopes document global-ocean redox-productivity relationships linked to cooling during the Frasnian-Famennian mass extinction. *Geology*, 45: 887-890.

Spalletta C. & Venturini C. (1995). Late Devonian-Early Carboniferous syn-sedimentary tectonic evolution of the Paleocarnic domain (southern Alps, Italy). *Giornale di Geologia*, 56[1994]: 211-222.

Spalletta C., Vai G.B. & Venturini C. (1982). La Catena Paleocarnica. *In* Castellarin A. & Vai G.B. (eds), Guida alla geologia del Sudalpino centro-orientale. Guide Geologiche Regionali, Società Geologica Italiana: 281-292.

Spalletta C., Perri M.C. & Vai G.B. (1983). Pattern of conodont reworking in the Upper Devonian of the Alps: palaeoenvironmental and palaeotectonic implication. *Lethaia*, 16: 51-66.

Spalletta C., Ferrari A., Kido E., Perri M.C., Pohler S.M.L., Pondrelli M., Schönlaub H.P., Suttner T.J. & Vai G.B. (2015a). Creta di Collina Formation. *In* Corradini C. & Suttner T.J. (eds), The Pre-Variscan sequence of the Carnic Alps (Austria and Italy). *Abhandlungen der Geologischen Bundesanstalt*, 69: 105-108.

Spalletta C., Perri M.C., Pondrelli M., Corradini C., Mossoni A. & Schönlaub H.P. (2015b). Pal Grande Formation. *In* Corradini C. & Suttner T.J. (eds), The Pre-Variscan sequence of the Carnic Alps (Austria and Italy). *Abhandlungen der Geologischen Bundesanstalt*, 69: 137-14.

Spalletta C., Perri M.C., Over D. & Corradini C. (2017). Famennian (Upper Devonian) conodont zonation: revised global standard. *Bullettin of Geoscience*, 92: 31-57.

Stauffer C. R. (1938). Conodonts of the Olentangy Shale. *Journal of Paleontology*, 12: 411-433.

Ulrich E.O. & Bassler R.S. (1926). A classification of the tooth-like fossils, conodonts, with descriptions of American Devonian and Mississippian species. *Proceedings of the United States National Museum*, 68: 1-63.

Vai G.B. (1976). Stratigrafia e paleogeografia ercinica delle Alpi. *Memorie della Società Geologica Italiana*, 13: 7-37.

Vai G.B. (1991). Palaezoic strike-slip rift pulses and palaeogeography in the circum-Meditarranean Tethyan realm. *Palaeogeography, Palaeoclimatology, Palaeoecology*, 87: 223-252.

Venturini C. (1990). Geologia delle Alpi Carniche centro-orientali. 220 pp. *Pubblicazioni del Museo Friulano di Storia Naturale*, 36, Udine.

Venturini C. (1991). Introduction to the geology of the Pramollo Basin (Carnic Alps) and its surroundings. *In* Venturini C. (ed.), Workshop Proceedings on Tectonics and Stratigraphy of the Pramollo Basin (Carnic Alps). *Giornale di Geologia*, 53: 13-47.

Venturini C. & Spalletta C. (1998). Remarks on the Palaeozoic stratigraphy and the Hercynian tectonics of the Palaeocarnic Chain (Southern Alps). *In* Perri M.C. & Spalletta C. (eds), Southern Alps field-trip guide-book, ECOS VII. *Giornale di Geologia*, Special Issue, 60: 69-88.

Walliser O.H. (1981). The geosynclinal development of the Rheinische Schiefergebirge. *Geologie en Mijnbouw*, 60: 89-96.

Walliser O.H. (1984). Geological processes and global events. *Terra Cognita*, 4: 17-20.

Walliser O.H. (1996). Global events in the Devonian and Carboniferous. *In* Walliser O.H. (ed.), Global Events and Event Stratigraphy in the Phanerozoic. Springer, Berlin: 225-250.

Walliser O.H., Gross-Uffenorde H., Schindler E. & Ziegler W. (1989). On the Upper Kellwasser Horizon (boundary Frasnian/Famennian). *Courier Forschungsinstitut Senckenberg*, 110: 247-255.

Yazdi M. (1999). Late Devonian-Carboniferous conodonts from Eastern Iran. *Rivista Italiana di Paleontologia e Stratigrafia*, 105: 167-200.

Youngquist W. (1945). Upper Devonian conodonts from the Independence Shale(?) of Iowa. *Journal of Paleontology*, 19: 355-367.

Youngquist W.L. & Peterson R.F. (1947). Conodonts from the Sheffield Formation of north-central Iowa. *Journal of Paleontology*, 21: 242-253.

Zhang J., Deng C., Liu W., Tang Z., Wangy Y., Ye T., Liang W. & Liu L. (2021). Mercury anomalies link to extensive volcanism across the Late Devonian Frasnian-Famennian boundary in South China. *Frontiers in Earth Science*, 9: 691827.

Zhao H., Shen J., Algeo T.J., Rackid G., Chen J., Huang C., Song J., Qie W. & Gong Y. (2022). Mercury isotope evidence for regional volcanism during the Frasnian-Famennian transition. *Earth and Planetary Science Letters*, 581: 117412.

Ziegler W. (1958). Conodontenfeinstratigraphische Untersuchungen an der Grenze Mitteldevon/Oberdevon und in der Adorfstufe. *Notizblatt des Hessischen Landesamtes für Bodenforschung*, 87: 7-77.

Ziegler W. (1960). Conodonten aus dem Rheinischen Untedevon (Gedinnium) des Remscheider sattels (Rheinisches Schiefergebirge). *Palaontologische Zeitschrift*, 34: 169-201.

Ziegler W. (1962). Taxionomie und Phylogenie Oberdevonischer Conodonten und ihre stratigraphische Bedeutung. *Abhandlungen des Hessischen Landesamtes für Bodenforschung*, 38: 1-166.

Ziegler W. & Huddle J.W. (1969). Die *Palmatolepis glabra*-Gruppe (Conodonta) nach der Revision der Typen von Ulrich & Bassler durch J. W. Huddle. *Fortschritte in der Geologie von Rheinland und Westfalen*, 16: 377-386.

Ziegler W. & Sandberg C.A. (1984). *Palmatolepis*-based revision of upper part of standard Late Devonian conodont zonation. *In* Clark D.L. (ed.), Conodont biofacies and provincialism. *Geological Society of America Special Paper*, 196: 179-194.

Ziegler W. & Sandberg C.A. (1990). The Late Devonian standard conodont zonation. *Courier Forschungsinstitut Senckenberg*, 121: 1-115.

Manuscript submitted 5 May 2023
Revised manuscript accepted 27 June 2023
Published online 23 September 2023
Editor Annalisa Ferretti

C O N O D O N T
P L A T E S

LEGEND TO THE PLATES

In Pls 1-16 abbreviations PRA and FRKT refer to Pramosio A section and Freikofel T section in the Carnic Alps.

Bed numbers refer to sampled beds (Figs 6, 14-16, Tabs 1-2, S3-S4 distribution charts).

Zone numbers refer to the Frasnian conodont zonation first developed in the Montagne Noire (Klapper, 1989) but since replicated at many sections in Devonian tropical areas (Klapper, 2007a). Zone names refer to the revised Famennian conodont zonation (Spalletta et al., 2017) based on the Famennian conodont biozonation of Sandberg & Ziegler (1990).

All figured specimens are P_1 elements.

EXPLANATION OF PLATE 1

Late Devonian conodonts from Pramosio A and Freikofel T sections, Carnic Alps. Scale bar corresponds to 500 μm.

Figs 1, 8-11 - *Ancyrodella hamata* Ulrich & Bassler, 1926.
1 - Upper (a) and lower (b) views of P216 245032, sample FRKT2, Frasnian Zone 13a.
8 - Upper (a) and lower (b) views of P178 212025, sample PRA0, Zone 12.
9 - Upper (a) and lower (b) views of P233 1823309, sample PRA5B, Zone 13b.
10 - Upper (a) and lower (b) views of P182 212053, sample PRA3, Zone 13a.
11 - Upper (a) and lower (b) views of P215 245030, sample FRKT5, Zone 13a.

Fig. 2 - *Ancyrodella ioides* Ziegler, 1958. Upper (a) and lower (b) views of P180 212044, sample PRA0, Zone 12.

Figs 3-7 - *Ancyrodella curvata* (Branson & Mehl, 1934).
3 - Lower (a) and upper (b) views of P215 245031, sample FRKT5, Zone 13a.
4 - Upper (a) and lower (b) views of P183 212060, sample PRA6BC, Zone 13b.
5 - Upper (a) and lower (b) views of P233 1823308, sample PRA5B, Zone 13b.
6 - Upper view of P223 922720, sample FRKT21D, Zone 13b.
7 - Upper view of P223 922719, sample FRKT21D, Zone 13b.

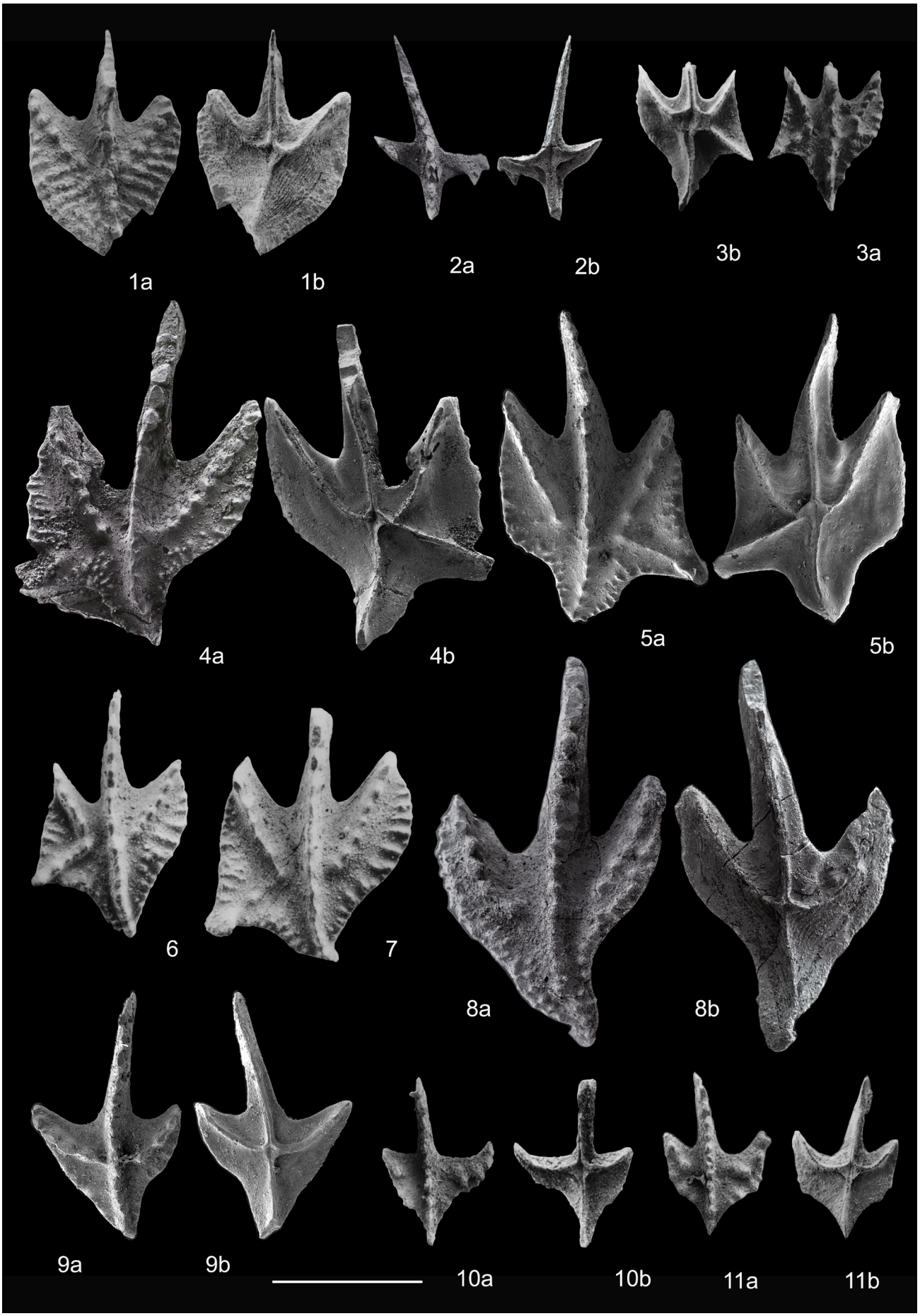
1a
1b
2a
2b
3b
3a
4a
4b
5a
5b
6
7
8a
8b
9a
9b
10a
10b
11a
11b

EXPLANATION OF PLATE 2

Late Devonian conodonts from Pramosio A and Freikofel T sections, Carnic Alps. Scale bar corresponds to 500 μm.

Figs 1-5 - *Icriodus alternatus alternatus* Branson & Mehl, 1934.
1 - Upper (a), lower (b) and lateral (c) views of P180 212046, sample PRA1, Frasnian Zone 12.
2 - Upper (a), lateral (b) and lower (c) views of P84 911276, sample PRA6, Zone 13b.
3 - Upper view of P223 922722, sample FRKT21D, Zone 13b.
4 - Upper (a) and lateral (b) views of P83 911269, sample PRA1, Zone 12.
5 - Upper (a), lateral (b) and lower (c) views of P180 212041, sample PRA10, *Pa. minuta minuta* Zone.

Fig. 6-8 - *Icriodus alternatus helmsi* Sandberg & Dreesen, 1984.
6 - Upper view of P240 1824006, sample PRA13, *Pa. minuta minuta* Zone.
7 - Upper (a) and lower (b) views of P240 1824004, sample PRA8B, *Pa. triangularis* Zone.
8 - Upper view of P223 922726, sample FRKT25, *Pa. triangularis* Zone.

Figs 9-13 - *Icriodus alternatus mawsonae* Yazdi, 1999.
9 - Upper view of P223 922725, sample FRKT21E, Zone 13c.
10 - Lower (a) and upper (b) views of P240 1824016, sample FRKT100, *Pa. crepida* Zone.
11 - Upper view of P240 1824009, sample PRA14, *Pa. minuta minuta* Zone.
12 - Upper (a) and lower (b) views of P240 1824007, sample PRA13, *Pa. minuta minuta* Zone.
13 - Upper view of P240 1824014, sample FRKT50, *Pa. minuta minuta* Zone.

Figs 14-16 - *Icriodus olivierii* Corradini, 1998.
14 - Upper (a) and lower (b) views of P240 1824012, sample PRA21, *Pa. rhomboidea* Zone.
15 - Upper (a) and lower (b) views of P240 1824013, sample PRA21, *Pa. rhomboidea* Zone.
16 - Upper (a) and lower (b) views of P240 1824011, sample PRA21, *Pa. rhomboidea* Zone.

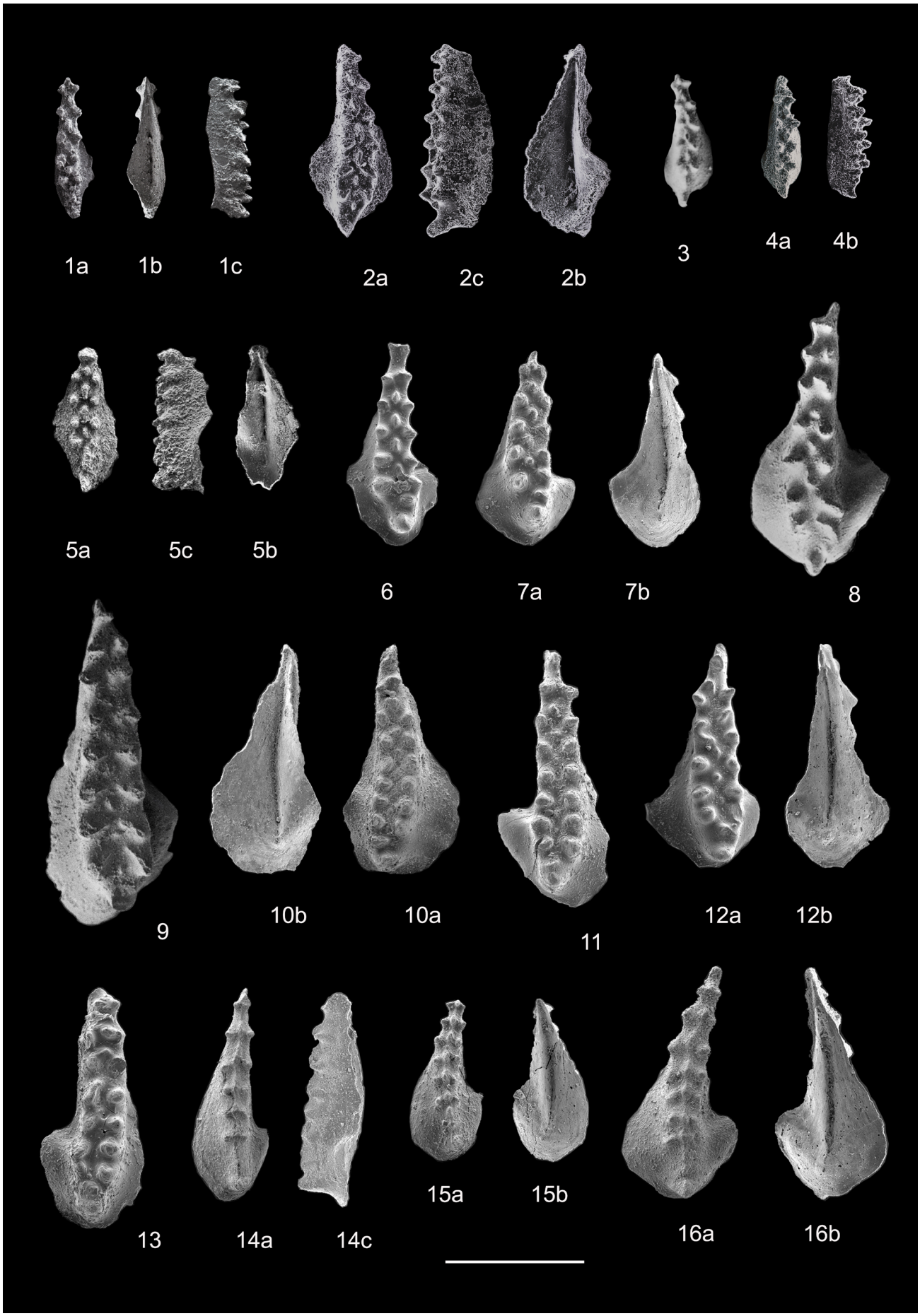
1a
1b
1c
2a
2c
2b
3
4a
4b
5a
5c
5b
6
7a
7b
8
9
10b
10a
11
12a
12b
13
14a
14c
15a
15b
16a
16b

EXPLANATION OF PLATE 3

Late Devonian conodonts from Pramosio A and Freikofel T sections, Carnic Alps. Scale bar corresponds to 500 μm.

Figs 1-4 - *Icriodus deformatus deformatus* Han, 1987.
1 - Upper (a) and lower (b) views of P240 1824003, sample PRA7B, *Pa. subperlobata* Zone.
2 - Upper view of P240 1824005, sample PRA12, *Pa. minuta minuta* Zone.
3 - Upper view of P223 922724, sample FRKT21E, Frasnian Zone 13c.
4 - Upper view of P223 922723, sample FRKT21E, Zone 13c.

Fig. 5 - *Icriodus multicostatus lateralis* Ji & Ziegler, 1993. Upper (a) and lateral (b) views of P240 1824017, sample FRKT132, *Pa. termini* Zone.

Figs 6-7 - *Icriodus deformatus asymmetricus* Ji, 1989.
6 - Upper (a) and lower (b) views of P240 1824002, sample PRA7A, *Pa. subperlobata* Zone.
7 - Upper view of P240 1824001, sample PRA6D, Zone 13c.

Fig. 8 - *Icriodus iowaensis iowaensis* Youngquist & Peterson, 1947. Upper view of P240 1824010, sample PRA20, *Pa. glabra prima* Zone.

Figs 9-10 - *Icriodus cornutus* Sannemann, 1955.
9 - Upper (a) and lateral (b) views of P240 1824008, sample PRA13, *Pa. minuta minuta* Zone.
10 - Upper (a), lower (b) and lateral (c) views of P240 1824015, sample FRKT72, *Pa. minuta minuta* Zone.

Figs 11-13 - *Pelekysgnathus planus* Sannemann, 1955.
11 - Upper (a) and lateral (b) views of P241 1824104, sample PRA13, *Pa. minuta minuta* Zone.
12 - Upper (a) and lateral (b) views of P241 1824102, sample PRA6B1A, Zone 13b.
13 - Lateral view of P241 1824103, sample PRA11B, *Pa. minuta minuta* Zone.

Fig. 14 - *Branmehla werneri* (Ziegler, 1962). Lateral view of P241 1824101, sample PRA30, *Pa. trachytera* Zone.

Fig. 15 - *Ancyrognathus amana* Müller & Müller, 1957. Lower (a) and upper (b) views of P84 911274, sample PRA6, Zone 13b.

Fig. 16 - *Ancyrognathus asymmetricus* (Ulrich & Bassler, 1926). Upper (a) and lower (b) views of P183 212059, sample PRA6, Zone 13b.

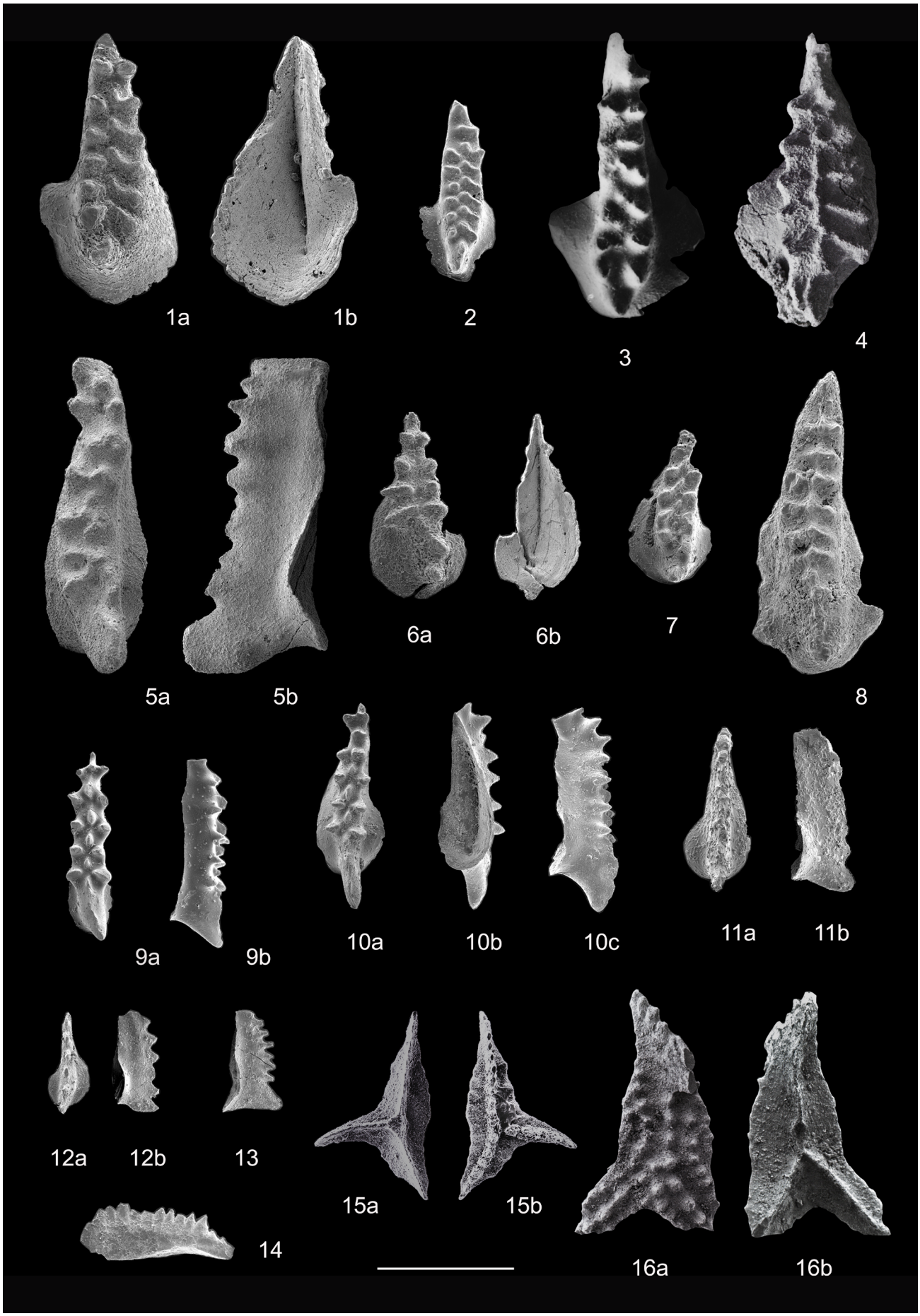
1a
1b
2
3
4
5a
5b
6a
6b
7
8
9a
9b
10a
10b
10c
11a
11b
12a
12b
13
14
15a
15b
16a
16b

EXPLANATION OF PLATE 4

Late Devonian conodonts from Pramosio A and Freikofel T sections, Carnic Alps. Scale bar corresponds to 500 μm.

Figs 1-3, 7 - *Palmatolepis winchelli* (Stauffer, 1938).
1 - Upper view of P222 922716, sample FRKT21E, Frasnian Zone 13c.
2 - Upper view of P216 245035, sample FRKT5, Zone 13a.
3 - Upper view of P185 212074, sample PRA6C, Zone 13c.
7 - Upper view of P234 1823405, sample PRA5B, Zone 13b.

Figs 4, 8 - *Palmatolepis bogartensis* (Stauffer, 1938).
4 - Morph. B, upper view of P234 1823404, sample PRA5B, Zone 13b.
8 - Morph. B, upper view of P234 1823406, sample PRA5B, Zone 13b.

Figs 5-6, 9 - *Palmatolepis hassi* Müller & Müller, 1957.
5 - Upper view of P181 212050, sample PRA2, Zone 13a.
6 - Upper view of P234 1823402, sample PRA0, Zone 12.
9 - Upper view of P84 911271, sample PRA2, Zone 13a.

Figs 10-11 - *Palmatolepis orlovi* Khrustchevae & Kuz'min, 1996.
10 - Upper view of P180 212042, sample PRA0, Zone 12.
11 - Upper view of P180 212043, sample PRA0, Zone 12.

Fig. 12 - *Palmatolepis anzhelae* Khrustchevae & Kuz'min, 1996. Upper view of P181 212048, sample PRA0, Zone 12.

Figs 13, 15 - *Palmatolepis jamieae* Ziegler & Sandberg, 1990.
13 - Upper view of P234 1823401, sample PRA0, Zone 12.
15 - Upper view of P178 212026, sample PRA0, Zone 12.

Fig. 14 - *Palmatolepis uyenoi* Klapper, 2007. Upper view of P181 212047, sample PRA0, Zone 12.

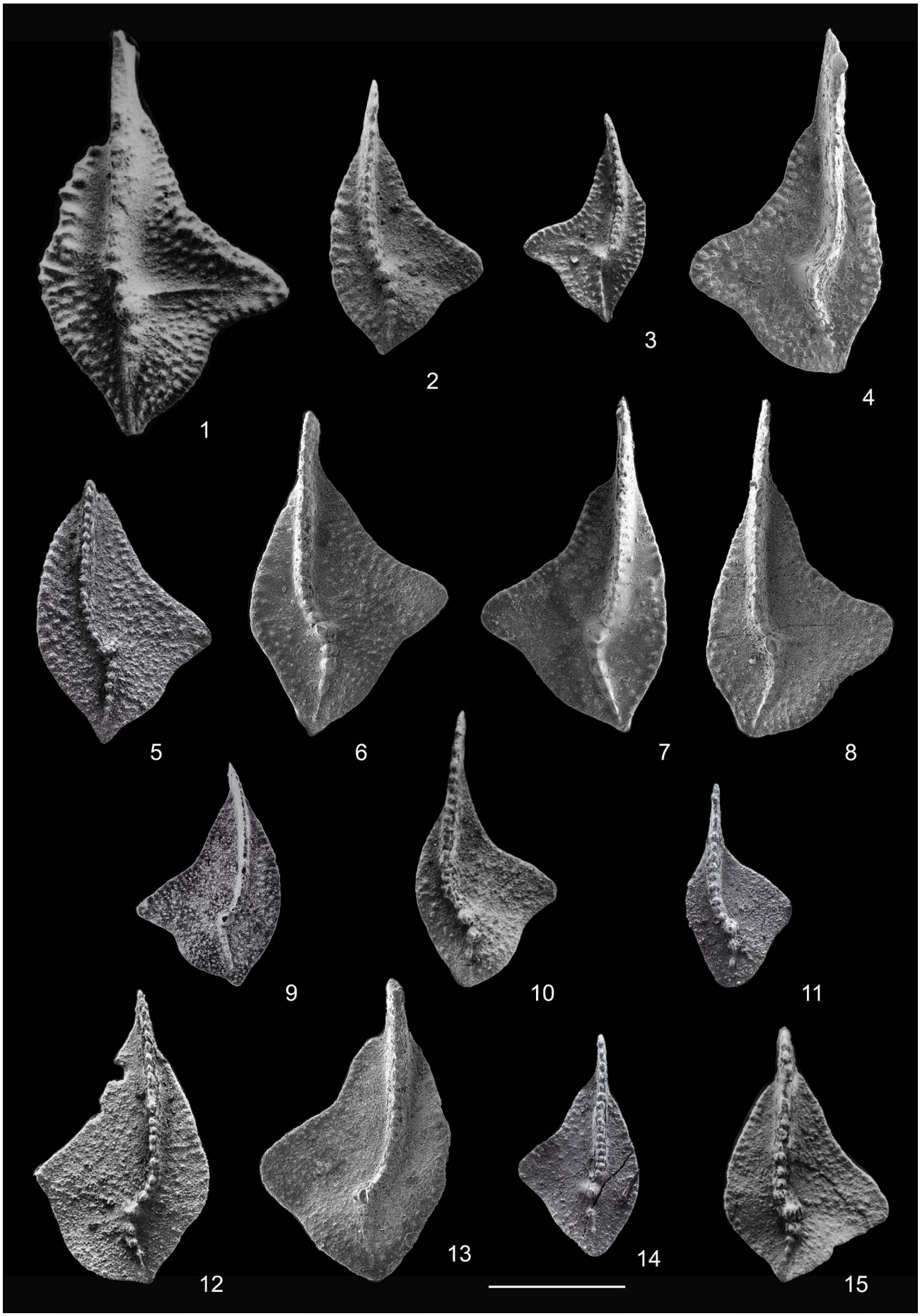
1
2
3
4
5
6
7
8
9
10
11
12
13
14
15

EXPLANATION OF PLATE 5

Late Devonian conodonts from Pramosio A and Freikofel T sections, Carnic Alps. Scale bar corresponds to 500 μm.

Figs 1-6 - *Palmatolepis boogaardi* Klapper & Foster, 1993.
1 - Upper view of P234 1823409, sample PRA0, Frasnian Zone 12.
2 - Upper view of P220 292702, sample FRKT21D, Zone 13b.
3 - Upper view of P234 1823414, sample PRA5C, Zone 13b.
4 - Upper view of P235 1823503, sample PRA6BC, Zone 13b.
5 - Upper view of P220 292701, sample FRKT21D, Zone 13b.
6 - Upper view of P234 1823413, sample PRA5C, Zone 13b.

Fig. 7 - *Palmatolepis nasuta* Müller, 1956. Upper view of P178 212027, sample PRA0, Zone 12.

Figs 8-9 - *Palmatolepis klugi* Klapper, 2007.
8 - Upper view of P187 212094, sample PRA6, Zone 13b.
9 - Upper view of P234 1823412, sample PRA5C, Zone 13b.

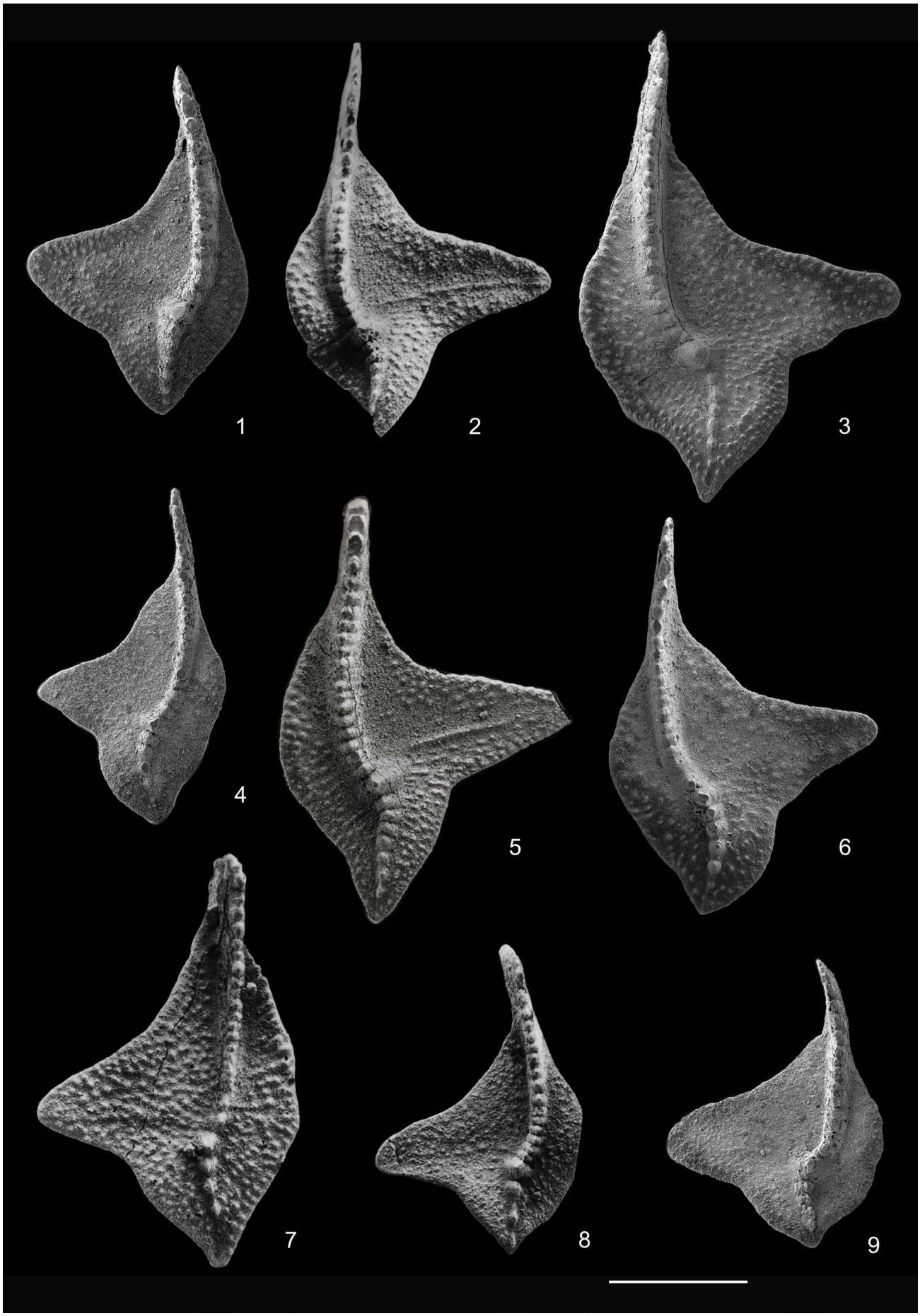
1
2
3
4
5
6
7
8
9

EXPLANATION OF PLATE 6

Late Devonian conodonts from Pramosio A and Freikofel T sections, Carnic Alps. Scale bar corresponds to 500 μm.

Figs 1-12 - *Palmatolepis bogartensis* (Stauffer, 1938).
1 - Morph. B, upper view of P221 922711, sample FRKT21D, Frasnian Zone 13b.
2 - Morph. A, upper view of P184 212067, sample PRA6D, Zone 13c.
3 - Morph. A, upper view of P183 212065, sample PRA6C, Zone 13c.
4 - Morph. B, upper view of P183 212064, sample PRA6C, Zone 13c.
5 - Morph. B, upper view of P217 245039, sample FRKT2, Zone 13a.
6 - Morph. B, upper view of P184 212072, sample PRA6, Zone 13b.
7 - Morph. B, upper view of P183 212061, sample PRA5, Zone 13a.
8 - Morph. B, upper view of P221 922708, sample FRKT21D, Zone 13b.
9 - Morph. C, upper view of P222 922715, sample FRKT21E, Zone 13c.
10 - Morph. C, upper view of P85 911279, sample PRA6, Zone 13b.
11 - Morph. C, upper view of P221 922712, sample FRKT21D, Zone 13b.
12 - Morph. C, upper view of P239 1823908, sample FRKT5, Zone 13a.

Fig. 13 - *Palmatolepis boogaardi* Klapper & Foster, 1993. Juv. element, upper view of P182 212055, sample PRA3, Zone 13a.

Figs 14-16 - *Palmatolepis winchelli* (Stauffer, 1938).
14 - Upper view of P184 212069, sample PRA5, Zone 13b.
15 - Upper view of P184 212070, sample PRA6, Zone 13b.
16 - Upper view of P184 212071, sample PRA6, Zone 13b.

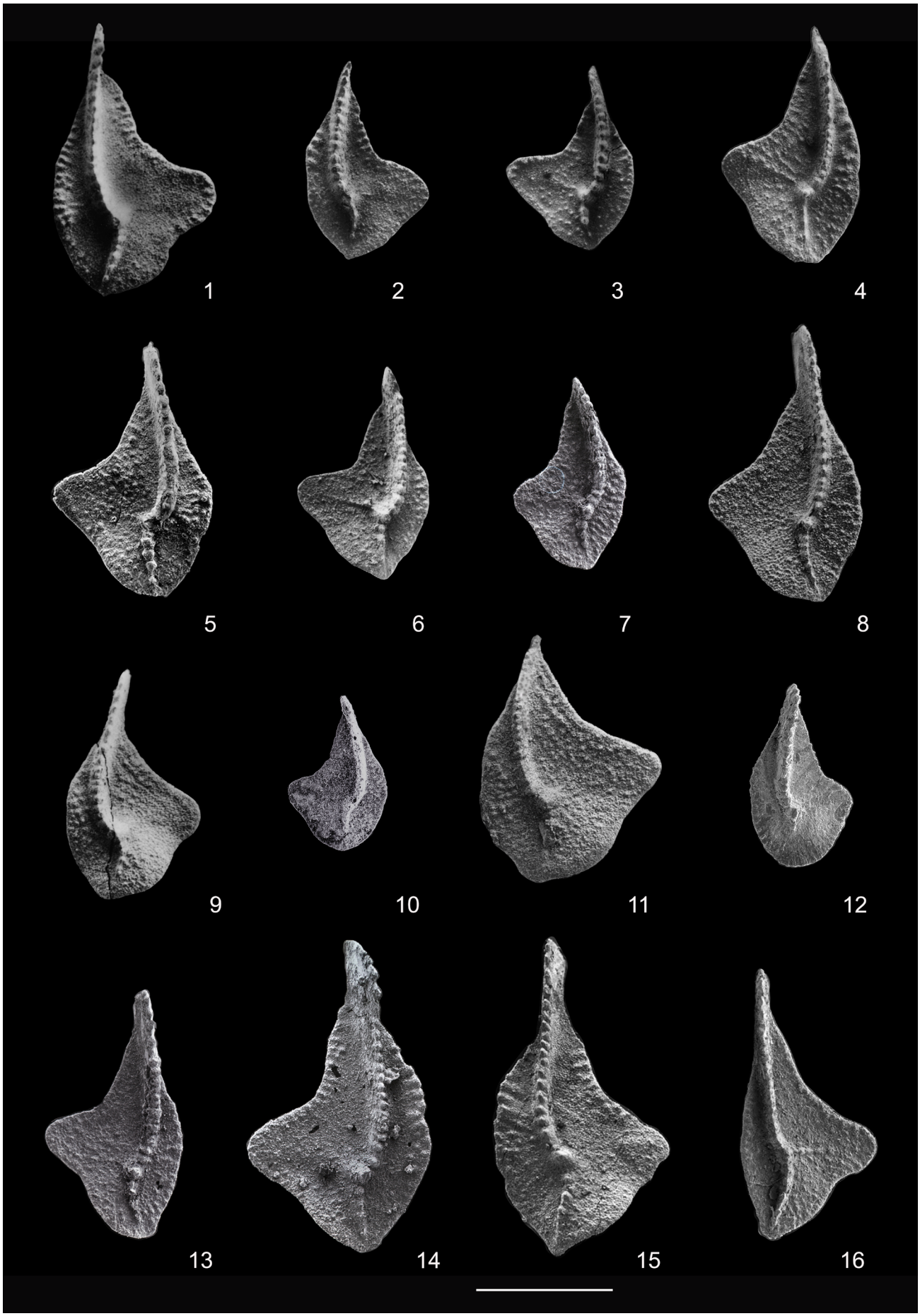
1
2
3
4
5
6
7
8
9
10
11
12
13
14
15
16

EXPLANATION OF PLATE 7

Late Devonian conodonts from Pramosio A and Freikofel T sections, Carnic Alps. Scale bar corresponds to 500 μm.

Figs 1-5 - *Palmatolepis triangularis* Sannemann, 1955.
1 - Upper view of P186 212089, sample PRA11, *Pa. minuta minuta* Zone.
2 - Upper view of P189 212107, sample PRA10, *Pa. minuta minuta* Zone.
3 - Upper view of P189 212108, sample PRA10, *Pa. minuta minuta* Zone.
4 - Upper view of P235 1823513, sample PRA8B, *Pa. triangularis* Zone.
5 - Upper view of P179 212036, sample PRA8B, *Pa. triangularis* Zone.

Figs 6, 8-11 - *Palmatolepis ultima* Ziegler, 1958.
6 - Upper view of P179 212033, sample PRA6C, Frasnian Zone 13c.
8 - Upper view of P235 1823509, sample PRA7A, *Pa. subperlobata* Zone.
9 - Upper view of P222 922718, sample FRKT21E, Zone 13c.
10 - Upper view of P235 1823510, sample PRA8A, *Pa. triangularis* Zone.
11 - Upper view of P225 922734, sample FRKT21E, Zone 13c.

Fig. 7 - *Palmatolepis subperlobata* Branson & Mehl, 1934. Upper view of P219 245054, sample FRKT41, *Pa. delicatula platys* Zone.

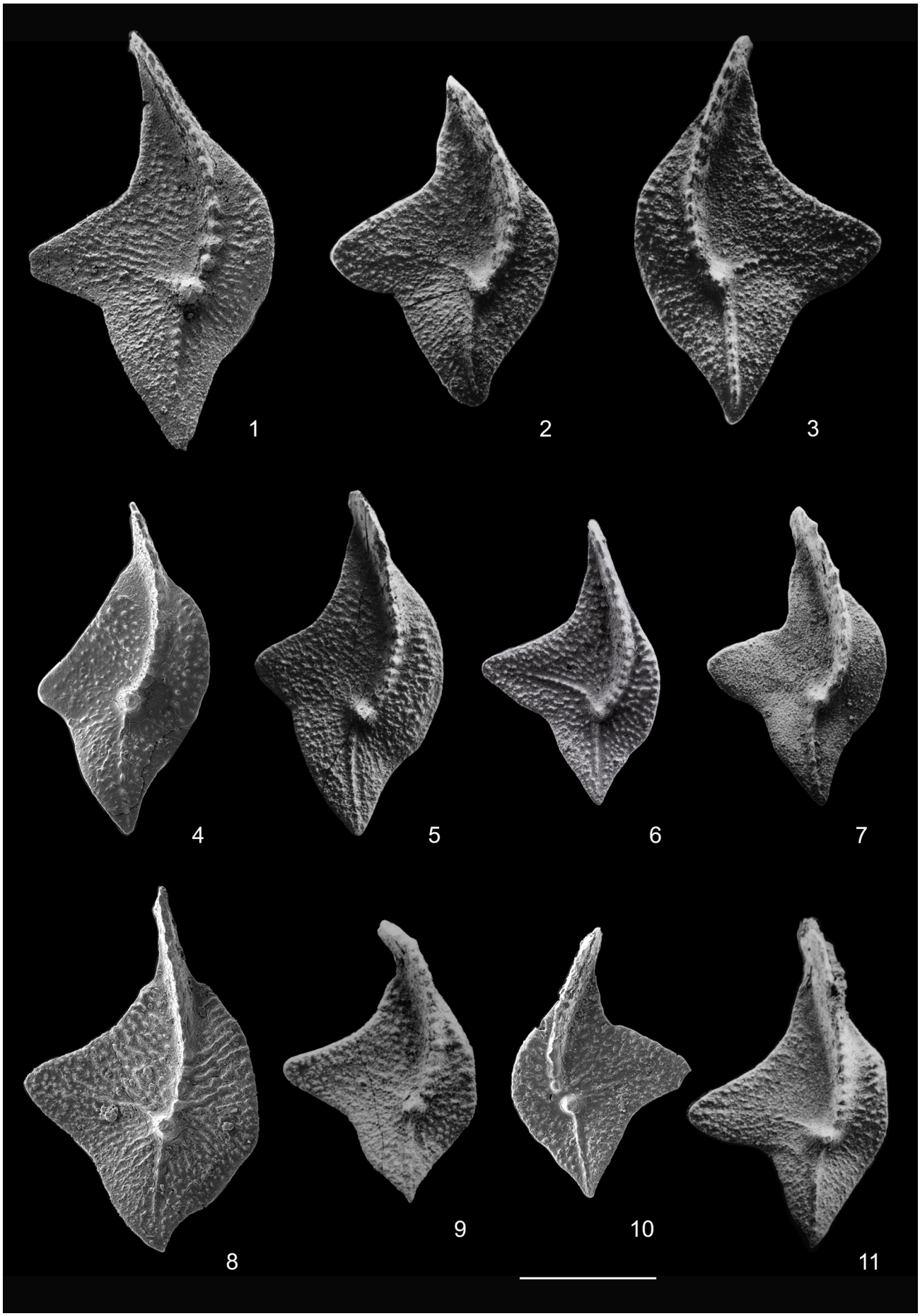
1
2
3
4
5
6
7
8
9
10
11

EXPLANATION OF PLATE 8

Late Devonian conodonts from Pramosio A and Freikofel T sections, Carnic Alps. Scale bar corresponds to 500 µm.

Figs 1-4, 8 - *Palmatolepis triangularis* Sannemann, 1955.
1 - Upper view of P237 1823701, sample PRA12, *Pa. minuta minuta* Zone.
2 - Upper view of P188 212105, sample PRA8A, *Pa. triangularis* Zone.
3 - Upper view of P236 1823601, sample PRA8C1, *Pa. delicatula platys* Zone.
4 - Upper view of P237 1823702, sample PRA12, *Pa. minuta minuta* Zone.
8 - Upper view of P239 1823910, sample FRKT25, *Pa. triangularis* Zone.

Figs 5-7, 9-12, 15 - *Palmatolepis subperlobata* Branson & Mehl, 1934.
5 - Upper view of P236 1823605, sample PRA11B, *Pa. minuta minuta* Zone.
6 - Upper view of P239 1823911, sample FRKT41, *Pa. delicatula platys* Zone.
7 - Upper view of P236 1823604, sample PRA11B, *Pa. minuta minuta* Zone.
9 - Upper view of P236 1823607, sample PRA12, *Pa. minuta minuta* Zone.
10 - Upper view of P239 1823913, sample FRKT72, *Pa. minuta minuta* Zone.
11 - Upper view of P235 1823511, sample PRA8A, *Pa. triangularis* Zone.
12 - Upper view of P239 1823909, sample FRKT22, *Pa. subperlobata* Zone.
15 - Upper view of P226 292744, with abraded surface, sample FRKT21F, *Pa. subperlobata* Zone.

Figs 13-14, 16 - *Palmatolepis ultima* Ziegler, 1958.
13 - Upper view of P225 922739, sample FRKT21E, Frasnian Zone 13c.
14 - Upper view of P235 1823508, sample PRA6E, Zone 13c.
16 - Upper view of P235 1823512, sample PRA8B, *Pa. triangularis* Zone.

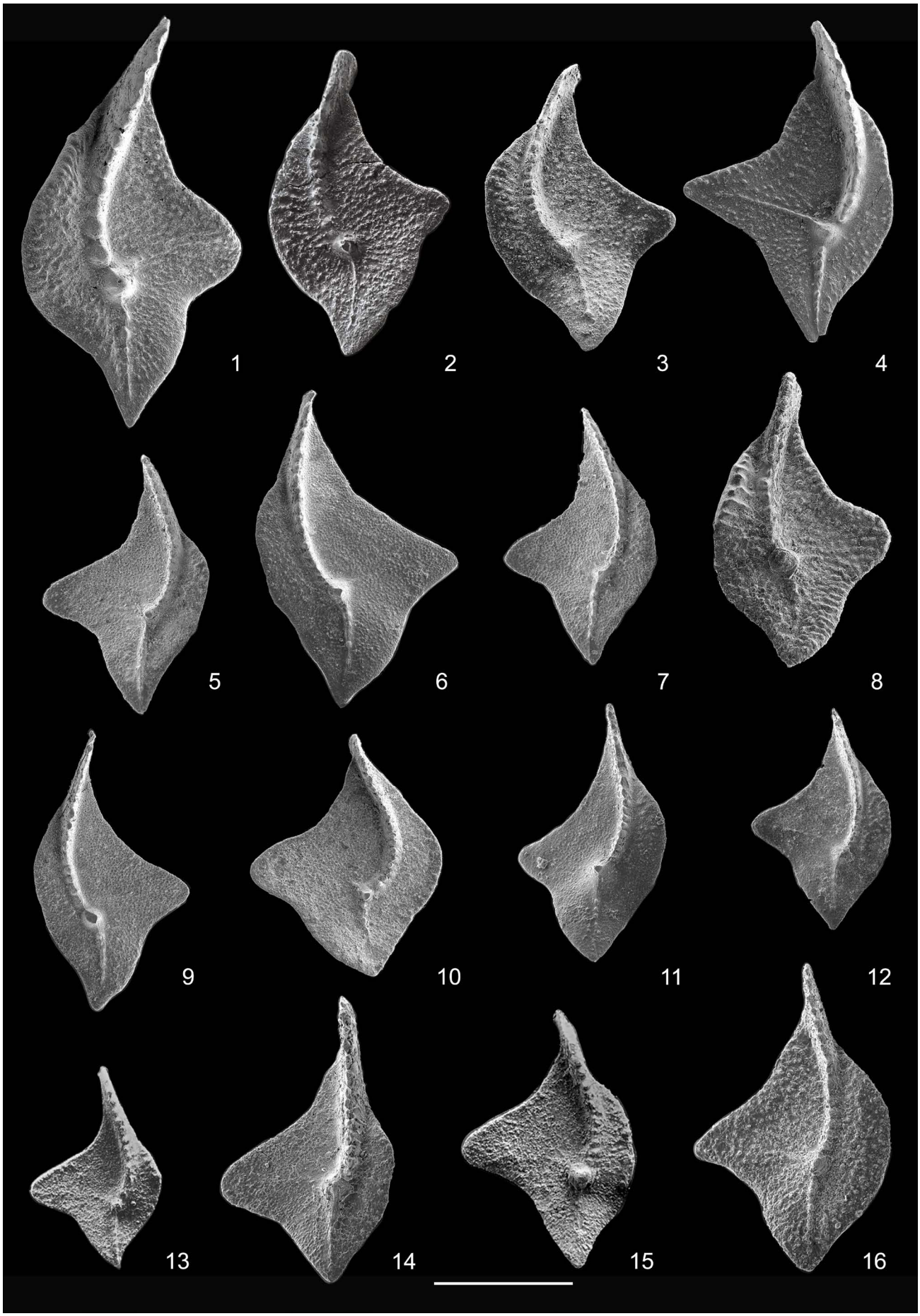
1
2
3
4
5
6
7
8
9
10
11
12
13
14
15
16

EXPLANATION OF PLATE 9

Late Devonian conodonts from Pramosio A and Freikofel T sections, Carnic Alps. Scale bar corresponds to 500 μm.

Fig. 1 - *Palmatolepis gracilis gracilis* Branson & Mehl, 1934. Upper-lateral view of P239 1823905, sample PRA31, *Ps. granulosus* Zone.

Fig. 2 - *Palmatolepis gracilis sigmoidalis* Ziegler, 1962. Upper-lateral view of P239 1823906, sample PRA31, *Ps. granulosus* Zone.

Figs 3-4 - *Palmatolepis regularis* Cooper, 1931.
3 - Upper view of P218 245050, sample FRKT132, *Pa. termini* Zone.
4 - Upper view of P237 1823709, sample PRA19, *Pa. glabra prima* Zone.

Figs 5-9, 13 - *Palmatolepis crepida* Sannemann, 1955.
5 - Upper view of P238 1823802, sample PRA18, *Pa. glabra prima* Zone.
6 - Upper view of P238 1823803, sample PRA18, *Pa. glabra prima* Zone.
7 - Upper view of P237 1823707, sample PRA19, *Pa. glabra prima* Zone.
8 - Upper view of P238 1823801, sample PRA18, *Pa. glabra prima* Zone.
9 - Upper view of P230 1823001b, sample PRA17, *Pa. glabra prima* Zone.
13 - Atypical element, upper view of P219 245056, sample FRKT132, *Pa. termini* Zone.

Figs 10-12, 14-17 - *Palmatolepis linguiformis* Müller, 1956.
10 - Upper view of P221 922706, sample FRKT21D, Frasnian Zone 13b.
11 - Upper view of P213 244995, sample FRKT19, Zone 13b.
12 - Upper view of P178 212030, sample PRA6, Zone 13b.
14 - Upper view of P221 922707, sample FRKT21D, Zone 13b.
15 - Upper view of P178 212028, sample PRA6, Zone 13b.
16 - Upper view of P179 212031, sample PRA6, Zone 13b.
17 - Upper view of P221 922705, sample FRKT21D, Zone 13b.

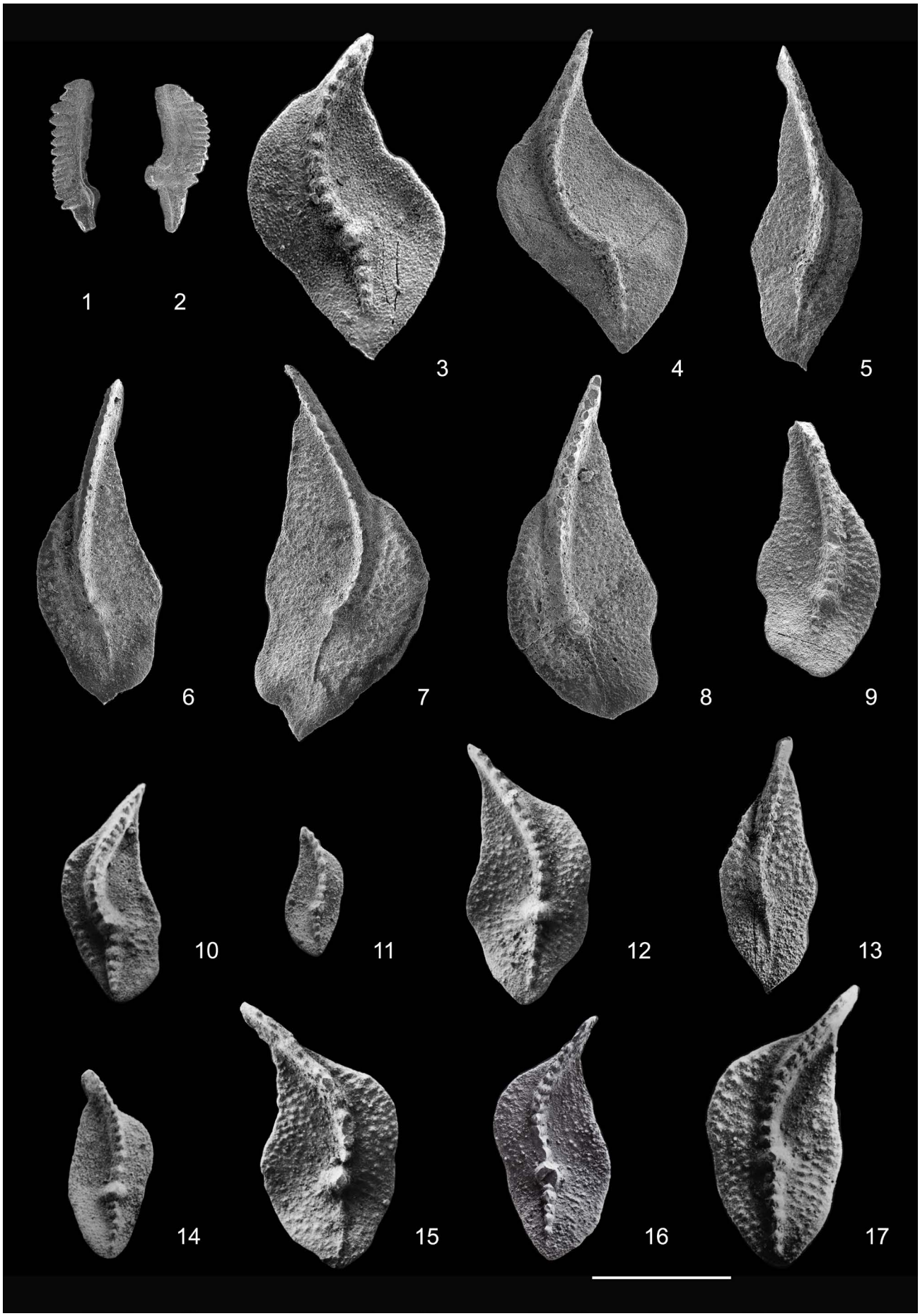
1
2
3
4
5
6
7
8
9
10
11
12
13
14
15
16
17

EXPLANATION OF PLATE 10

Late Devonian conodonts from Pramosio A and Freikofel T sections, Carnic Alps. Scale bar corresponds to 500 μm.

Figs 1-5 - *Palmatolepis clarki* Ziegler, 1962.
1 - Upper view of P236 1823602, sample PRA10, *Pa. minuta minuta* Zone.
2 - Upper view of P180 212039, sample PRA12, *Pa. minuta minuta* Zone.
3 - Upper view of P186 212085, sample PRA10, *Pa. minuta minuta* Zone.
4 - Upper view of P189 212109, sample PRA12, *Pa. minuta minuta* Zone.
5 - Upper view of P219 245052, sample FRKT72, *Pa. minuta minuta* Zone.

Figs 6-10 - *Palmatolepis protorhomboidea* Sandberg & Ziegler, 1973.
6 - Upper view of P236 1823603, sample PRA10, *Pa. minuta minuta* Zone.
7 - Upper view of P236 1823613, sample PRA12, *Pa. minuta minuta* Zone.
8 - Upper view of P179 212038, sample PRA8C, *Pa. delicatula platys* Zone.
9 - Upper view of P180 212045, sample PRA10, *Pa. minuta minuta* Zone.
10 - Upper view of P218 245046, sample FRKT55, *Pa. minuta minuta* Zone.

Fig. 11 - *Palmatolepis minuta minuta* Branson & Mehl, 1934. Atypical element, upper view of P186 212084, sample PRA12, *Pa. minuta minuta* Zone.

Figs 12-17, 23 - *Palmatolepis delicatula platys* Ziegler & Sandberg, 1990.
12 - Upper view of P186 212088, sample PRA11, *Pa. minuta minuta* Zone.
13 - Upper view of P217 245044, sample FRKT41, *Pa. delicatula platys* Zone.
14 - Upper view of P217 245043, sample FRKT41, *Pa. delicatula platys* Zone.
15 - Upper view of P236 1823612, sample PRA12, *Pa. minuta minuta* Zone.
16 - Upper view of P236 1823608, sample PRA12, *Pa. minuta minuta* Zone.
17 - Upper view of P236 1823606, sample PRA11B, *Pa. minuta minuta* Zone.
23 - Upper view of P236 1823614, sample PRA12, *Pa. minuta minuta* Zone.

Figs 18-22 - *Palmatolepis delicatula delicatula* Branson & Mehl, 1934.
18 - Upper view of P219 245055, sample FRKT55, *Pa. minuta minuta* Zone.
19 - Upper view of P236 1823611, sample PRA12, *Pa. minuta minuta* Zone.
20 - Upper view of P218 245045, sample FRKT55, *Pa. minuta minuta* Zone.
21 - Upper view of P236 1823610, sample PRA12, *Pa. minuta minuta* Zone.
22 - Upper view of P236 1823609, sample FRKT50, *Pa. minuta minuta* Zone.

Figs 24-28 - *Palmatolepis juntianensis* Han, 1987.
24 - Upper view of P186 212091, sample PRA3, Frasnian Zone 13a.
25 - Upper view of P217 245040, sample FRKT13, Zone 13a.
26 - Upper view of P85 911278, sample PRA6, Zone 13b.
27 - Upper view of P189 212111, sample PRA6, Zone 13b.
28 - Upper view of P189 212110, sample PRA6, Zone 13b.

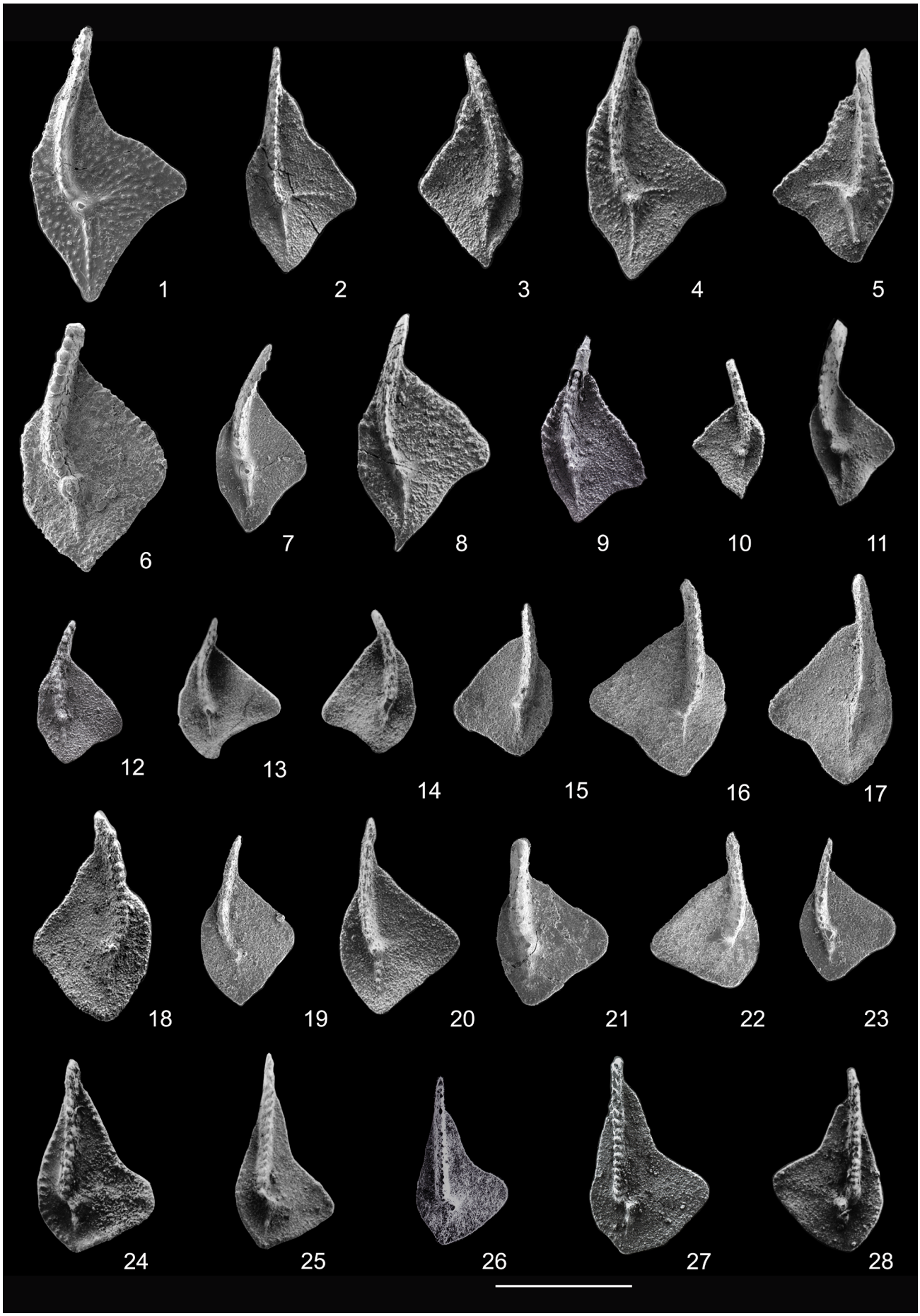
1
2
3
4
5
6
7
8
9
10
11
12
13
14
15
16
17
18
19
20
21
22
23
24
25
26
27
28

EXPLANATION OF PLATE 11

Late Devonian conodonts from Pramosio A and Freikofel T sections, Carnic Alps. Scale bar corresponds to 500 μm.

Fig. 1 - *Palmatolepis klapperi* Sandberg & Ziegler, 1973. Upper view of P238 1823813, sample PRA23, *Pa. gracilis gracilis* Zone.

Figs 2-5 - *Palmatolepis glabra pectinata* Ziegler, 1962.
2 - Upper view of P238 1823810, sample PRA22, *Pa. rhomboidea* Zone.
3 - Upper view of P238 1823814, sample PRA24, *Pa. gracilis gracilis* Zone.
4 - Upper view of P238 1823815, sample PRA24, *Pa. gracilis gracilis* Zone.
5 - Upper view of P239 1823901, sample PRA24, *Pa. gracilis gracilis* Zone.

Fig. 6 - *Palmatolepis glabra lepta* Ziegler & Huddle, 1969. Upper view of P239 1823904, sample PRA31, *Ps. granulosus* Zone.

Fig. 7 - *Palmatolepis glabra glabra* Ulrich & Bassler, 1926. Upper view of P238 1823808, sample PRA21, *Pa. rhomboidea* Zone.

Figs 8-10 - *Palmatolepis glabra prima* Ziegler & Huddle, 1969.
8 - Upper view of P238 1823804, sample PRA20, *Pa. glabra prima* Zone.
9 - Upper view of P238 1823809, sample PRA21, *Pa. rhomboidea* Zone.
10 - Upper view of P237 1823708, sample PRA19, *Pa. glabra prima* Zone.

Figs 11-12, 14-15 - *Palmatolepis tenuipunctata* Sannemann, 1955.
11 - Upper view of P237 1823710, sample PRA18, *Pa. glabra prima* Zone.
12 - Upper view of P237 1823711, sample PRA18, *Pa. glabra prima* Zone.
14 - Upper view of P237 1823706, sample PRA19, *Pa. glabra prima* Zone.
15 - Upper view of P237 1823712, sample PRA18, *Pa. glabra prima* Zone.

Fig. 13 - *Palmatolepis subperlobata* Branson & Mehl, 1934. Upper view of P239 1823915, sample FRKT100, *Pa. crepida* Zone.

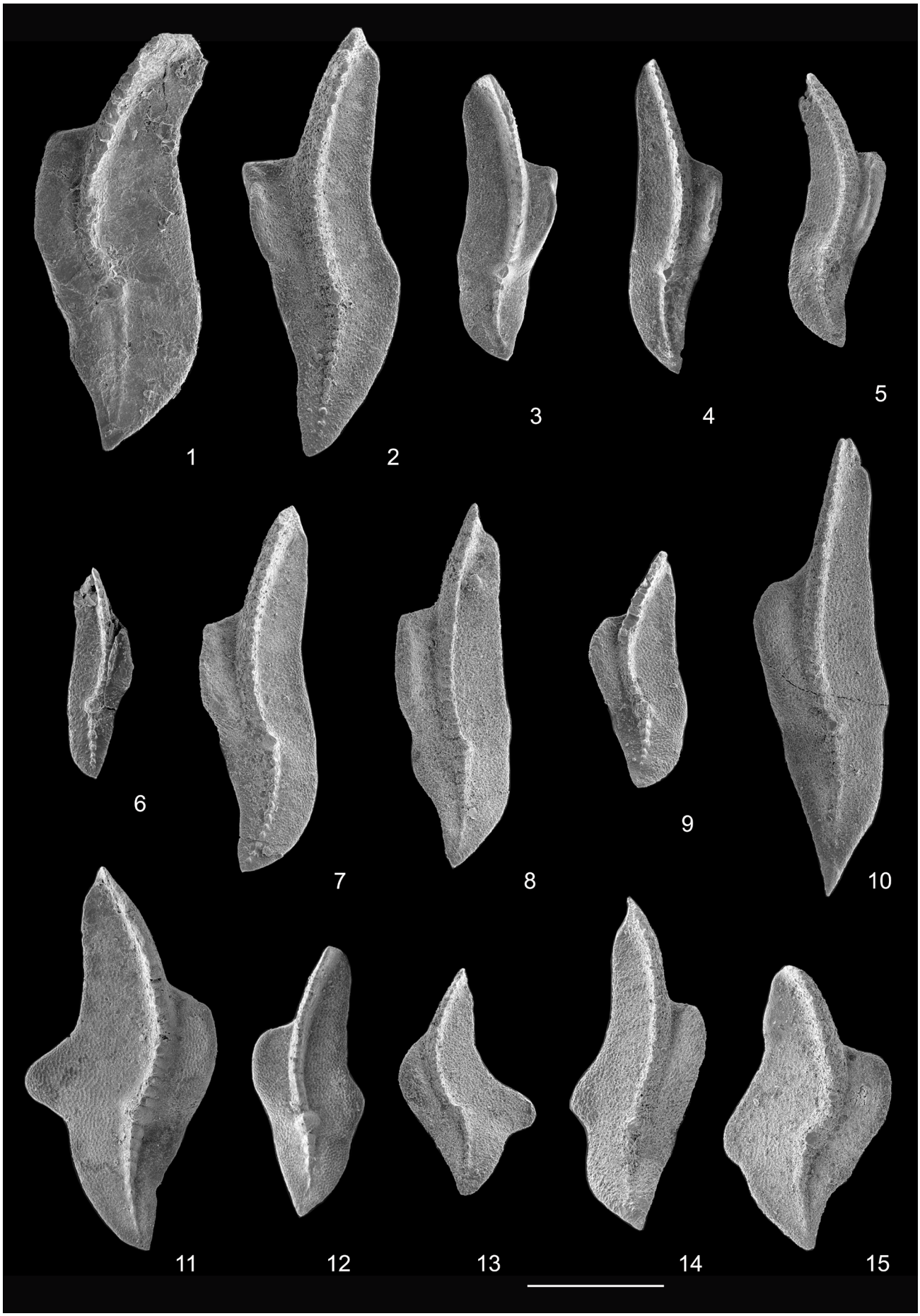
1
2
3
4
5
6
7
8
9
10
11
12
13
14
15

EXPLANATION OF PLATE 12

Late Devonian conodonts from Pramosio A and Freikofel T sections, Carnic Alps. Scale bar corresponds to 500 μm.

Fig. 1 - *Palmatolepis marginifera utahensis* Ziegler & Sandberg, 1984. Upper view of P239 1823903, sample PRA26, *Pa. marginifera utahensis* Zone.

Fig. 2 - *Palmatolepis marginifera marginifera* Helms, 1959. Upper view of P239 1823902, sample PRA26, *Pa. marginifera utahensis* Zone.

Fig. 3 - *Palmatolepis subperlobata* Branson & Mehl, 1934. Upper view of P238 1823807, sample PRA21, *Pa. rhomboidea* Zone.

Fig. 4 - *Palmatolepis minuta minuta* Branson & Mehl, 1934. Upper view of P238 1823812, sample PRA22, *Pa. rhomboidea* Zone.

Fig. 5 - *Palmatolepis minuta loba* Helms, 1963. Upper view of P237 1823705, sample PRA17, *Pa. glabra prima* Zone.

Figs 6-7 - *Palmatolepis poolei* Sandberg & Ziegler, 1973.
6 - Upper view of P238 1823805, sample PRA21, *Pa. rhomboidea* Zone.
7 - Upper view of P238 1823811, sample PRA22, *Pa. rhomboidea* Zone.

Fig. 8 - *Palmatolepis quadrantinodosalobata* Sannemann, 1955. Upper view of P238 1823806, sample PRA21, *Pa. rhomboidea* Zone.

Fig. 9 - *Palmatolepis sandbergi* Ji & Ziegler, 1993. Upper view of P239 1823914, sample FRKT100, *Pa. crepida* Zone.

Fig. 10 - *Palmatolepis termini* Sannemann, 1955. Upper view of P237 1823703, sample PRA16, *Pa. termini* Zone.

Figs 11-17 - *Palmatolepis lobicornis* Schülke, 1995.
11 - Upper view of P230 1823002, sample PRA17, *Pa. glabra prima* Zone.
12 - Upper view of P230 1823003, sample PRA15, *Pa. crepida* Zone.
13 - Upper view of P230 1823004, sample PRA15, *Pa. crepida* Zone.
14 - Upper view of P230 1823005, sample FRTK72, *Pa. minuta minuta* Zone.
15 - Upper view of P230 1823006, sample FRTK72, *Pa. minuta minuta* Zone.
16 - Upper view of P230 1823007, sample FRTK72, *Pa. minuta minuta* Zone.
17 - Upper view of P231 1823103, sample FRKT50, *Pa. minuta minuta* Zone.

Figs 18-19 - *Palmatolepis robusta* Schülke, 1995.
18 - Upper view of P230 1823008, sample FRKT72, *Pa. minuta minuta* Zone.
19 - Upper view of P230 1823009, sample PRA14, *Pa. minuta minuta* Zone.

Figs 20-26 - *Palmatolepis spathula* Schülke, 1995.
20 - Upper view of P231 1823106, sample PRA13, *Pa. minuta minuta* Zone.
21 - Upper view of P231 1823101, sample FRKT55, *Pa. minuta minuta* Zone.
22 - Upper view of P231 1823102, sample FRKT55, *Pa. minuta minuta* Zone.
23 - Upper view of P231 1823104, sample FRKT50, *Pa. minuta minuta* Zone.
24 - Upper view of P231 1823107, sample PRA11B, *Pa. minuta minuta* Zone.
25 - Upper view of P231 1823108, sample PRA14, *Pa. minuta minuta* Zone.
26 - Upper view of P231 1823109, sample PRA14, *Pa. minuta minuta* Zone.

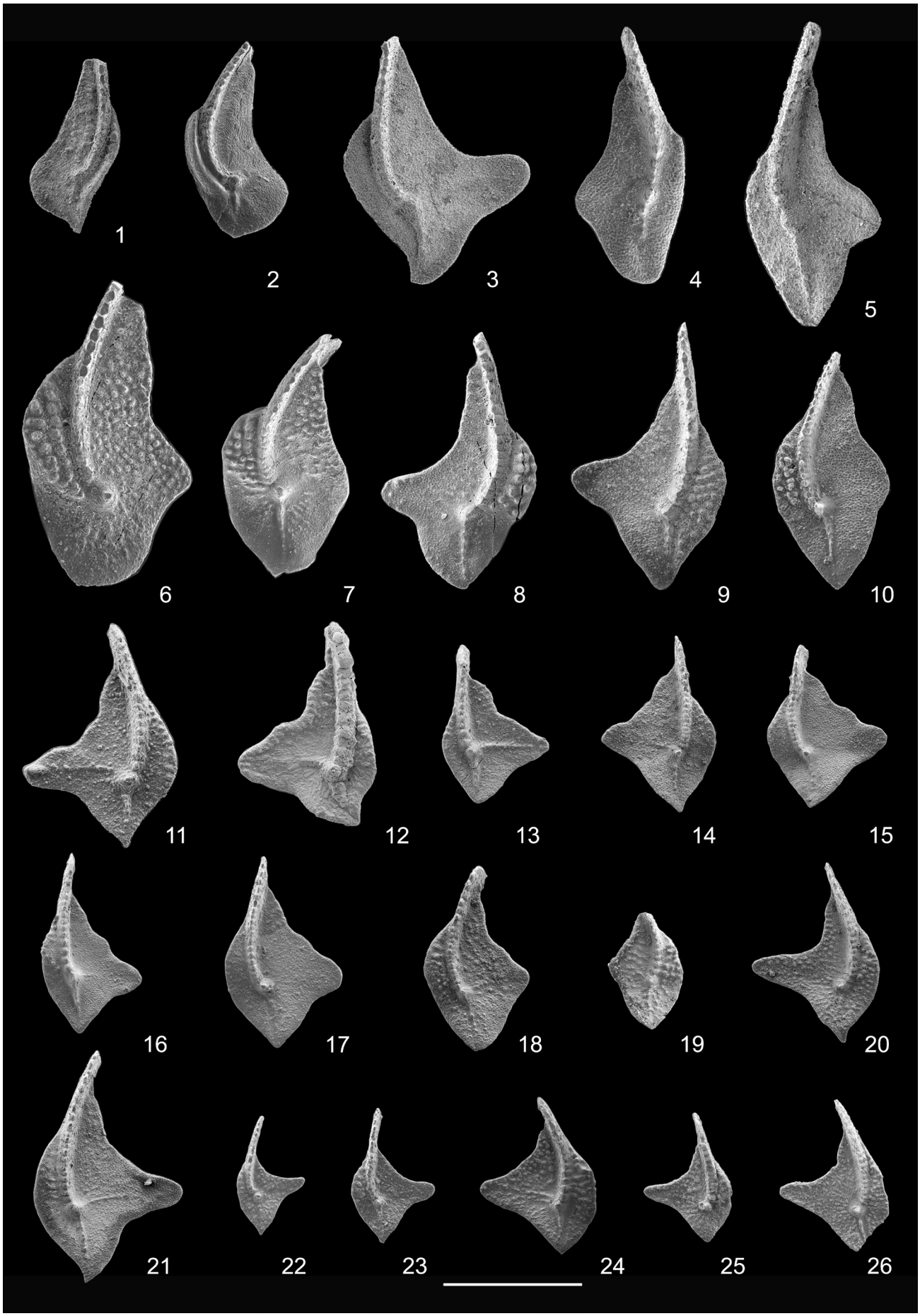
1
2
3
4
5
6
7
8
9
10
11
12
13
14
15
16
17
18
19
20
21
22
23
24
25
26

EXPLANATION OF PLATE 13

Late Devonian conodonts from Pramosio A and Freikofel T sections, Carnic Alps. Scale bar corresponds to 500 µm.

Figs 1-4 - *Polygnathus brevilaminus* Branson & Mehl, 1934.
1 - Upper (a), lower (b) and lateral (c) views of P86 911283, sample PRA7A, *Pa. subperlobata* Zone.
2 - Upper view of P179 212037, sample PRA8A, *Pa. triangularis* Zone.
3 - Upper (a) and lower (b) views of P180 212040, sample PRA6C, Frasnian Zone 13c.
4 - Upper (a) and lower (b) views of P232 1823204, sample PRA7A, *Pa. subperlobata* Zone.

Fig. 5 - *Polygnathus angustidiscus* Branson & Mehl, 1934. Upper (a) and lower (b) views of P232 1823203, sample PRA11A, *Pa. minuta minuta* Zone.

Figs 6, 8-10 - *Polygnathus decorosus* Stauffer, 1938.
6 - Upper (a) and lower (b) views of P181 212051, sample PRA3, Zone 13a.
8 - Upper (a) and lower (b) views of P232 1823208, sample PRA6B1A, Zone 13b.
9 - Upper (a) and lower (b) views of P232 1823212, sample PRA5B, Zone 13b.
10 - Upper (a) and lower (b) views of P232 1823202, sample PRA6BB, Zone 13b.

Figs 7, 11-12 - *Polygnathus lodinensis* Pölsler, 1969.
7 - Upper (a) and lower (b) views of P179 212032, sample PRA6, Zone 13b.
11 - Upper view of P232 1823210, sample FRKT20, Zone 13b.
12 - Upper (a) and lower (b) views of P232 1823207, sample PRA6B1A, Zone 13b.

Figs 13, 15-16 - *Polygnathus praepolitus* Kononova, Alekseev, Barskov & Reimers, 1996.
13 - Upper (a) and lower (b) views of P233 1823303, sample PRA0, Zone 12.
15 - Upper (a) and lower (b) views of P232 1823211, sample PRA5B, Zone 13b.
16 - Upper view of P233 1823302, sample PRA0, Zone 12.

Fig. 14 - *Polygnathus politus* Ovnatanova, 1969. Upper (a) and lower (b) views of P2331823301, sample PRA5D, Zone 13b.

Figs 17-18 - *Polygnathus eoglaber* Ji & Ziegler, 1993.
17 - Upper (a) and lower (b) views of P214 245024, sample FRKT87, *Pa. minuta minuta* Zone.
18 - Upper (a) and lower (b) views of P214 245025, sample FRKT87, *Pa. minuta minuta* Zone.

Fig. 19 - *Polygnathus glaber glaber* Ulrich & Bassler, 1926. Upper (a) and lower (b) views of P232 1823213, sample PRA24, *Pa. gracilis gracilis* Zone.

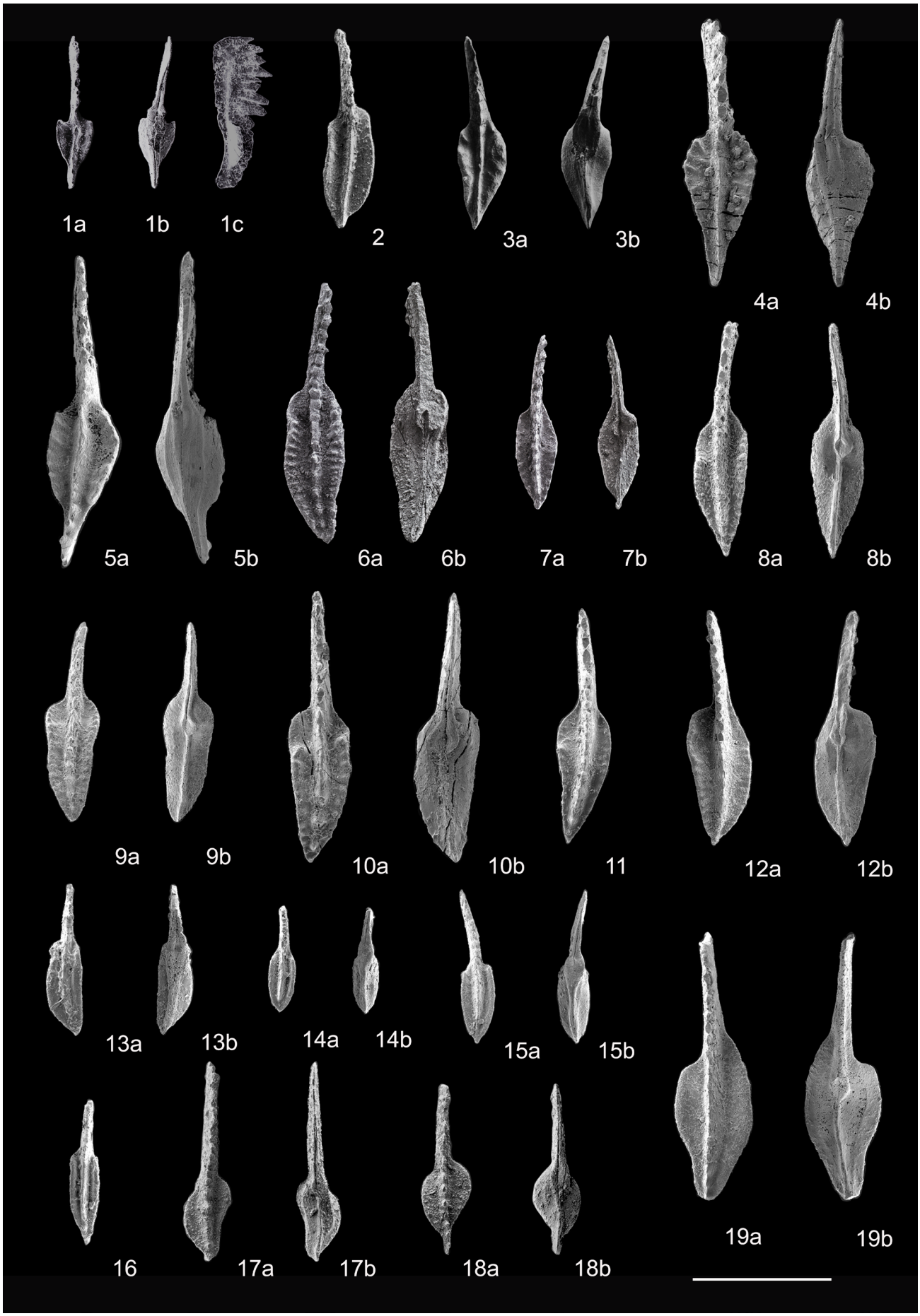
1a
1b
1c
2
3a
3b
4a
4b
5a
5b
6a
6b
7a
7b
8a
8b
9a
9b
10a
10b
11
12a
12b
13a
13b
14a
14b
15a
15b
16
17a
17b
18a
18b
19a
19b

EXPLANATION OF PLATE 14

Late Devonian conodonts from Pramosio A and Freikofel T sections, Carnic Alps. Scale bar corresponds to 500 µm.

Figs 1-2 - *Polygnathus aequalis* Klapper & Lane, 1985.
1 - Upper (a) and lower (b) views of P241 1824115, sample PRA6BC, Frasnian Zone 13b.
2 - Upper (a) and lower (b) views of P241 1824114, sample PRA6, Zone 13b.

Figs 3-4 - *Polygnathus webbi* Stauffer, 1938.
3 - Upper (a) and lower (b) views of P214 245022, sample FRKT20, Zone 13b.
4 - Upper view of P181 212052, sample PRA3, Zone 13a.

Fig. 5 - *Polygnathus procerus* Sannemann, 1955. Upper (a) and lower (b) views of P241 1824108, sample PRA15, *Pa. crepida* Zone.

Figs 6-10 - *Polygnathus praecursor* Matyja, 1993.
6 - Upper (a) and lower (b) views of P179 212035, sample PRA7A, *Pa. subperlobata* Zone.
7 - Upper (a) and lower (b) views of P241 1824105, sample PRA13, *Pa. minuta minuta* Zone.
8 - Lower (a) and upper (b) views of P215 245027, sample FRKT100, *Pa. crepida* Zone.
9 - Upper (a) and lower (b) views of P241 1824118, sample PRA12, *Pa. minuta minuta* Zone.
10 - Upper (a) and lower (b) views of P241 1824117, sample PRA14, *Pa. minuta minuta* Zone.

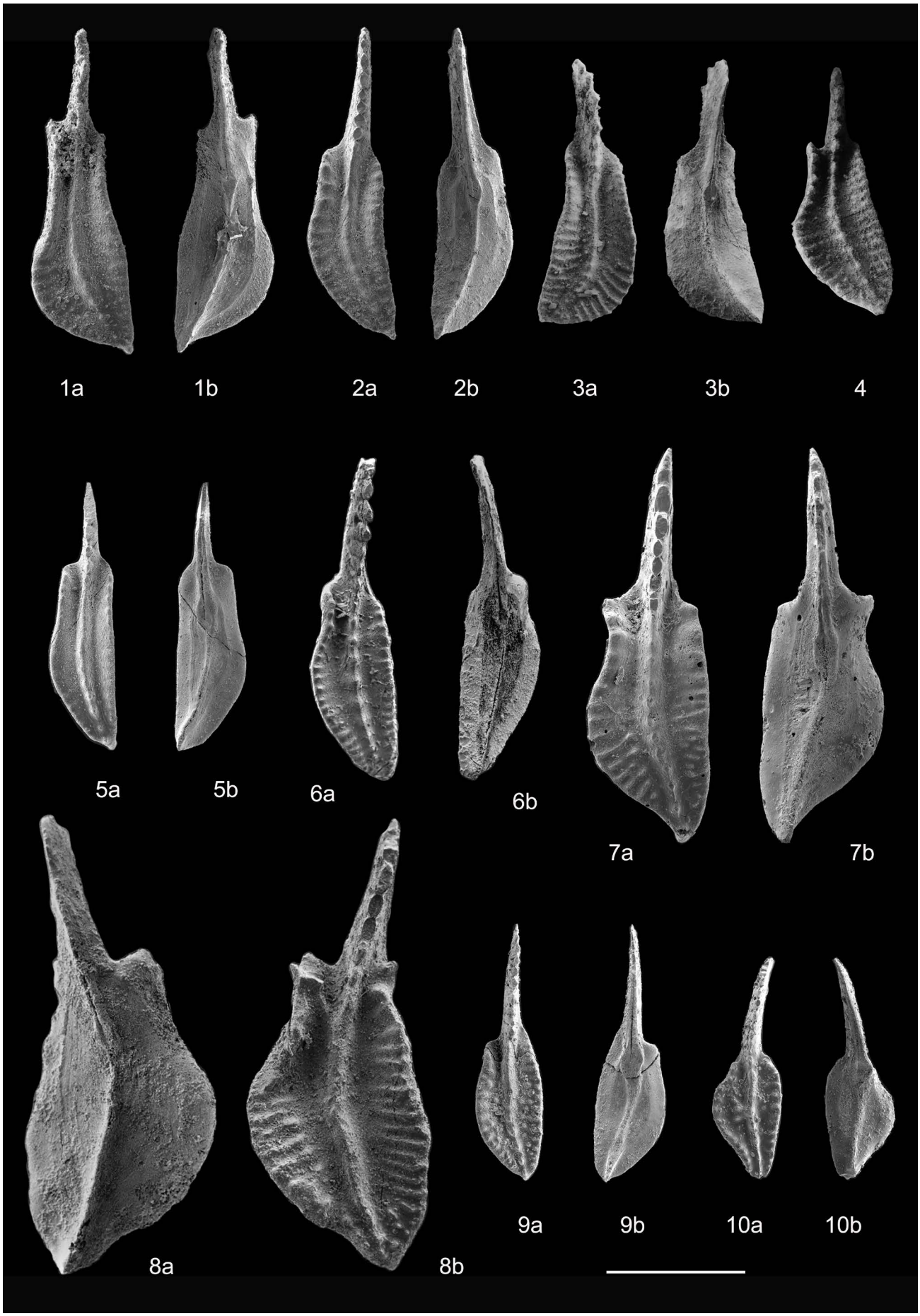
1a
1b
2a
2b
3a
3b
4
5a
5b
6a
6b
7a
7b
8a
8b
9a
9b
10a
10b

EXPLANATION OF PLATE 15

Late Devonian conodonts from Pramosio A and Freikofel T sections, Carnic Alps. Scale bar corresponds to 500 μm.

Figs 1-6 - *Polygnathus procerus* Sannemann, 1955.
1 - Upper (a) and lower (b) views of P241 1824110, sample FRKT72, *Pa. minuta minuta* Zone.
2 - Upper (a) and lower (b) views of P241 1824112, sample FRKT132, *Pa. termini* Zone.
3 - Upper (a) and lower (b) views of P216 245034, sample FRKT132, *Pa. termini* Zone.
4 - Upper (a) and lower (b) views of P216 245033, sample FRKT132, *Pa. termini* Zone.
5 - Upper (a) and lower (b) views of P241 1824111, sample FRKT72, *Pa. minuta minuta* Zone.
6 - Upper (a) and lower (b) views of P241 1824109, sample PRA17, *Pa. glabra prima* Zone.

Fig. 7 - *Polygnathus procerus* Sannemann, 1955 sensu Schülke, 1999. Lower (a) and upper (b) views of P215 245029, sample FRKT50, *Pa. minuta minuta* Zone.

Figs 8-9, 12 - *Polygnathus semicostatus* Branson & Mehl, 1934.
8 - Morph. trend 1 of Dreesen & Dusar, 1974. Upper (a) and lower (b) views of P233 1823306, sample PRA18, *Pa. glabra prima* Zone.
9 - Morph. trend 8 of Dreesen & Dusar, 1974. Upper (a) and lower (b) views of P233 1823305, sample PRA18, *Pa. glabra prima* Zone.
12 - Morph. trend 8 of Dreesen & Dusar, 1974. Upper (a) and lower (b) views of P233 1823304, sample PRA18, *Pa. glabra prima* Zone.

Figs 10-11, 13 - *Polygnathus praecursor* Matyja, 1993.
10 - Upper (a) and lower (b) views of P241 1824119, sample PRA13, *Pa. minuta minuta* Zone.
11 - Upper (a) and lower (b) views of P232 1823216, sample PRA7B, *Pa. subperlobata* Zone.
13 - Upper (a) and lower (b) views of P232 1823205, sample PRA7A, *Pa. subperlobata* Zone.

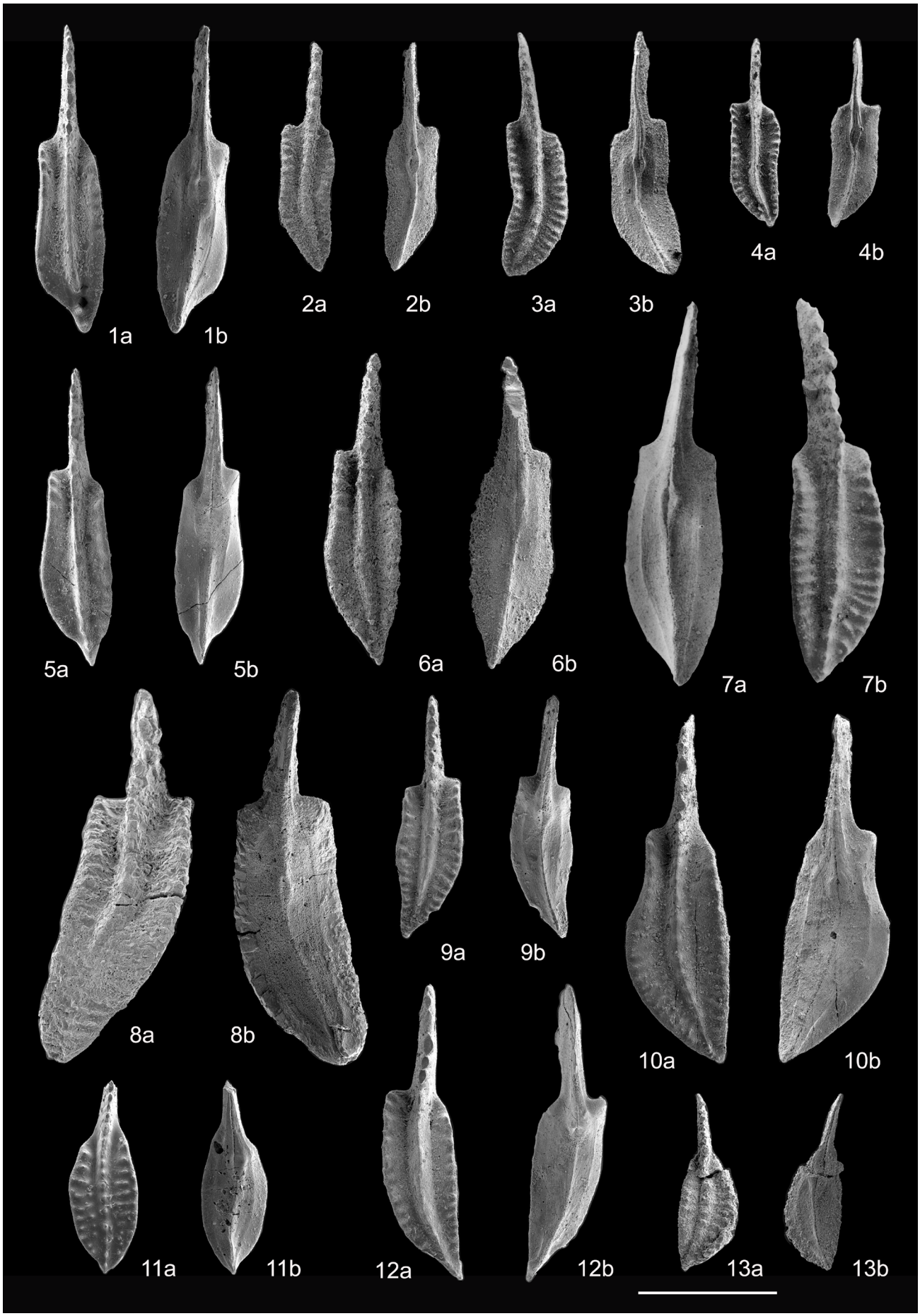
1a
1b
2a
2b
3a
3b
4a
4b
5a
5b
6a
6b
7a
7b
8a
8b
9a
9b
10a
10b
11a
11b
12a
12b
13a
13b

EXPLANATION OF PLATE 16

Late Devonian conodonts from Pramosio A and Freikofel T sections, Carnic Alps. Scale bar corresponds to 500 μm.

Figs 1, 11-12 - *Polygnathus webbi Stauffer*, 1938.
1 - Upper (a) and lower (b) views of P232 1823209, sample PRA6B1A, Frasnian Zone 13b.
11 - Upper (a) and lower (b) views of P182 212058, sample PRA4, Zone 13a.
12 - Upper-lateral view of P224 922733, sample FRKT21D, Zone 13b.

Figs 2-3 - *Polygnathus aequalis* Klapper & Lane, 1985.
2 - Upper (a) and lower (b) views of P241 1824113, sample PRA6, Zone 13b.
3 - Upper (a) and lower (b) views of P232 1823201, sample PRA6BB, Zone 13b.

Fig. 4 - *Polygnathus praecursor* Matyja, 1993. Upper (a) and lower (b) views of P214 245026, sample FRKT50, *Pa. minuta minuta* Zone.

Fig. 5 - *Polygnathus* cf. *Po. procerus* Sannemann, 1955 sensu Schülke, 1999 in Klapper, 2007a (fig. 7.4). Upper (a) and lower (b) views of P232 1823214, sample PRA5C, Zone 13b.

Fig. 6 - *Polygnathus semicostatus* Branson & Mehl, 1934. Morph. trend 1 of Dreesen & Dusar, 1974. Upper-lateral view of P233 1823307, sample PRA22, *Pa. rhomboidea* Zone.

Figs 7-8 - *Polygnathus brevis* Miller & Youngquist, 1947.
7 - Upper (a) and lower (b) views of P182 212056, sample PRA3, Zone 13a.
8 - Upper view of P224 922727, sample FRKT21D, Zone 13b.

Fig. 9 - *Polygnathus* cf. *morgani* Klapper & Lane, 1985. Upper view of P224 922730, sample FRKT21E, Zone 13c.

Fig. 10 - *Polygnathus* cf. *Po. churkini* Savage & Funai, 1980. Upper view of P232 1823206, sample PRA6B1A, Zone 13b.

Fig. 13 - *Polygnathus nodocostatus nodocostatus* Branson & Mehl, 1934. Upper (a) and lower (b) views of P232 1823215, sample PRA21, *Pa. rhomboidea* Zone.

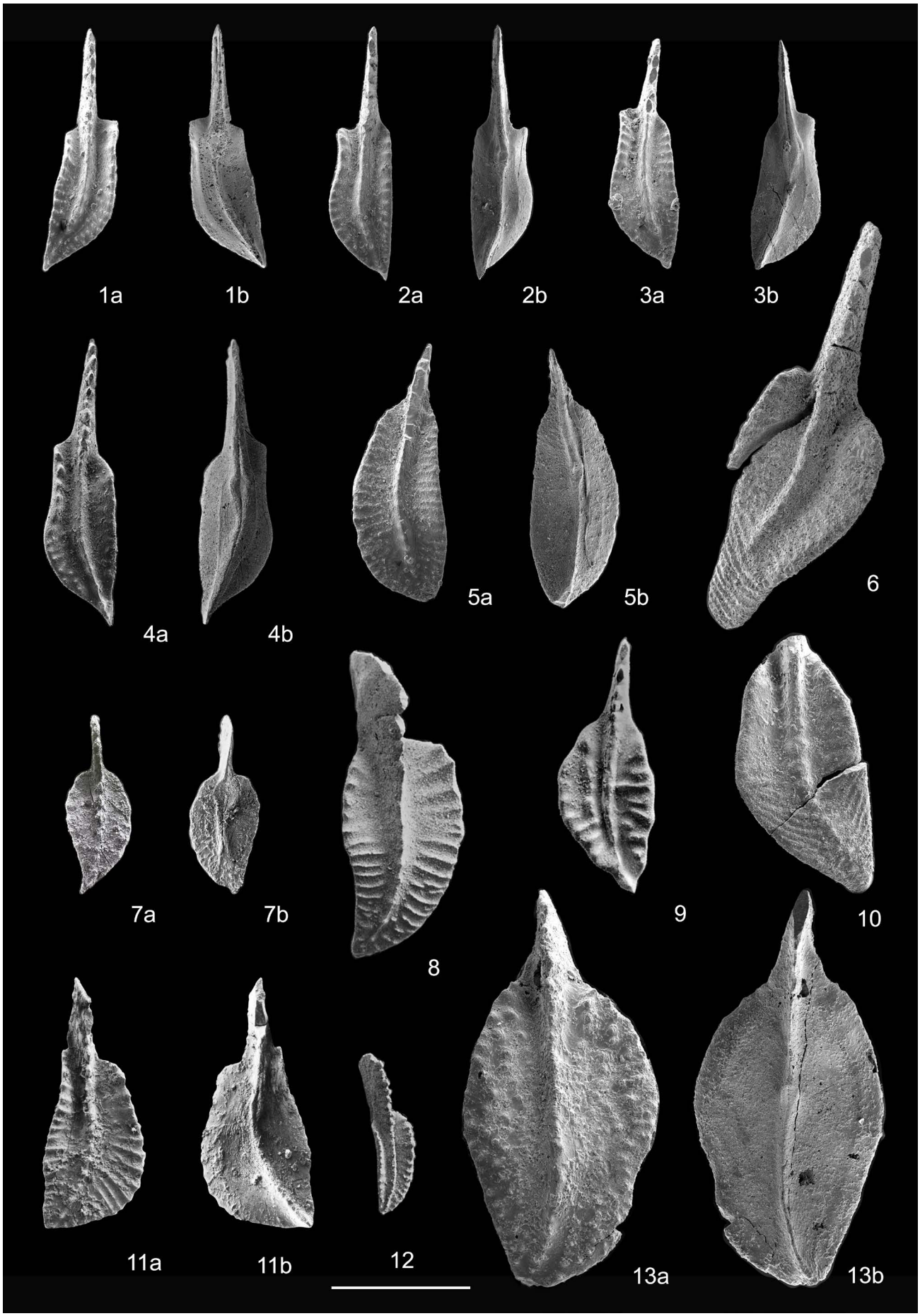
1a
1b
2a
2b
3a
3b
4a
4b
5a
5b
6
7a
7b
8
9
10
11a
11b
12
13a
13b